Study of generation, growth and breakdown of streamwise streaks in a Blasius boundary layer.

by

Luca Brandt

May 2001
Technical Reports from
Royal Institute of Technology
Department of Mechanics
SE-100 44 Stockholm, Sweden

Typsatt i $\mathcal{AMS}$-LaTeX.

Akademisk avhandling som med tillstånd av Kungliga Tekniska Högskolan i Stockholm framlägges till offentlig granskning för avläggande av teknologie licentiatexamen onsdagen den 6:e juni 2001 kl 13.15 i sal E3, Huvudbyggnaden, Kungliga Tekniska Högskolan, Osquars Backe 14, Stockholm.

Kopiecenter, Stockholm 2001

Study of generation, growth and breakdown of streamwise streaks in a Blasius boundary layer.

Luca Brandt 2001
Department of Mechanics, Royal Institute of Technology
SE-100 44 Stockholm, Sweden.

Abstract

Transition from laminar to turbulent flow has been traditionally studied in terms of exponentially growing eigensolutions to the linearized disturbance equations. However, experimental findings show that transition may occur also for parameters combinations such that these eigensolutions are damped. An alternative non-modal growth mechanism has been recently identified, also based on the linear approximation. This consists of the transient growth of streamwise elongated disturbances, mainly in the streamwise velocity component, called streaks. If the streak amplitude reaches a threshold value, secondary instabilities can take place and provoke transition. This scenario is most likely to occur in boundary layer flows subject to high levels of free-stream turbulence and is the object of this thesis. Different stages of the process are isolated and studied with different approaches, considering the boundary layer flow over a flat plate. The receptivity to free-stream disturbances has been studied through a weakly non-linear model which allows to disentangle the features involved in the generation of streaks. It is shown that the non-linear interaction of oblique waves in the free-stream is able to induce strong streamwise vortices inside the boundary layer, which, in turn, generate streaks by the lift-up effect. The growth of steady streaks is followed by means of Direct Numerical Simulation. After the streaks have reached a finite amplitude, they saturate and a new laminar flow, characterized by a strong spanwise modulation is established. Using Floquet theory, the instability of these streaks is studied to determine the features of their breakdown. The streak critical amplitude, beyond which unstable waves are excited, is 26% of the free-stream velocity. The instability appears as spanwise (sinuous-type) oscillations of the streak. The late stages of the transition, originating from this type of secondary instability, are also studied. We found that the main structures observed during the transition process consist of elongated quasi-streamwise vortices located on the flanks of the low speed streak. Vortices of alternating sign are overlapping in the streamwise direction in a staggered pattern.

Descriptors: Fluid mechanics, laminar-turbulent transition, boundary layer flow, transient growth, streamwise streaks, *lift-up* effect, receptivity, free-stream turbulence, nonlinear mechanism, streak instability, secondary instability, Direct Numerical Simulation.

Preface

This thesis considers the study of the generation, growth and breakdown of streamwise streaks in a zero pressure gradient boundary layer. The thesis is based on and contains the following papers

Paper 1. Brandt, L., Henningson, D. S., & Ponziani D. 2001 Weakly non-linear analysis of boundary layer receptivity to free-stream disturbances. *submitted to Phisics of Fluids*.

Paper 2. Andersson, P., Brandt, L., Bottaro, A. & Henningson, D. S. 2001 On the breakdown of boundary layer streaks. *Journal of Fluid Mechanics*, **428**, pp. 29-60.

Paper 3. Brandt, L. & Henningson, D. S. 2001 Transition of streamwise streaks in zero pressure gradient boundary layers. *To appear in Proceedings of the second international symposium on Turbulence and Shear Flow Phenomena (TSFP2)*, Stockholm, June 2001.

The papers are re-set in the present thesis format.

Division of work between authors

The Direct Numerical Simulations were performed with a numerical code already in use mainly for transitional research, developed originally by Anders Lundbladh and Dan Henningson (DH). It is based on a pseudo-spectral technique and has been further developed by Luca Brandt (LB) for generating new inflow conditions and extracting flow quantities needed during the work.

The numerical implementation of the perturbation model presented in Paper 1 was done in collaboration between LB and Donatella Ponziani (DP). The writing was done by LB and DP with great help from DH.

The DNS data and secondary instability calculations presented in Paper 2 were done by LB, who also collaborated in the writing process. The theory and the writing was done by Paul Andersson, Alessandro Bottaro and DH.

The DNS in Paper 3 was performed by LB. The writing was done by LB with help from DH.

Contents

CHAPTER 1

Introduction

The motion of a fluid is usually defined as *laminar* or *turbulent*. A laminar flow is an ordered, predictable and layered flow (from Latin "lamina": layer, sheet, leaf) as opposed to the chaotic, swirly and fluctuating turbulent flow. In a laminar flow the velocity gradients and the shear stresses are smaller; consequently the drag force over the surface of a vehicle is much lower than in a turbulent flow. One of the major challenges in aircraft design is in fact to obtain a laminar flow over the wings to reduce the friction in order to save fuel. On the other hand a turbulent flow provides an excellent mixing in the flow because of the chaotic motion of the fluid particles, and it is therefore required in chemical reactors or combustion engines.

In real applications, as the velocity of the fluid or the physical dimension limiting the flow increase, a laminar motion cannot be sustained; the perturbations inevitably present within the flow are amplified and the flow evolves into a turbulent state. This phenomenon is called *transition*.

Transition and its triggering mechanisms are today not fully understood, even though the first studies on this field dates back to the end of the nineteenth century. The very first piece of work is traditionally considered the classical experiment of Osborne Reynolds in 1883 performed at the hydraulics laboratory of the Engineering Department at Manchester University. Reynolds studied the flow inside a glass tube injecting ink at the centerline of the pipe inlet. If the flow stayed laminar, he could observe a straight colored line inside the tube. When transition occurred, the straight line became irregular and the ink diffused all over the pipe section. He found that the value of a non dimensional parameter, later called Reynolds number, $Re = \frac{Ur}{\nu}$, where U is the bulk velocity, r the pipe radius and ν the kinematic viscosity, governed the passage from the laminar to the turbulent state. Reynolds stated quite clearly, however, that there is no a single *critical* value of the parameter Re, above which the flow becomes unstable and transition may occur; the whole matter is much more complicated. He also noted the sensitivity of the transition to disturbances in the flow before entering the tube.

The knowledge of why, where and how a flow becomes turbulent is of great practical importance in almost all the application involving flows either internal or external; at the present state models able to predict transition onset are available only for simple specific cases. In gas turbines, where a turbulent free stream is present, the flow inside the boundary layer over the surface of

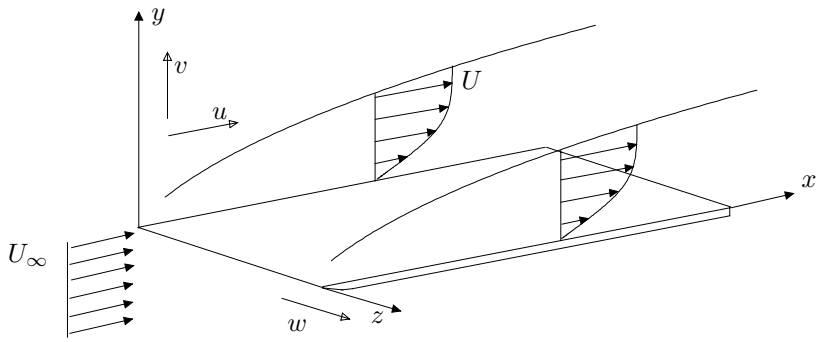

FIGURE 1.1. Boundary layer flow with free-stream velocity U_∞. The velocity has components u, v and w in the coordinate system x, y and z.

a blade is transitional for $50 - 80\%$ of the chord length. Wall shear stresses and heat transfer rates are increased during transition and a correct design of the thermal and shear loads on the turbine blades must take into account the features of the transitional process.

The present thesis deals with transition in the simplified case of the boundary layer over a flat plate subject to a uniform oncoming flow. The friction at the wall will slow down the fluid particles; due to viscosity the velocity of the flow will vary from the free stream value a distance above the wall (boundary layer thickness) to zero at the plate surface, with the thickness growing as the flow evolves downstream, see figure 1.1. This flow is also referred to as *Blasius boundary layer* after the scientist who, under certain assumptions, solved the governing fluid dynamics equations (Navier–Stokes equations) for this particular configuration. This is probably the most simple configuration, but still helps us to gain some physical insight in the transition process. It has been in fact observed that independently of the background disturbances and environment the flow eventually becomes turbulent further downstream. The background environment determines, however, the route the transition process will follow and the location of its onset. Other effects present in real applications such as curvature of the surface or pressure gradients, which give an accelerating or decelerating flow outside the boundary layer, will not be considered.

The transition process may be divided into three sages: receptivity, disturbance growth and breakdown. In the *receptivity* stage the disturbance is initiated inside the boundary layer. This is the most difficult phase of the full transition process to predict because it requires the knowledge of the ambient disturbance environment, which is stochastic in real applications. The main sources of perturbations are free stream turbulence, free stream vortical disturbances, acoustic waves and surface roughness. Once a small disturbance is introduced, it may *grow* or decay according to the stability characteristics of the flow. Examining the equation for the evolution of the kinetic energy of

the perturbation (Reynolds–Orr equation), a strong statement can be made on the non linear effects: the non linear terms redistribute energy among different frequencies and scales of the flow but have no net effect on the instantaneous growth rate of the energy. This implies that linear growth mechanisms are responsible for the energy of a disturbance of any amplitude to increase (Henningson 1996). After the perturbation has reached a finite amplitude, it often saturates and a new, more complicated, laminar flow is established. This new steady or quasi-steady state is usually unstable; this instability is referred to as "secondary", to differentiate it from the "primary" growth mechanism responsible for the formation of the new unstable flow pattern. It is at this stage that the final non linear *breakdown* begins. It is followed by other symmetry breaking instability and non linear generation of the multitude of scales and frequencies typical of a turbulent flow. The breakdown stage is usually more rapid and characterized by larger growth rates of the perturbation compared to the initial linear growth.

CHAPTER 2

Transition in zero pressure gradient boundary layers

2.1. Natural transition

Historically, the first approach to transition was the analysis of the stability of a flow. Equations for the evolution of a disturbance, linearized around a mean velocity profile were first derived by Lord Rayleigh (1880) for an inviscid flow; later Orr (1907) and Sommerfeld (1908) included the effects of viscosity, deriving independently what we today call the Orr–Sommerfeld equation. Assuming a wave–like form of the velocity perturbation and Fourier transforming the equation, it reduces to an eigenvalue problem for exponentially growing or decaying disturbances. The first solutions for unstable waves, traveling in the direction of the flow (two-dimensional waves), were presented by Tollmien (1929) and Schlichting (1933). The existence of such solutions (TS-waves) was experimentally proofed by Schubauer & Skramstad in 1947.

About at the same time, Squire's theorem (1933), stating that two dimensional waves are the first to become unstable, directed the early studies on stability towards two-dimensional perturbations. The stability of such eigenmodes of the Orr–Sommerfeld problem depends on their wavelength, frequency, and on the Reynolds number, defined for a boundary later flow as $Re = \frac{U_\infty \delta}{\nu}$, with δ the boundary layer thickness. Since δ is increasing in the downstream direction, see figure 1.1, the Reynolds number varies and the TS-waves growth rate is also function of the downstream position along the plate. The classical stability theory assumes that the boundary layer has a constant thickness, the so called *parallel flow* assumption, implying that the base flow is characterized only by its streamwise velocity component which varies only in the wall normal direction. The stability of a disturbance is evaluated for different Reynolds numbers, mimicking the downstream evolution of the Blasius flow. This proofed to be a reasonable approximation, even if different models have been now developed to include the boundary layer growth in the stability calculations (see for example the Parabolized Stability Equations introduced by Herbert & Bertolotti 1987).

If an amplified Tollmien–Schlichting wave grows above an amplitude in u_{rms} of 1% of the free-stream velocity, the flow become susceptible to secondary instability. Klebanoff, Tidstrom & Sargent (1962) observed that three-dimensional perturbations, which are present in any natural flow, were strongly

amplified. The three-dimensional structure of the flow was characterized by regions alternating in the spanwise direction of enhanced and diminished perturbation velocity amplitudes, denoted by them "peaks and valleys". The spanwise scale of the new pattern was of the same order of the streamwise wavelength of the TS-waves and the velocity time signal showed the appearance of high frequency disturbance spikes at the peak position. This transition scenario was later denoted as K-type after Klebanoff but also fundamental since the frequency of the secondary, spanwise periodic, fluctuations is the same as the one of the TS-waves. In the non-linear stages of the K-type scenario, rows of "Λ-shaped" vortices, aligned in the steamwise directions, have been observed. An other scenario was also observed, first by Kachanov, Kozlov & Levchenko (1977). This is denoted N-type after Novosibirsk, where the experiments were carried out or H-type after Herbert, who performed a theoretical analysis of the secondary instability of TS-waves (Herbert 1983). In this scenario, the frequency of the secondary instability mode is half the one of the TS-waves and, thus, this is also known as subharmonic breakdown. "Λ-shaped" vortices are present also in this case, but they are arranged in a staggered pattern. Experiments and computations reveals that the N-type scenario is the first to be induced, when small three-dimensional perturbations are forced in the flow.

Transition originating from exponentially growing eigenfunctions is usually called *classical* or *natural* transition. This is observed in natural flows only if the background turbulence is very small; as a rule of thumb it is usually assumed that natural transition occurs for free-stream turbulence levels less than 1%. For higher values, the disturbances inside the boundary layer are large enough that other mechanisms play an important role and the natural scenario is bypassed.

2.2. By–pass transition

In 1969 Morkovin coined the expression "bypass transition", noting that "we can bypass the TS-mechanism altogether". In fact, experiments reveal that many flows, including channel and boundary layer flows, may undergo transition for Reynolds numbers well below the critical ones from linear stability theory. The first convincing explanation for this was proposed by Ellingsen & Palm (1975). They considered, in the inviscid case, an initial disturbance independent of the streamwise coordinate in a shear layer and showed that the streamwise velocity component may grow linearly in time, producing alternating low- and high-velocity *streaks*. Hultgren & Gustavsson (1981) considered the temporal evolution of a three-dimensional disturbance in a boundary layer and found that in a viscous flow the initial growth is followed by a viscous decay (*transient growth*).

Landahl (1980) proposed a physical explanation for this growth. A wall normal displacement of a fluid element in a shear layer will cause a perturbation in the streamwise velocity, since the fluid particle will initially retain its horizontal momentum. It was observed that weak pairs of quasi streamwise

counter rotating vortices are able to lift up fluid with low velocity from the wall and bring high speed fluid towards the wall, and so they are the most effective in forcing streamwise oriented *streaks* of high and low streamwise velocity, alternating in the spanwise direction. This mechanism is denoted *lift-up effect* and it is inherently a three-dimensional phenomenon. Some insight in it may also be gained from the equation for the wall normal vorticity of the perturbation (Squire equation), which is proportional to the streamwise velocity for streamwise independent disturbances. The equation is, in fact, forced by a term due to the interaction between the spanwise variation of the wall normal velocity perturbation and the mean shear of the base flow.

From a mathematical point of view, it is now clear that since the linearized Navier–Stokes operator is non-normal for many flow cases (e.g. shear flows), a significant transient growth may occur before the subsequent exponential behavior (see Schmid & Henningson 2001). Such growth is larger for disturbances mainly periodic in the spanwise direction, that is with low frequency or streamwise wavenumbers; it can exist for sub-critical values of the Reynolds number and it is the underlying mechanism in bypass transition phenomena.

For real applications, the most interesting case in which disturbances originating from non-modal growth are responsible for transition, is probably in the presence of free-stream turbulence. Inside the boundary layer the turbulence is highly damped, but low frequency oscillations, associated with long streaky structures, appear. As the streaks grow downstream, they breakdown into regions of intense randomized flow, turbulent *spots*. The leading edge of these spots travels at nearly the free-stream velocity, while the trailing edge at about half of the speed; thus a spot grows in size and merges with other spots until the flow is completely turbulent. This scenario is usually observed for higher levels of free-stream turbulence and transition occurs at Reynolds numbers lower than in case of natural transition.

An other case where transient growth plays an important role is in the so called *oblique transition*. In this scenario, streamwise aligned vortices are generated by non-linear interaction between a pair of oblique waves with equal angle but opposite sign in the flow direction. These vortices, in turn, induce streamwise streaks, which may grow over a certain amplitude and become unstable, initiating the breakdown to a turbulent flow. Oblique transition has been studied in detail both numerically and experimentally by Berlin, Wiegel & Henningson (1999).

Transition to turbulence may, thus, follow different routes, according to the disturbance environment. In general, as soon as streamwise vortices are present in the flow, strong streamwise streaks are created, and the breakdown to turbulence occurs through their growth and breakdown. In this thesis, bypass transition is analyzed, isolating the different stages of the process and studying them with different approaches. These will be shortly introduced in the next sections.

2.2.1. *Receptivity*

The occurrence of streamwise elongated structures in boundary layers subject to free-stream turbulence was first identified by Klebanoff (1971) in terms of low frequency oscillations in hot wire signals, caused by slow spanwise oscillations of the streaks. Kendall (1985) denoted these disturbances as Klebanoff modes. He also observed streamwise elongated structures with narrow spanwise scales, with the maximum of the streamwise velocity perturbation located in the middle of the boundary layer. The appearance of streaks has been identified as the dominant mechanism in transition in boundary layers subject to free-stream turbulence (see Matsubara & Alfredsson 2001). However, a number of important parameters affect the receptivity of the boundary layer; not only the level of free-stream turbulence, but also its spatial scales, its energy spectrum, the degree of isotropy and homogeneity play an important role. In fact, as observed by Westin *et al.* (1994), different experiments with apparently similar conditions can disagree on the location and extent of transition.

From a theoretical point of view, Bertolotti (1997) has considered disturbances which are free-stream modes, periodic in all directions. He found receptivity to modes with zero streamwise wavenumbers and has shown that the growth is connected to the theories of non modal growth. Andersson, Berggreen & Henningson (1999) and Luchini (2000) used an optimization technique to determine which disturbance present at the leading edge will give the largest disturbance in the boundary layer. They also found a pair of counter rotating streamwise vortices as the most effective in streak's generation. Besides these linear models for receptivity, Berlin & Henningson (1999) have proposed a non-linear mechanism. Numerical simulations have shown that oblique waves in the free-steam can interact to generate streamwise vortices and subsequent streaks inside the boundary layer.

Here we develop a theoretical analysis with the aim to isolate the features involved in the generation of streamwise streaks. We consider a weakly non-linear model based on a perturbation expansion of the disturbance truncated at second order. The perturbation equations are derived directly from the Navier–Stokes equations, superimposing a perturbation field to the base flow, the Blasius profile. This is assumed of constant thickness so that the problem may be transformed in Fourier space in the directions parallel to the wall. A single, decoupled equation is then obtained for each wavenumber pair (α, β) of the perturbation velocity field, with α and β the streamwise and spanwise wavenumber respectively. It is shown that both the problem for the first order disturbance velocity and for the second order correction are governed by the Orr-Sommerfeld/Squire operator, the one describing the linear evolution of three-dimensional disturbances in the flow. The solution for the first order perturbation velocity field is induced by an external forcing of small amplitude ϵ. At second order, $O(\epsilon^2)$, the problem is forced by non-linear interactions of first order solutions with wavenumber pairs such that their combination is equal to the wave-vector of the perturbation we want to study. In particular,

we study the long time response of the system to a couple of oblique modes oscillating with a given frequency ω. The oblique modes are associated to $(\alpha, \pm\beta)$ wavenumbers and their quadratic interactions produce perturbations with $(0, \pm 2\beta)$ wavenumbers that correspond, in physical terms, to streamwise elongated structures.

2.2.2. *Disturbance growth*

Data from different experiments in boundary layers subject to free-stream turbulence show that the growth of the maximum u_{rms} of the low frequency perturbation is initially linear with the Reynolds number based on the local displacement thickness. Thereafter the streaks reach a maximum amplitude and then saturate. The linear analysis of Andersson *et al.* (1999) also shows that optimal disturbances (streamwise streaks) grow linearly with the downstream distance.

Here, Direct Numerical Simulations (DNS), that is numerical solutions of the governing equations without any simplifying assumptions, are used to follow the non-linear saturation of the optimally growing streaks in a spatially evolving boundary layer. The complete velocity vector field from the linear results by Andersson *et al.* (1999) is used as input close to the leading edge and the downstream non-linear development is monitored for different initial amplitudes of the perturbation. The numerical code used is described in Lundbladh *et al.* (1999); it uses a pseudo-spectral algorithm to solve the three dimensional, time-dependent, incompressible Navier–Stokes equations. In a spectral method the solution is approximated by an expansion in smooth functions, trigonometric functions and Chebyshev polynomials in our case. The algorithm is defined pseudo-spectral because the multiplications in the non-linear terms are performed in physical space, to avoid the evaluation of convolution sums. The transformation between physical and spectral space can be performed efficiently using Fast Fourier Transforms algorithms and this allows for efficient implementations of these methods. Due to the fast convergence rate of the spectral approximation of a function, the spectral methods have higher accuracy compared to finite-element of finite difference approximations. However, they are limited to applications in simple geometry.

2.2.3. *Breakdown*

Very carefully controlled experiments on the breakdown of streaks in channel flow were conducted by Elofsson, Kawakami & Alfredsson (1999). They generated elongated streamwise streaky structures by applying wall suction, and triggered a secondary instability by the use of earphones. They observed that the growth rate of the secondary instability modes was unaffected by a change of the Reynolds number of their flow and that the instability appeared as spanwise (sinuous-type) oscillations of the streaks in cross-stream planes.

To determine the characteristic features of streak breakdown, we study the *temporal, inviscid secondary instability* of the saturated streak calculated by

means of DNS. With *temporal stability* we indicate the unstable disturbances are assumed to grow in time, rather than in a space as it would be more natural in comparison with laboratory experiments.

The linear secondary stability calculations are carried out on the basis of the boundary layer approximation, i.e. the mean field to leading order will consist only of the streamwise velocity component U. Such a mean field varies on a slow streamwise scale, whereas the secondary instability varies rapidly in the streamwise direction x, as observed in flow visualizations (see Alfredsson & Matsubara 1996 as example). Therefore we will assume a parallel mean flow, with perturbation mode shapes dependent only on the cross-stream coordinates.

The equations governing the stability of the streak are obtained by substituting $U+\mathbf{u}$, where $\mathbf{u}(x,y,z,t)=(u,v,w)$ is the perturbation velocity and U is the streaky velocity profile, into the Navier–Stokes equations and dropping non-linear terms in the perturbation. If viscosity is neglected it is possible to find an uncoupled equation for the pressure. This is expanded in an infinite sum of Fourier modes and only perturbation quantities consisting of a single wave component in the streamwise direction are considered. Since the base flow is periodic in the spanwise directions, Floquet theory can be used to express the solution as

$$p(x,y,z,t) = Real\{e^{i\alpha(x-ct)} \sum_{k=-\infty}^{\infty} \hat{p}_k(y) e^{i(k+\gamma)\beta z}\},$$

where α is the real streamwise wavenumber and $c = c_r + ic_i$ is the phase speed. Here β is the spanwise wavenumber of the primary disturbance field and γ is the (real) Floquet exponent. Because of symmetry of the streaks it is sufficient to study values of γ between zero and one half, with $\gamma = 0$ corresponding to a *fundamental* instability mode, and $\gamma = 0.5$ corresponding to a *subharmonic* mode. Here fundamental and subharmonic refer to the spanwise periodicity of the modes: in the fundamental instability, perturbations have the same periodicity of the streaks, while in the subharmonic case, the spanwise wavenumber is half the one of the streaks. The most commonly used definitions of *sinuous* or *varicose* modes of instability are adopted with reference to the visual appearance of the motion of the *low-speed streaks*; the symmetries of the subharmonic sinuous/varicose fluctuations of the low-speed streaks are always associated to staggered (x) varicose/sinuous oscillations of the high-speed streaks.

The following highly non-linear stages of streak's breakdown are also studied in this thesis, again using direct numerical simulations. These computations require now many more points and computer resources since the flow is approaching a turbulent state and many scales have to been well resolved to correctly follow the flow evolution. In particular, the performed analysis is devoted to the identification of the large flow structures characteristic of this type of transition.

CHAPTER 3

Conclusions and outlook

In the present work different aspects of the transition process in a Blasius boundary layer have been isolated and analyzed to identify and better understand the mechanisms involved in transition induced by free-stream turbulence. As said in the previous chapter, experimental findings show that, in this scenario, the process is characterized by the occurrence and successive breakdown of streamwise elongated streaks.

We have investigated how free-stream disturbances affect a laminar boundary layer. In particular, we have analyzed the receptivity to oblique waves in the free-stream and to free-stream turbulence–like disturbances. In both cases, the generation of strong streamwise velocity component of the disturbance in streamwise–independent modes is the dominant feature. The underlying mechanism can be reduced to a two-step process, first the non linear generation of streamwise vorticity forced by the interactions between disturbances in the free-stream and then the linear formation of streaks by the *lift–up* effect. A remarkable result is that the importance of the two steps in the process is comparable. In fact the analysis of the equations derived applying a weakly non linear model shows that an amplification of $O(Re)$ occurs both for the generation of streamwise vortices and, afterwards, for the formation of streaks induced by the interaction of the wall normal disturbance velocity and the shear of the Blasius flow.

In the second paper presented in this thesis the non linear downstream evolution of streaks is followed by means of direct numerical simulations, using as inflow condition close to the leading edge of the flat plate the optimal perturbations derived in Andersson *et al.* (1999) in a linear contest. A new mean field characterized by a strong spanwise modulation is established and its secondary stability is studied. The importance of considering a base flow which includes mean flow modification and harmonics of the fundamental streak is demonstrated. The streak critical amplitude, defined as one half of the difference between the highest and lowest streamwise velocity in a cross stream plane, beyond which disturbances are amplified is about 26% of the free-stream velocity. This value is larger than the typical ones of $1 - 2\%$ characteristic of the secondary instability of Tollmien-Schlichting waves. The sinuous instability is clearly the most dangerous one resulting in harmonic spanwise oscillations of the low speed region.

Also using DNS, the breakdown to a turbulent flow resulting from the sinuous secondary instability of streaks is studied. The late stages of the process are investigated and flow structures identified. The main structures observed during the transition process consist of elongated quasi-streamwise vortices located on the flanks of the low speed streak. Vortices of alternating sign are overlapping in the streamwise direction in a staggered pattern. They are different from the case of transition initiated by Tollmien-Schlichting waves and their secondary instability (see Rist & Fasel 1995 as example) or by-pass transition initiated by oblique waves (Berlin *et al.* 1999). In these latter two scenarios Λ-vortices with strong shear layer on top, streamwise vortices deforming the mean flow and inflectional velocity profiles are observed. The present case shows analogies with streak instability and breakdown found in the near wall region of a turbulent boundary layer (see Schoppa & Hussain 1997 or Kawahara *et al.* 1998).

In this first half of my graduate studies, some parts of the phenomena observed and considered relevant in transition in boundary layer subject to free-stream turbulence have been analyzed in detail using simple flow configurations and known repeatable disturbances. In the receptivity study or in the secondary stability calculations limiting assumptions have also been made, but still some interesting results, summarized above, are believed to have been obtained. However, in a recent paper by Jacobs & Durbin (2001), full direct numerical simulations of a transitional Blasius boundary layer under free-stream turbulence have been presented. The authors write that no evidence of sinuous, or other prefatory streak instability, is observed in their simulations, even though they appear in a number of flow visualizations (Matsubara & Alfredsson 2001 as example). Perturbations enter the boundary layer in form of long and intense "backward jets" (corresponding to what we call low-speed streaks) that are lifted in the outer part of the boundary layer. They speculate that backward jets are a link between free-stream eddies and the boundary layer. The breakdown is on isolated jets, originating turbulent patches and spots.

Preliminary DNS of laminar-turbulent transition in a boundary layer subject to free-stream turbulence have been performed using the spectral code also here at KTH (Schlatter 2001). The next step in this research project will then be devoted to the detailed study of this transition scenario through extensive numerical computations. The goal is to try to identify secondary instabilities or other mechanisms responsible for the formation of turbulent spots. Moreover the influence of the free-stream turbulence intensity and characteristic length scales on the location of transition will be investigated. Figures 3.1 and 3.2 show some preliminary results. The simulations are reasonably well resolved, but the limited dimensions of the computational domain may influence the streak growth and the consequently location and frequency of spot's appearance. Anyway strong streamwise streaks, turbulent spots and a turbulent region at the end of the computational domain may be clearly seen; also periodic oscillations of single streaks before spot formation are identified.

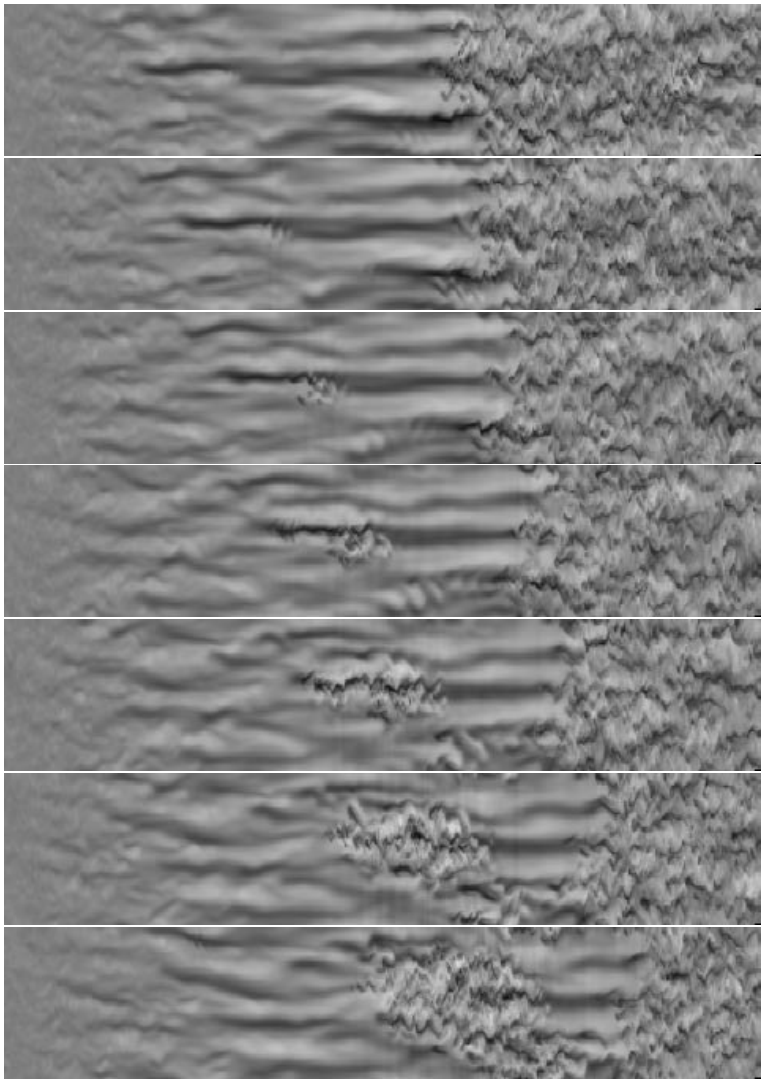

FIGURE 3.1. Visualization of streaks and the spot formation showing the streamwise velocity u of the disturbance. $Re_{\delta_0^*} = 300$, $x/\delta_0^* = [0, 900]$, $z/\delta_0^* = [-25, 25]$, $y/\delta_0^* = 2.5$. Dark areas indicate lower and light areas higher speed. The velocity ranges from about $-35\%, 35\%$ of the local mean velocity. The difference between to frames is 75 non-dimensional time units.

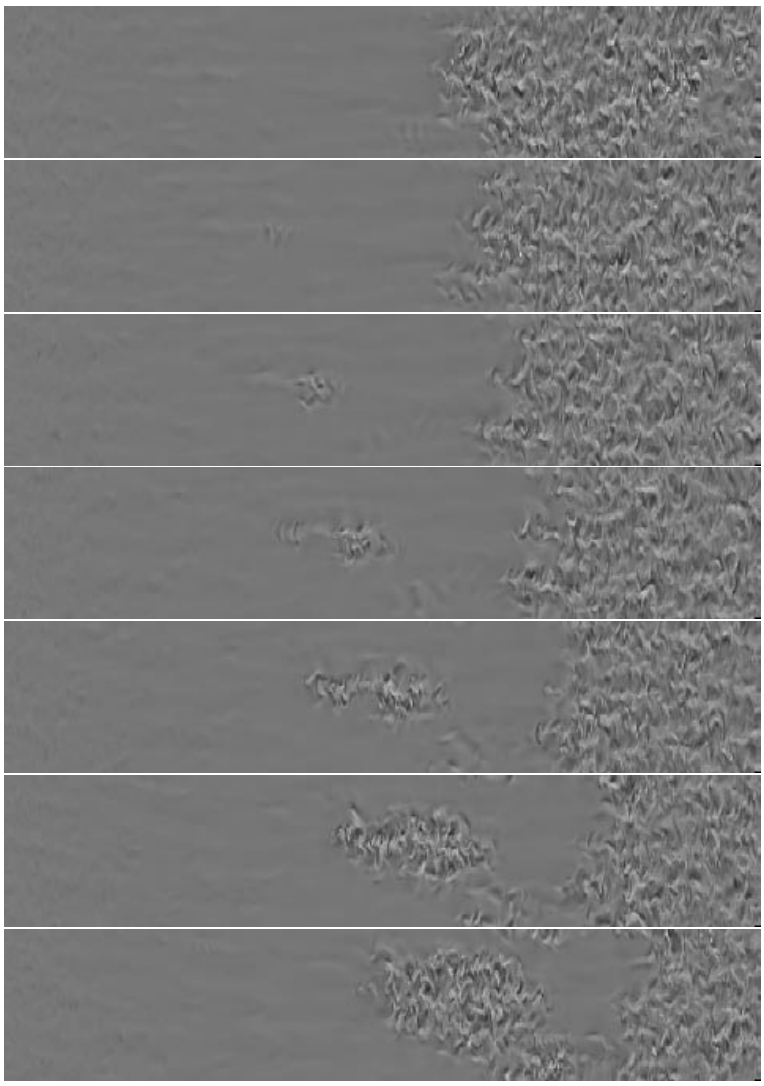

FIGURE 3.2. Visualization of the spot formation showing the amplitude of the normal velocity v. $Re_{\delta_0^*} = 300$, $x/\delta_0^* = [0, 900]$, $z/\delta_0^* = [-25, 25]$, $y/\delta_0^* = 2.5$. Dark areas indicate lower and light areas higher speed, whereas grey indicates zero velocity. The velocity ranges from $-28\%, 28\%$ of the free-stream velocity. The difference between to frames is 75 non-dimensional time units.

Acknowledgment

First of all, I want to thank my supervisor, Professor Dan Henningson, for giving me the opportunity to study and work in *the fascinating world of fluid mechanics*. He has always been available and helpful.

I also want to thank all the people I worked with during these years: Paul Andersson, Alessandro Bottaro, Donatella Ponziani and Philipp Schlatter; I surely learned from all of them.

People at the Department provided a nice atmosphere and I especially enjoyed innebandy very much. I also want to name some of my friends and colleagues in Stockholm: Janne Pralits, Markus Högberg, Martin Skote, Arnim Brüger, Björn Lindgren, Mårtensson Gustaf, Francois Gurniki, MarcoC, Claudio Altafini and Christophe Duwig.

Grazie a *mia moglie* Giulia per tanto, ai miei genitori e al piccolo Lorenzo.

Bibliography

Alfredsson, P. H. & Matsubara, M. 1996 Streaky structures in transition. In *Proc. Transitional Boundary Layers in Aeronautics.* (ed. R. A. W. M. Henkes & J. L. van Ingen), pp. 373-386, Royal Netherlands Academy of Arts and Sciences. Elsevier Science Publishers.

Andersson, P., Berggren, M. & Henningson, D. 1999 Optimal disturbances and bypass transition in boundary layers. *Phys. Fluids.* **11** (1), 134–150.

Berlin, S. & Henningson, D.S. 1999 A nonlinear mechanism for receptivity of free-stream disturbances *Phys. Fluids* **11** , (12), 3749–3760.

Berlin, S., Wiegel, M. & Henningson, D. S. 1999 Numerical and experimental investigations of oblique boundary layer transition. *J. Fluid Mech.*, **393**, 23-57.

Bertolotti, F. P. 1997 Response of the Blasius boundary layer to free-stream vorticity. *Phys. Fluids.* **9** (8), 2286–2299.

Blasius, H. 1907 Grenzschichten in Flüssigkeiten mit kleiner Reibung. Diss. Göttingen. Z. Math. u. Phys. 56, 1-37 (1908). (English translation NACA TM 1256).

Ellingsen, T. & Palm, E. 1975 Stability of linear flow. *Phys. Fluids* **18**, 487.

Elofsson, P. A., Kawakami, M. & Alfredsson, P. H. 1999 Experiments on the stability of streamwise streaks in plane Poiseuille flow. *Phys. Fluids* **11**, 915.

Henningson, D. S. 1996 Comment on "Transition in shear flows. Nonlinear normality versus non-normal linearity" [Phys. Fluids 7 3060 (1995)] *Phys. Fluids* **8**, 2257.

Herbert, T. 1983 Secondary instability of plane channel flow to subharmonic three-dimensional disturbances. *Phys. Fluids* **26**, 871–874.

Herbert, T. & Bertolotti, F. 1987 Stability analysis of non parallel boundary layers. *Bull. Am. Phys. Soc.* **32**, 2079.

Hultgren, L. S. & Gustavsson, L. H. 1981 Algebraic growth of disturbances in a laminar boundary layer *Phys. Fluids.* **24** (6), 1000–1004.

Jacobs, R. J. & Durbin, P. A. 2001 Simulations of bypass transition. *J. Fluid Mech.*, **428**, 185-212.

Kachanov, Yu S. and Kozlov, V.V. & Levchenko, V. Yu 1977 Nonlinear development of a wave in a boundary layer. *Izv. Akad. Nauk SSSR, Mekh. Zhidk. Gaza* **3**, 49-53 (in Russian).

KAWAHARA, G., JIMÉNEZ, J., UHLMANN, M. & PINELLI, A. 1998 The instability of streaks in near-wall turbulence. Center for Turbulence Research, Annual Research Briefs 1998, 155-170.

KENDALL, J. M. 1985 Experimental study of disturbances produced in a pretransitional laminar boundary layer by weak free-stream turbulence. AIAA Paper 85-1695.

KLEBANOFF, P. S. 1971 Effect of free-stream turbulence on the laminar boundary layer. *Bull. Am. Phys. Soc.* **10**, 1323.

KLEBANOFF, P. S. AND TIDSTROM, K. D. & SARGENT, L. M. 1962 The three-dimensional nature of boundary layer instability. *J. Fluid Mech.*, **12**, 1-34.

LANDAHL, M. T. 1980 A note on an algebraic instability of inviscid parallel shear flows. *J. Fluid Mech.* **98**, 243.

LUCHINI, P. 2000 Reynolds-number-independent instability of the boundary layer over a flat surface: optimal perturbations. Accepted *J. Fluid Mech.* **404**, 289.

LUNDBLADH, A., BERLIN, S., SKOTE, M., HILDINGS, C., CHOI, J., KIM, J. & HENNINGSON, D. S. 1999 An efficient spectral method for simulation of incompressible flow over a flat plate. *TRITA-MEK Technical Report* 1999:11, Royal Institute of Technology, Stockholm, Sweden

MATSUBARA, M., ALFREDSSON, P.H. 2001 Disturbance growth in boundary layers subjected to free stream turbulence *J. Fluid Mech.*, **430**, , 149-168.

RAYLEIGH, L. 1880 On the stability of certain fluid motions. *Proc. Math. Soc. Lond.* **11**, 57-70.

REYNOLDS, O. 1883 *Phil. Trans. R. Soc. Lond.* **174**, 935-982.

ORR, W. M. F. 1907 The stability or instability of the steady motions of a perfect liquid and of a viscous liquid. Part I: A perfect liquid. Part II: A viscous liquid. *Proc. R. Irish Acad. A* **27**, 9-138.

RIST, U. & FASEL, H. 1995 Direct numerical simulation of controlled transition in a flat-plate boundary layer. *J. Fluid Mech.*, **298**, 211-248.

SCHLATTER, P. 2001 Direct numerical simulation of laminar-turbulent transition in boundary layer subject to free-stream turbulence *Diploma Thesis, Department of Mechanics, Royal Institute of Technology, Stockholm, Sweden*

SCHLICHTING, H. 1933 Berechnung der Anfachung kleiner Störungen bei der Plattenströmung. *ZAMM* **13**, 171-174.

SCHMID, P. J. & HENNINGSON, D.S. 2001 Stability and Transition in Shear Flows. *Springer.*

SCHOPPA, W. & HUSSAIN, F. 1997 Genesis and dynamics of coherent structures in near-wall turbulence: a new look. In *Self-Sustaining Mechanisms of Wall Turbulence.* (ed. R. L. Panton), pp. 385-422. Computational Mechanics Publications, Southampton.

SCHUBAUER, G. B. & SKRAMSTAD, H. F. 1947 Laminar boundary layer oscillations and the stability of laminar flow. *J. Aero. Sci.* **14**, 69-78.

SOMMERFELD, A. 1908 Ein Beitrag zur hydrodynamischen Erklärung der turbulenten Flüssigkeitbewegungen. *Atti. del 4. Congr. Internat. dei Mat. III*, pp 116-124, Roma.

SQUIRE, H. B. 1933 On the stability of three-dimensional disturbances of viscous fluid flow between parallel walls. *Proc. Roy. Soc. Lond. Ser. A* **142**, 621-628.

Tollmien, W. 1929 Über die Entstehung der Turbulenz. Nachr. Ges. Wiss. Göttingen 21-24, (English translation NACA TM 609, 1931).

Westin, K. J. A., Boiko, A. V., Klingmann, B. G. B., Kozlov, V. V. & Alfredsson, P. H., 1994 Experiments in a boundary layer subject to free-stream turbulence. Part I: Boundary layer structure and receptivity. *J. Fluid Mech.* **281**, 193–218.

1

Paper 1

Weakly non-linear analysis of boundary layer receptivity to free-stream disturbances

By Luca Brandt[†], Dan S. Henningson[†], and Donatella Ponziani[‡1]

[†]Department of Mechanics, Royal Institute of Technology (KTH), S-100 44 Stockholm, Sweden

[‡]Department of Mechanics and Aeronautics, *University of Rome "La Sapienza"*, 18 Via Eudossiana, 00184 Rome, Italy

The intent of the present paper is to study the receptivity of a zero pressure gradient boundary layer to free-stream disturbances with the aim to isolate the essential features involved in the generation of streamwise streaks. A weakly non-linear formulation based on a perturbation expansion in the amplitude of the disturbance truncated at second order is used. It is shown that the perturbation model provide an efficient tool able to disentangle the sequence of events in the receptivity process. Two types of solutions are investigated: the first case amounts to the receptivity to oblique waves oscillating in the free-stream, the second the receptivity to free-stream turbulence-like disturbances, represented as a superposition of modes of the continuous spectrum of the Orr–Sommerfeld and Squire operators. A scaling property of the governing equations with the Reynolds number is also shown to be valid.

1. Introduction

The objective of the present work is the study of the stability of the boundary layer subjected to free-stream disturbances. From a theoretical point of view, boundary layer stability has mainly been analyzed in terms of the eigensolutions of the Orr-Sommerfeld, Squire equations that reduces the study to exponentially growing disturbances. Experimental findings show that transition is also characterized by the occurrence of streamwise elongated structures which are very different from the exponentially growing perturbations. These streamwise structures (or streaks) were first identified by Klebanoff (1971) in terms of low frequency oscillations in hot wire signals caused by low spanwise oscillations of the streaks (Kendall 1985; Westin *et al.* 1994) and are commonly referred to as Klebanoff-modes.

Further analysis of the Orr-Sommerfeld, Squire equations (Gustavsson 1991; Butler & Farrel 1992; Reddy & Henningson 1993; Trefethen *et al.* 1993)

[1]Authors listed in alphabetical order

have confirmed that disturbances other than exponentially growing perturbations may lead to boundary layer instability. From a mathematical point of view this is due to the non–normality of the Orr-Sommerfeld, Squire operator. The physical mechanism behind this linear mechanism is the lift-up induced by streamwise vortices that interact with the boundary layer shear thus generating streaks in the streamwise velocity component. Transition due to these types of disturbances is generally called by-pass transition.

The understanding and prediction of transition require the knowledge of how a disturbance can enter and interact with the boundary layer, commonly referred to as receptivity of the boundary layer. The disturbances are often characterized as either acoustic or vortical disturbances convected by the free-stream. Both types of disturbances have been investigated by asymptotic methods and a summary of the results can be found in the reviews by Goldstein & Hultgren (1989) and Kerschen (1990). Bertolotti (1997) has assumed disturbances which are free-stream modes, periodic in all directions, and has studied the boundary layer receptivity in a "linear region" excluding the leading edge. He has found receptivity to modes with zero streamwise wavenumber and have shown that the growth is most likely connected to the theories of non-modal growth. To answer the question of which disturbance present at the leading edge gives the largest disturbance in the boundary layer at a certain downstream position, Andersson *et al.* (1999) and Luchini (2000) have used an optimization technique adapted from optimal-control theory. The disturbances they found were also streamwise vortices that caused the growth of streaks, and both the wall normal disturbance shape and growth rates agreed well with the findings of Bertolotti (1997).

Berlin & Henningson (1999) have carried out numerical experiments on how simple vortical free-stream disturbances interact with a laminar boundary layer, and have identified a linear and a new non-linear receptivity mechanism. The non-linear one was found to force streaks inside the boundary layer similar to those found in experiments on free-stream turbulence and it worked equally well for streamwise and oblique free-stream disturbances. The boundary layer response caused by the non-linear mechanism was, depending on the initial disturbance energy, comparable to that of the linear mechanism, which was only efficient for streamwise disturbances.

In the present work we develop a theoretical analysis with the aim to isolate the features involved in the generation of streamwise streaks in flows subjected to free-stream turbulence. We consider a weakly non-linear model based on a perturbation expansion in terms of the amplitude of the disturbance, truncated at second order. The model, originally developed in a previous work for the case of Poiseuille flow (Ponziani 2000; Ponziani *et al.* 2000), is here extended to boundary layer flows. This implies the inclusion of the continuous spectrum eigenfunctions in the representation of the first and the second order solutions. To validate the model we first investigate a receptivity mechanisms in a boundary layer imposing a localized disturbance both in the boundary

layer and in the free-stream. In particular, we study the long time response of the system to a couple of oblique modes oscillating with a given frequency ω. For this case the linearized stability equations are driven at first order by the external disturbance and at second order by the quadratic interactions between first order terms. For the type of disturbance considered, the presence of oblique waves generates streamwise vortices which, in turn, induce the formation of streaks inside the boundary layer. The oblique modes are associated to $(\alpha, \pm\beta)$ wavenumbers and their quadratic interactions produce $(0, 2\,\beta)$ wavenumbers that correspond, in physical terms, to an elongated vortical structure, i.e. streamwise counter-rotating vortices. The results show that the generation of streamwise vorticity, which is a non-linear mechanism, and its subsequent lift-up can indeed be recovered through the weakly non-linear formulation. The theory is validated through comparison with direct numerical simulations.

The model is also applied to investigate the response of the boundary layer to continuous spectrum modes. The latter are fundamental for the understanding of the interaction between free-stream vortical eddies and the boundary layer since they reduce to simple sines and cosines in the free-stream and can easily be used to represent a free-stream turbulence spectrum. By using continuous modes, which are solutions of the linear problem, the model reduces to solve a second order equation where the forcing is given by the weakly non-linear interactions between continuous modes. An extensive parametric study is carried out to analyze the interaction between Orr-Sommerfeld as well as Squire modes, in particular considering the effect of the disturbance wavenumbers. A scaling property of the resolvent of the Orr–Sommerfeld and Squire problem with the Reynolds number is shown to be valid for the results obtained.

2. The perturbation model

In the following we define the streamwise, wall normal and spanwise directions as x, y and z, respectively, with velocity perturbation $\underline{u} = (u, v, w)$. All variables are made dimensionless with respect to the constant displacement thickness δ_0^* and the free-stream velocity U_∞ (time is made non dimensional with respect to δ_0^*/U_∞). The perturbation equations are derived directly from the Navier-Stokes equations where we have superimposed a perturbation field to the base flow, namely the Blasius profile. In order to impose periodic boundary conditions in the directions parallel to the wall we assume a parallel base flow and we consider no-slip boundary conditions and solenoidal initial conditions.

We study the evolution of a disturbance in a boundary layer over a flat plate via perturbation theory by expanding the relevant variables in terms of the amplitude of the disturbance ϵ

$$\begin{aligned} \underline{u} &= \underline{u}^{(0)} + \epsilon\,\underline{u}^{(1)} + \epsilon^2\,\underline{u}^{(2)} + \dots . \\ p &= p^{(0)} + \epsilon\,p^{(1)} + \epsilon^2\,p^{(2)} + \dots . \end{aligned} \tag{1}$$

where $\underline{u}^{(0)}, p^{(0)}$ is the given base flow, while remaining terms are unknowns to be determined by the perturbation analysis. We consider a general case in which the perturbation equations are forced by an external forcing

$$F(x,y,z,t) = \epsilon\, F^{(1)}(x,y,z,t)\,,$$

with a given initial condition.

Substituting the expansion (1), truncated at second order, into the Navier-Stokes equations and collecting terms of like powers in ϵ, one obtains the governing equations for the first and the second order. These equations, can be rewritten in the normal velocity $v^{(j)}$, normal vorticity $\eta^{(j)}(\ j = 1, 2)$ formulation, thus obtaining the following Orr-Sommerfeld, Squire system

$$[\,(\frac{\partial}{\partial t} + u^{(0)}\,\frac{\partial}{\partial x})\Delta - D^2\,u^{(0)}\frac{\partial}{\partial x} - \frac{1}{Re}\,\Delta^2\,]\,v^{(j)} \;=\; N_v^{(j)} + F_v^{(j)} \qquad (2)$$

$$[\,\frac{\partial}{\partial t} + u^{(0)}\,\frac{\partial}{\partial x} - \frac{1}{Re}\,\Delta\,]\,\eta^{(j)} + Du^{(0)}\,\frac{\partial\, v^{(j)}}{\partial\, z} \;=\; N_\eta^{(j)} + F_\eta^{(j)} \qquad (3)$$

where

$$N_v^{(j)} \;=\; -[(\frac{\partial^2}{\partial\, x^2} + \frac{\partial^2}{\partial\, z^2})\,S_2^{(j)} - \frac{\partial^2}{\partial\, x\,\partial\, y}\,S_1^{(j)} - \frac{\partial^2}{\partial\, y\,\partial\, z}\,S_3^{(j)}] \qquad (4)$$

$$N_\eta^{(j)} \;=\; -(\frac{\partial}{\partial\, z}S_1^{(j)} - \frac{\partial}{\partial\, x}S_3^{(j)}) \qquad (5)$$

with

$$S_1^{(j)} \;=\; \frac{\partial}{\partial\, x}u^{(j-1)}u^{(j-1)} + \frac{\partial}{\partial\, y}u^{(j-1)}v^{(j-1)} + \frac{\partial}{\partial\, z}u^{(j-1)}w^{(j-1)} \qquad (6)$$

$$S_2^{(j)} \;=\; \frac{\partial}{\partial\, x}u^{(j-1)}v^{(j-1)} + \frac{\partial}{\partial\, y}v^{(j-1)}v^{(j-1)} + \frac{\partial}{\partial\, z}v^{(j-1)}w^{(j-1)} \qquad (7)$$

$$S_3^{(j)} \;=\; \frac{\partial}{\partial\, x}u^{(j-1)}w^{(j-1)} + \frac{\partial}{\partial\, y}v^{(j-1)}w^{(j-1)} + \frac{\partial}{\partial\, z}w^{(j-1)}w^{(j-1)} \qquad (8)$$

The first and second order equations have constant coefficients with respect to the streamwise and spanwise directions, hence we consider the Fourier transform in the (x, z) plane by making the following form assumption for the solution $q^{(j)} = (v^{(j)},\ \eta^{(j)})^T$

$$q^{(j)}(x,y,z,t) = \sum_m \sum_n\ \hat{q}_{mn}^{(j)}(y,t)\, e^{i(\alpha_m\, x + \beta_n z)}$$

and likewise for the external forcing. The wave numbers are defined as follows

$$\alpha_m \;=\; m\ 2\pi/L_x \qquad (9)$$

$$\beta_n \;=\; n\ 2\pi/L_z \qquad (10)$$

$$k_{mn}^2 \;=\; \alpha_m^2 + \beta_n^2 \qquad (11)$$

where L_x and L_z are, respectively, the streamwise and spanwise lengths of the periodic domain. Hereafter, for reading convenience, the subscript m and n are

omitted and we refer to the equations for the individual wave number (α_m, β_n) as (α, β). The resulting equations in matrix form read

$$(\frac{\partial}{\partial t}\hat{M} - \hat{L})\,\hat{q}^{(1)} = \hat{P}\,\hat{F}\,, \tag{12}$$

$$(\frac{\partial}{\partial t}\hat{M} - \hat{L})\,\hat{q}^{(2)} = \hat{P}\sum_{k+p=m}\sum_{l+q=n}[\,\hat{N}(\underline{\hat{u}}^{(1)}_{kl}\underline{\hat{u}}^{(1)^T}_{pq})\,]^T \tag{13}$$

where

$$\hat{L} = \begin{pmatrix} \mathcal{L}_{OS} & 0 \\ \mathcal{C} & \mathcal{L}_{SQ} \end{pmatrix}, \quad \hat{M} = \begin{pmatrix} k^2 - D^2 & 0 \\ 0 & 1 \end{pmatrix},$$

$$\hat{N} = \begin{pmatrix} i\,\alpha \\ D \\ i\,\beta \end{pmatrix}, \qquad \hat{P} = \begin{pmatrix} -i\,\alpha\,D & k^2 & -i\,\beta\,D \\ -i\,\beta & 0 & i\,\alpha \end{pmatrix}.$$

$\hat{L}$ is the linear operator that defines the classical Orr-Sommerfeld, Squire problem

$$\begin{aligned} \mathcal{L}_{OS} &= i\,\alpha\,u^{(0)}(D^2 - k^2) - i\,\alpha\,D^2u^{(0)} - \frac{1}{Re}(D^2 - k^2)^2 \\ \mathcal{C} &= -i\,\beta\,Du^{(0)} \\ \mathcal{L}_{SQ} &= -i\,\alpha\,u^{(0)} + \frac{1}{Re}(D^2 - k^2)\,. \end{aligned} \tag{14}$$

In this investigation we consider two different types of solutions. In the first case the system of equations at first order is forced by an external force that we assume pulsating with a given frequency ω

$$\hat{F}^{(1)} = \hat{f}(y)\,e^{i\,\omega\,t} + \hat{f}^*(y)\,e^{-i\,\omega\,t}\,,$$

where the $*$ indicates the complex conjugate. At second order, the problem is forced by the non-linear interactions of first order terms

$$\hat{T} = \hat{P}\sum_{k+p=\bar{m}}\sum_{l+q=\bar{n}}[\,N(\underline{\hat{u}}^{(1)}_{kl}\underline{\hat{u}}^{(1)^T}_{pq})\,]^T\,. \tag{15}$$

In the second case, we assume that the solution for the first order is given by a continuous spectrum mode representation, and we solve only the second order problem.

The initial conditions are

$$\hat{q}^{(j)}(t=0) = \hat{q}_0, \quad j = 1, 2. \tag{16}$$

With regard to the boundary conditions we enforce no-slip conditions

$$\hat{v}^{(j)} = D\hat{v}^{(j)} = \hat{\eta}^{(j)} = 0 \tag{17}$$

while we assume boundedness in the free-stream. The remaining velocities are recovered by

$$\hat{u}^{(j)} = \frac{i}{k^2}(\alpha D\hat{v}^{(j)} - \beta\hat{\eta}^{(j)}) \tag{18}$$

$$\hat{w}^{(j)} = \frac{i}{k^2}(\beta D\hat{v}^{(j)} + \alpha\hat{\eta}^{(j)}) \tag{19}$$

2.1. *The solution to the forced problem*

We like here to consider the harmonically forced problem described by the system of Eqs. (12), (13) whose solution can be split into two parts (see Ponziani *et al.* 2000): one representing the long time asymptotic solution $\hat{q}^{(j)^L}$ and the other describing the initial transient behavior $\hat{q}^{(j)^T}$,

$$\hat{q}^{(j)} \;=\; \hat{q}^{(j)^T} + \hat{q}^{(j)^L}, \qquad j = 1, 2\,. \tag{20}$$

First we consider the equations for the long time behavior at first order

$$\begin{aligned} (\pm i\,\omega\,\hat{M} - \hat{L})\,\hat{q}^{(1)^L} &= \hat{P}\,\hat{F}\,, \\ \hat{v}^{(1)^L} = D\hat{v}^{(1)^L} &= \hat{\eta}^{(1)^L} = 0, \qquad y = 0, \qquad y = y_\infty \end{aligned} \tag{21}$$

whose long time response to the harmonic forcing is given by

$$\hat{q}^{(1)^L}_{\pm\omega} \;=\; (\pm i\,\omega\,\hat{M} - \hat{L})^{-1}\,\hat{P}\,\hat{f}(y)\,e^{\pm i\,\omega\,t}. \tag{22}$$

The equations that describe the transient at first order are given by

$$\begin{aligned} \frac{\partial}{\partial t}\hat{M}\,\hat{q}^{(1)^T} &= \hat{L}\,\hat{q}^{(1)^T} \\ \hat{q}^{(1)^T} &= -\hat{q}^{(1)^L}, \qquad t = 0 \\ \hat{v}^{(1)^T} = D\hat{v}^{(1)^T} &= \eta^{(1)^T} = 0, \qquad y = 0, \qquad y = y_\infty \end{aligned} \tag{23}$$

Equations (21), (23) provide a complete description of the harmonic forced linear problem; the solution of Eq. (23) is obtained as described in a later section.

With regard to the second order solution, the structure of the quadratic interaction term implies that several frequency components are excited at second order. As for the first order problem we can split the governing equations into two parts that describe the long time and the transient behavior. With regard to the former, we point out that at first order the asymptotic solution in time is characterized by given frequencies $\pm\omega$, which implies that only the zero and 2ω frequency components are excited at second order. However, as demonstrated by Trefethen *et al.* (1993), the maximum response of a system occurs for $\alpha = 0$ and $\omega = 0$; hence we reduce our analysis to the most effective part, that is the one associated to zero frequency and zero streamwise wavenumber

$$-\hat{L}\hat{q}_0^{(2)^L} \;=\; \hat{T}_0^L \tag{24}$$

Here the terms $\hat{T}_0^L$ represent the convolution sum in (15) where only the contribution with zero frequency is considered. Observe that this procedure can also be applied to the solution corresponding to the continuous spectrum modes. Indeed, if a first order solution is represented as a continuous spectrum mode, it is still characterized by a given frequency that corresponds to the real part of the associated eigenvalue.

The equations that describe the transient behavior at second order accounts for different forcing terms that arise from the self interactions between first order transient solutions and the quadratic interactions between the transient solution and the long time solutions.

2.2. *Scaling of forced solution*

For the forced problem it is possible to show a Reynolds number dependence for the norm of the resolvent. Let us introduce a new set of variables to rescale the Orr-Sommerfeld, Squire problem as in Gustavsson (1991); Reddy & Henningson (1993); Kreiss *et al.* (1994)

$$t^* = t/Re, \;\; s^* = s\,Re, \;\; \hat{v}^* = \hat{v}/\,\beta\,Re, \;\; \hat{\eta}^* = \hat{\eta}; \tag{25}$$

with the new scaling we can rewrite (14) as

$$\begin{aligned} \mathcal{L}^*_{OS} &= i\,\alpha\,Re\,u^{(0)}(D^2-k^2) - i\,\alpha\,Re\,D^2u^{(0)} - (D^2-k^2)^2 \\ \mathcal{C}^* &= -i\,Du^{(0)} \\ \mathcal{L}^*_{SQ} &= -i\,\alpha\,Re\,u^{(0)} + (D^2-k^2)\,. \end{aligned} \tag{26}$$

The scaled equations exhibit a dependency only on the two parameters, αRe and k^2, rather than $\alpha,\ \beta,\ Re$ as in the original Orr-Sommerfeld, Squire equations. In the new variables the resolvent can be written as

$$\|(sI-\hat{L})^{-1}\|_E = Re\|(s^*I-\hat{L}^*\|_{E^*} \tag{27}$$

where E is the energy norm with respect to the original variables and E^* is the energy norm with respect to the scaled ones. It is possible to show, see Kreiss *et al.* (1994), that for $\alpha Re = 0$ (that corresponds to the maximum response of the system) the norm of the resolvent $\|(s^*I-\hat{L}^*\|_{E^*}$ scales as the Reynolds number. Hence, Eq. (27) implies that the norm of the original resolvent $\|(sI-\hat{L})^{-1}\|_E$ scales as the square of the Reynolds number.

Further, it is possible to show (see e.g. Kreiss *et al.* 1994) that if we consider Reynolds number independent forcing the amplitude of the response in the original unscaled problem is $O(Re)$ for v and $O(Re^2)$ for η.

2.3. *The initial value problem*

In accounting for the transient solution it is worth making some observations. Since the eigenfunctions of the eigenvalue problem associated to the Orr-Sommerfeld, Squire system form a complete set, see DiPrima (1969) and Salwen & Grosch (1981), we can expand the perturbation solution $\hat{q}^{(i)^T}$ $(i = 1, 2)$ as a superposition of modes. For Blasius boundary layer flow, the

domain is semi-bounded and the spectrum has a continuous and a discrete part, see Grosch & Salwen (1978). These authors have shown that in this case the solution can be expanded in a sum over the discrete modes and in an integration over the continuous spectrum. This analysis can be simplified using a discrete representation of the continuous spectrum by cutting the upper unbounded domain at a given y_∞. Although the eigenvalues differ from the exact representation of the continuous spectrum, particularly as the decay rate increases, their sum has been found to describe correctly the solution to the initial value problem, see Butler & Farrel (1992). Observe that formally, it is possible to expand the solution using integrals over the continuous spectrum. However, the added computational complexity, without any significant gain in accuracy, justifies the use of the present simpler formulation.

With regard to the selection of a set of functions that are orthogonal to the set of Orr-Sommerfeld, Squire eigenfunctions, we exploit the orthogonality relation between the eigenfunctions of the Orr-Sommerfeld, Squire system ($\tilde{q}$) and those of the adjoint Orr-Sommerfeld, Squire problem ($\tilde{q}^+$). From the definition of adjoint, it is easy to show that the eigenvalues of the adjoint are the complex conjugate to the eigenvalue of the of the Orr-Sommerfeld, Squire system. This leads to the orthogonality condition

$$(\hat{M}\,\tilde{q}_j, \tilde{q}_k^+) \quad = \quad C\,\delta_{jk} \tag{28}$$

where δ_{jk} is the Kronecker symbol and C a constant that normalizes the eigenfunctions and that needs to be determined. Hence, for the initial value problem, we can exploit the completeness of the Orr-Sommerfeld, Squire eigenmodes for bounded flows to recover ${\hat{q}^{(i)}}^T$

$$\begin{pmatrix} {\hat{v}^{(i)}}^T \\ {\hat{\eta}^{(i)}}^T \end{pmatrix} \quad = \quad \sum_l K_l \begin{pmatrix} \tilde{v}_l \\ \tilde{\eta}_l^P \end{pmatrix} e^{-i\,\lambda_l^{OS}\,t} + \sum_j B_j \begin{pmatrix} 0 \\ \tilde{\eta}_j \end{pmatrix} e^{-i\,\lambda_j^{Sq}\,t} \tag{29}$$

where (λ_l^{OS}, $\tilde{v}_l$) and (λ_j^{Sq}, $\tilde{\eta}_j$), respectively, are the eigenvalues and eigenvectors of the non-normal $\mathcal{L}_{OS}$ operator, and the homogeneous $\mathcal{L}_{SQ}$ operator and $\tilde{\eta}_l^P$ is the solution of the Squire problem forced by the Orr-Sommerfeld eigenfunctions. The coefficient K_l and B_j are determined from a given initial condition $(\hat{v}_0, \hat{\eta}_0)$ according to (28)

$$K_l \quad = \quad \frac{1}{2\,k^2} \int_0^{y_\infty} \begin{pmatrix} \tilde{\xi}_l \\ 0 \end{pmatrix}^H \begin{pmatrix} k^2 - D^2 & 0 \\ 0 & 1 \end{pmatrix} \begin{pmatrix} \hat{v}_0 \\ \hat{\eta}_0 \end{pmatrix} dy \tag{30}$$

$$B_j \quad = \quad \frac{1}{2\,k^2} \int_0^{y_\infty} \begin{pmatrix} \tilde{\xi}_j^P \\ \zeta_j \end{pmatrix}^H \begin{pmatrix} k^2 - D^2 & 0 \\ 0 & 1 \end{pmatrix} \begin{pmatrix} \hat{v}_0 \\ \hat{\eta}_0 \end{pmatrix} dy \tag{31}$$

where

$$\begin{pmatrix} \tilde{\xi} \\ 0 \end{pmatrix}, \qquad \begin{pmatrix} \tilde{\xi}^P \\ \tilde{\zeta} \end{pmatrix}. \tag{32}$$

are the modes of the adjoint system, see Schmid & Henningson (2001).

2.4. *Continuous spectrum modes*

The Orr-Sommerfeld eigenvalue problem in a semi-bounded domain is characterized by a continuous and a discrete spectrum. The discrete modes decay exponentially with the distance from the wall, while the modes of the continuous spectrum are nearly sinusoidal, whereby the free-stream disturbances can be expanded as a superposition of continuous modes. Since they are associated to stable eigenvalues, they are not relevant for the classical linear stability analysis; however they are fundamental for the understanding of the interaction between free-stream vortical eddies and the boundary layer. In order to determine the eigenfunctions of the continuous spectrum we consider first the Orr-Sommerfeld equations for a small 3-D disturbance with no-slip boundary conditions at the wall $\tilde{v}(0) = D\tilde{v}(0) = 0$ and boundedness at $y \to \infty$. In particular in the free-stream the mean flow is constant (i.e. $u^{(0)} = 1$ as $y/\delta^* > 3$) and the Orr-Sommerfeld equation reduces to

$$(D^2 - k^2)^2\,\tilde{v} - i\,\alpha\,Re\,\{(1-c)(D^2-k^2)\}\tilde{v} \;\; = \;\; 0 \tag{33}$$

where c is the phase velocity. The above equation admits the following solution, see Grosch & Salwen (1978),

$$\tilde{v} \;\; = \;\; A\,e^{i\,\gamma\,y} \,+\, B\,e^{-i\,\gamma\,y} \,+\, C\,e^{-k\,y}, \;\; y \to \infty \tag{34}$$

where

$$k^2 + \gamma^2 + i\,\alpha\,Re(1-c) = 0.$$

From this, an analytical expression for the eigenvalues is derived

$$c = 1 - i\,(1 + \frac{\gamma^2}{k^2})\,\frac{k^2}{\alpha Re} \tag{35}$$

where γ represents the wave number in the wall-normal direction and assumes any positive real value.

From a numerical point of view the crucial point is to enforce the boundedness of the eigenfunctions at $y \to \infty$. We follow the method introduced by Jacobs & Durbin (1998) to recover the correct behavior of the solution in the free-stream solving the equation as a two-point boundary value problem using the spectral collocation method based on Chebyshev polynomial.

We need a total of four boundary conditions: the first two are the no slip at the wall. The arbitrary normalization is $\tilde{v}(y_\infty) = 1$, where y_∞ is the maximum value of y in the wall-normal direction. The condition of boundedness as $y \to \infty$

is converted to a numerical condition at two specific values of y. In fact Eq. (34) implies

$$D^2\tilde{v} + \gamma^2\,\tilde{v} \quad = \quad C\,(k^2 + \gamma^2)e^{-k\,y} \tag{36}$$

in the free-stream. The missing boundary condition is derived evaluating relation (36) at two different point in the free-stream y_1, y_2

$$\frac{(D^2\tilde{v}+\gamma^2\tilde{v})_{y_1}}{(D^2\tilde{v}+\gamma^2\tilde{v})_{y_2}} \quad = \quad e^{k(y_2-y_1)}\,. \tag{37}$$

A similar procedure is used to determine the continuous modes of the Squire equation. However in this case the free-stream behavior of the solution is given only by the two complex exponentials. Hence, from a numerical point of view it suffices to enforce the arbitrary normalization condition $\tilde{\eta}(y_\infty) = 1$.

2.5. *The numerical method*

The temporal eigenvalue systems and the forced problems derived in the previous sections are solved numerically using a spectral collocation method based on Chebychev polynomials. In particular, we consider the truncated Chebychev expansion

$$\phi(\eta) = \sum_{n=0}^{N} \bar{\phi}^n T_n(\eta),$$

where

$$T_n(\eta) = \cos(n\,\arccos(\eta)) \tag{38}$$

is the Chebychev polynomial of degree n defined in the interval $-1 \le \eta \le 1$, and the discretization points are the Gauss–Lobatto collocation points,

$$\eta_j = \cos\frac{\pi j}{N}, \qquad j = 0, 1, \ldots, N,$$

that is, the extrema of the Nth-order Chebyshev polynomial T_N plus the endpoints of the interval. The calculations are performed using at least 301 Chebyshev collocation points in y. The wall-normal domain varies in the range $(0, y_\infty)$, with y_∞ well outside the boundary layer (typically $y_\infty = 50$). The Chebyshev interval $-1 \le \eta \le 1$ is transformed into the computational domain $0 \le y \le y_\infty$ by the use of the mapping

$$y = y_\infty \frac{1-\eta}{2}. \tag{39}$$

The unknown functions $\hat{q} = \hat{q}(y)$ are then approximated by

$$\hat{q}^N(y) = \sum_{n=0}^{N} \bar{q}^n T_n(\eta),$$

The Chebyshev coefficients $\bar{q}^n$, $n = 0, \ldots, N$ are determined by requiring the different equations derived from (12),(13) to hold for $\hat{q}^N$ at the collocation points y_j, $j = p, \ldots, N-p$, with $p = 2$ for the fourth order Orr–Sommerfeld

equation and $p = 1$ for the second order Squire equation. The boundary conditions are enforced by adding the equations

$$\sum_{n=0}^{N} \bar{q}^n T_n(0) = \sum_{n=0}^{N} \bar{q}^n T_n(y_\infty) = 0,$$

and the two additional conditions for the Orr–Sommerfeld problem

$$\sum_{n=0}^{N} \bar{q}^n DT_n(0) = \sum_{n=0}^{N} \bar{q}^n DT_n(y_\infty) = 0,$$

where DT_n denotes the y-derivative of the n-th Chebyshev polynomial.

3. Receptivity to localized forcing

3.1. *Disturbance generation and parameter settings*

In order to trigger the formation of streamwise streaks in the boundary layer we consider the response of the system to a couple of oblique waves. This is similar to the investigations of Berlin & Henningson (1999), although here we are able to understand the mechanism in more detail since we use an analytical formulation. In this section we also compare our analytical results to direct numerical simulations of the type presented by Berlin & Henningson (1999). The oblique waves are generated by an harmonic localized wall–normal volume force given by

$$\underline{F} \quad = \quad f(y)\, cos(\alpha\, x)\, cos(\beta\, z)\, e^{j\,\omega\, t} \tag{40}$$

with

$$f(y) \quad = \quad \frac{1}{\sqrt{2\pi}\sigma} e^{-\frac{(y-y_0)^2}{2\sigma^2}}$$

In our computations we chose $Re = 400$, and $(\alpha, \pm\beta) = (0.2, \pm 0.2)$. We analyze two cases: for the first one the forcing is in the boundary layer ($y_0 = 2.2$), for the second the forcing is in the free-stream ($y_0 = 8.$). The results presented here correspond to the latter case with $\sigma = 0.5$.

The formation of streamwise streaks in the boundary layer is initiated by two oblique waves characterized by wave numbers $(\alpha,\, \pm\beta) = (\,0.2,\, \pm 0.2)$. In the linear long time response of the system to the external forcing, there is no evidence of streaks generation. However, if one accounts for the second order interactions (in particular those that force the wave number $(0,\, 2\,\beta)$) it is easy to observe that the second order correction corresponds to a system of strong streamwise longitudinal vortices in the boundary layer. These results are in agreement with the work of Berlin & Henningson (1999) where the generation of streaks in the boundary layer is triggered by the non-linear evolution of two oblique waves.

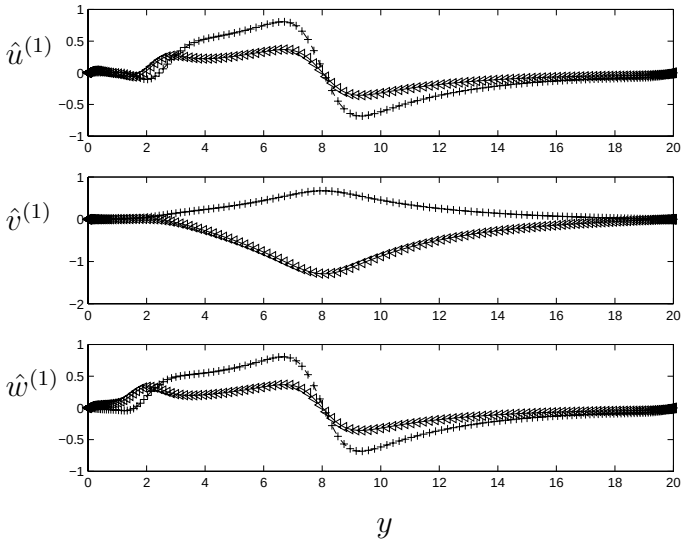

FIGURE 1. Velocity components of the linear perturbation velocity for the oblique wave with $(\alpha, \beta) = (0.2, 0.2)$. Forced problem for $Re = 400$, $y_\infty = 20$, $y_0 = 8$, $\sigma = 0.5$, $\omega = 0.2$ and $t = 100$. DNS result: $+$ real part, $\lhd$ imaginary part. Perturbation model: - - -, real part; ——, imaginary part .

3.2. *Comparison to DNS data: linear and non-linear case*

In order to validate the perturbation model and its capability to select the most effective interactions as a second order correction, we compare our results with direct numerical simulations of the forced evolution problem and an initial value problem. The DNS code, reported in Lundbladh *et al.* (1999), is used to solve the temporal problem for a parallel Blasius base flow. For a quantitative comparison we analyze the DNS results in terms of an amplitude expansion, so as to isolate the linear, quadratic and cubic part of the solution, see Henningson *et al.* (1993). We in fact run the same case with three different small amplitude disturbances. Different Fourier modes are then extracted and compared with the results obtained using the perturbation model.

We first consider the velocity field at early times, where the problem is governed by Eq. (23) and the initial value problem is solved as a superposition of the discretized eigenmodes. Comparisons of the three velocity component for the Fourier mode $(\alpha, \beta) = (0.2, 0.2)$ are shown in Fig. 1 at time $t = 100$. The good agreement confirms the validity of the discrete representation of the continuous spectrum.

With regards to the asymptotic time behavior, the numerical simulations are run to time $t = 50000$ and the response is compared with the perturbation results. Figure 2 depicts the velocity components associated to the mode

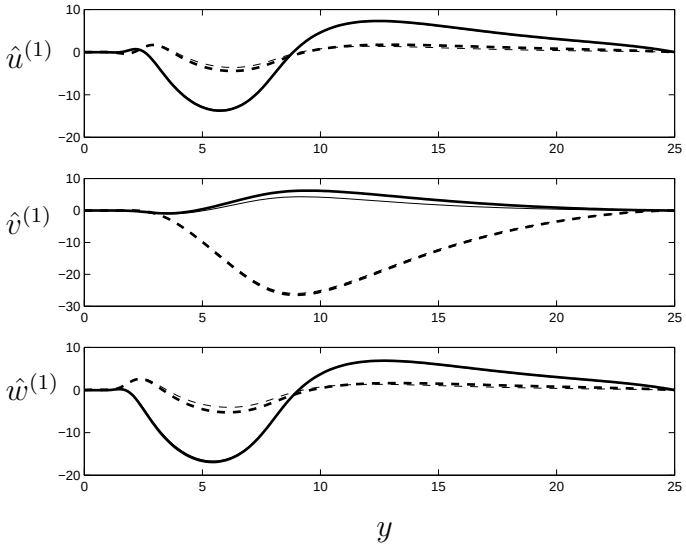

FIGURE 2. Velocity components of the linear perturbation velocity for the oblique wave with $(\alpha, \beta) = (0.2, 0.2)$. Forced problem for $Re = 400$, $y_\infty = 25$, $y_0 = 8$, $\sigma = 0.5$, $\omega = 0.2$ and $t = 50000$. DNS result: - - -, real part; ——, imaginary part (thick lines). Perturbation model: - - - real part; ——, imaginary part (thin lines).

$(\alpha, \beta) = (0.2, 0.2)$. The small differences observed in the figures are probably due to the accumulation of truncation errors in the DNS after such a long time integration. For the same problem, the second order correction with $(0, 2\beta)$ and $\omega = 0$ is displayed in Fig. 3. The formation of streamwise streaks in the longitudinal component is clearly seen. A similar result (not reported) is observed in the case of localized forcing inside the boundary layer ($y_0 = 2.2$, $\sigma = 0.4$). However, in the latter case, the streaks exhibit an amplitude smaller than the previous case (about one third).

Let us consider the transient part of the solution. The time evolution of the energy of the response of the forced problems corresponding to two different wave numbers ($(0.2, 0.2)$, $(1., 1.)$) and for the same values of y_0 and σ ($y_0 = 8$, $\sigma = 0.5$) is shown in Fig. 4. The figure shows that the energy of the high wave number disturbances attains its asymptotic value on a scale that is one order of magnitude less than the one associated to the short wave number (both for the first and the second order corrections).

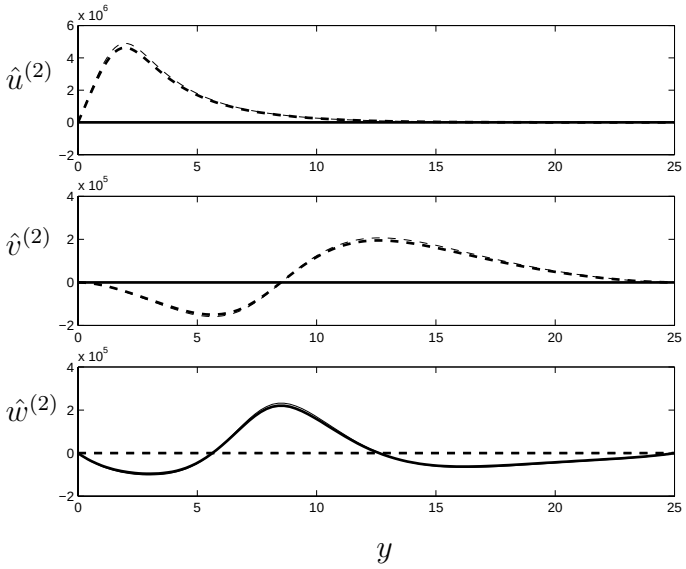

FIGURE 3. Velocity components of the second order perturbation velocity for $(\alpha, \beta) = (0, 0.4)$. Forced problem for $Re = 400$, $y_\infty = 25$, $y_0 = 8$, $\sigma = 0.5$ and $t = 50000$. DNS result: - - -, real part; ——, imaginary part (thick lines). Perturbation model: - - -, real part; ——, imaginary part (thin lines).

4. Role of Continuous Spectra in the Receptivity Mechanism

4.1. *Reynolds number scaling*

As shown in section 2.1, it is possible to prove that the resolvent, which governs the solution to the forced Orr-Sommerfeld, Squire system, is $O(Re^2)$. For the second problem we address, the forcing is given by non-linear interactions between continuous spectrum modes, and we analyze the forced solution at different values of the Reynolds number. In Fig. 5 we compare the continuous spectrum modes of the Orr-Sommerfeld operator for $\alpha = 1$, $\beta = 0.2$ and $\gamma = 0.628$ at two different Reynolds numbers ($Re = 300$ and $Re = 500$). We observe that the modes differ only at the edge of the boundary layer and these differences are small. Hence, we assume that the forcing term is Re independent. This assumption is confirmed for large Reynolds number by the findings of Jacobs & Durbin (1998), who have shown that the penetration depth of the modes is proportional to $(\alpha Re)^{-0.13}$ which implies that for large values of Re this depth becomes smaller and smaller.

In Fig. 6 we report the plot of the maximum of the streamwise second order velocity (normalized by the first order energy and by the square of Re) as a function of the streamwise and spanwise wave numbers for a given value of γ,

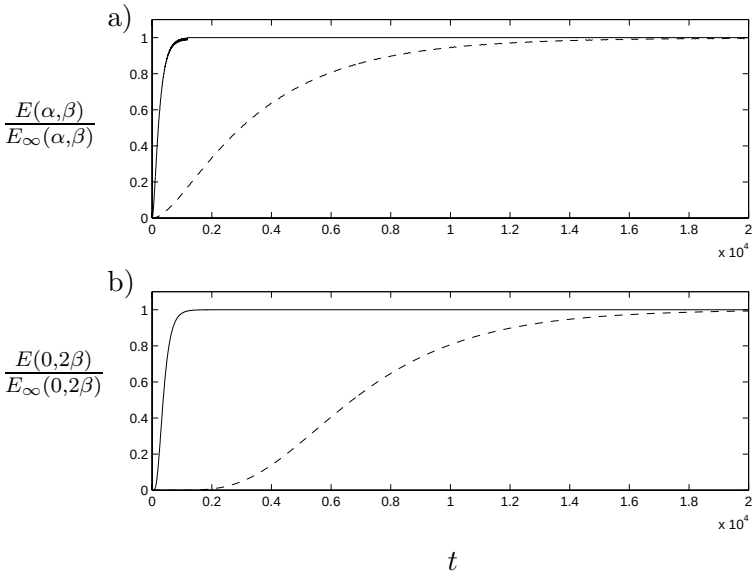

FIGURE 4. Time evolution of the energy normalized with respect to its asymptotic value. a) first order correction; b), second order correction; ——, $(\alpha, \beta) = (1, 1)$; - - - , $(\alpha, \beta) = (0.2, 0.2)$.

note that the second order distribution is displayed with reference to the (α, β) values of the corresponding first order terms. The figure clearly confirms the scaling in the energy norm found in section 2.1. The results show that the maximum amplitude is obtained for $\alpha \approx 2$ and $\beta \approx 0.15$. Further computations (not reported) verify the validity of the scaling down to $Re \approx 100$. However, for lower values of the Reynolds number the maximum response is obtained for values of β less than the one associated to $Re > 100$. Thus, it suffices to investigate the forced results only at one Reynolds number, since they can be subsequently scaled to arbitrary $Re > 100$.

4.2. *Non-linear interaction and linear forcing*

In a previous work it has been demonstrated that nonlinearities play a fundamental role in boundary layer receptivity, see Berlin & Henningson (1999). In the present work we use a model based on a perturbation expansion in the amplitude of the disturbance truncated at second order to single out the mechanisms at work during the generation of streamwise streaks in flat plate boundary layers subject to free-stream turbulence.

Since it is possible to rather well represent free-stream turbulence as a superposition of modes associated to the continuous spectrum, see for example Jacobs & Durbin (2000), we simplify the problem analyzing the weakly

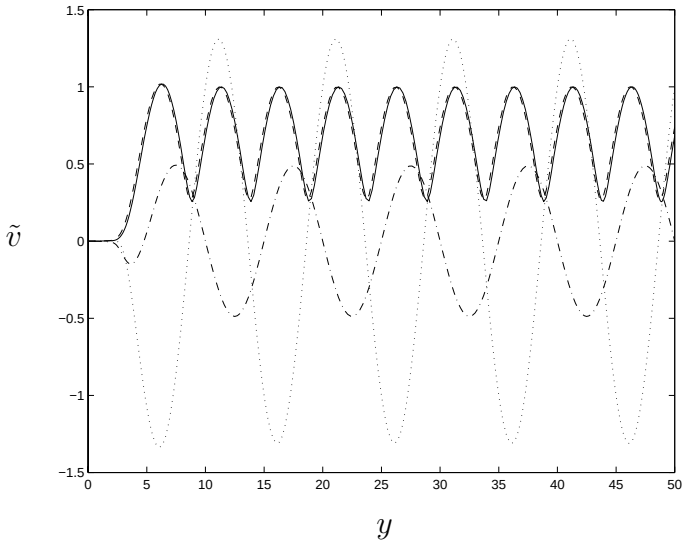

FIGURE 5. Distribution of the Orr-Sommerfeld eigenfunction *vs* y for $\alpha = 1$, $\beta = 0.2$: ——, $\|\tilde{v}\|$ for $Re = 500$; - - -, $\|\tilde{v}\|$ for $Re = 300$; $\cdots$, $Re(\tilde{v})$ for $Re = 300$; $\cdot$ - $\cdot$, $Im(\tilde{v})$ for $Re = 300$.

non-linear response of the system to a single pair of oblique continuous spectrum modes.

First we analyze the problem associated to the Orr-Sommerfeld continuous spectrum modes. The first order solution corresponds to two eigenmodes of the continuous spectrum with wave numbers (α, β, γ) and $(\alpha, -\beta, \gamma)$ whose damping rate is set to zero. At second order we account for the quadratic interactions between the two continuous spectrum modes and we focus our attention on the $(0, 2\beta)$ contribution. The transient part of the solution is neglected and the asymptotic time response is analyzed. We observe that the second order forcing to the $(0, 2\beta)$ modes induces strong streamwise vorticity, that in turn forces the formation of streaks inside the boundary layer by the linear lift-up mechanism. This two-step process, first the non-linear generation of streamwise vortices and then the linear forcing of the streamwise streaks, is completely captured by the weakly non-linear model. Figure 7 shows that the non-linear forcing of the Orr-Sommerfeld, Squire system (T_0^L, shown in Fig. 7(a)) induces second order spanwise and normal to wall velocities (see Fig. 7(b)). As a consequence, streamwise vorticity is produced which then creates streamwise streaks (see Fig. 7(c)) through the forcing of the Squire equation due to the coupling term (which is approximately ten times larger than the corresponding second order forcing, compare Figs. 7(a) and (d)).

The same analysis has been carried out also considering the second order forcing induced by Squire continuous spectrum modes. The results show that

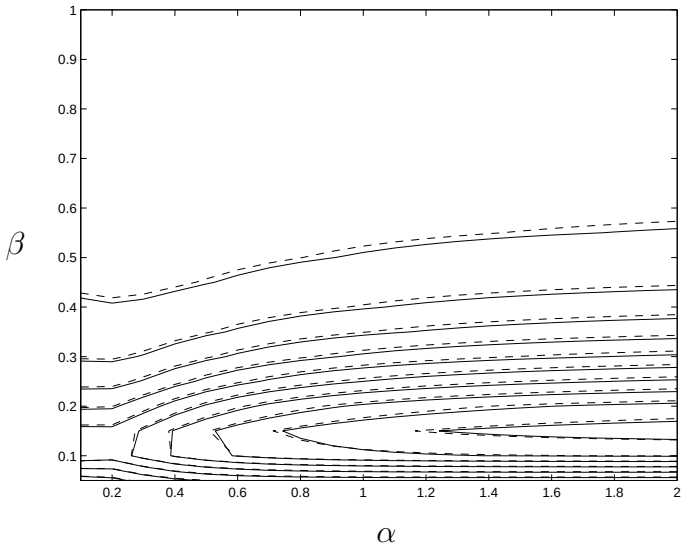

FIGURE 6. Forcing induced by Orr-Sommerfeld continuous spectrum modes for $\gamma = 0.27$. Contour levels of the maximum of the streamwise second order velocity (normalized by the first order energy and Re^2). Note that the second order distribution is displayed with reference to the (α, β) values of the corresponding first order terms. Maximum value 0.1056, contour spacing 0.011.

the same physical mechanism is induced and the amplitude of the generated streaks is comparable for the two different classes of modes.

4.3. *Parametric study*

In order to find the most effective interactions between continuous spectrum modes we carried out a parametric study varying the wave numbers in the range $0.1 < \alpha < 2$, $0.05 < \beta < 1$ and $0.25 < \gamma < 20.9$ at a given Reynolds number. In Figs. 8 and 9 we report, respectively, the results corresponding to forcing induced by Orr-Sommerfeld and Squire continuous spectrum modes. The figures depict the maximum amplifications of the streamwise velocity component normalized with respect to the energy density E of the non-linearly interacting modes. In particular, we plot

$$\begin{aligned} A(\alpha,\beta) &= max_\gamma \frac{u^{(2)}(\alpha,\beta,\gamma)}{E}, \\ B(\alpha,\gamma) &= max_\beta \frac{u^{(2)}(\alpha,\beta,\gamma)}{E}, \\ C(\beta,\gamma) &= max_\alpha \frac{u^{(2)}(\alpha,\beta,\gamma)}{E}. \end{aligned}$$

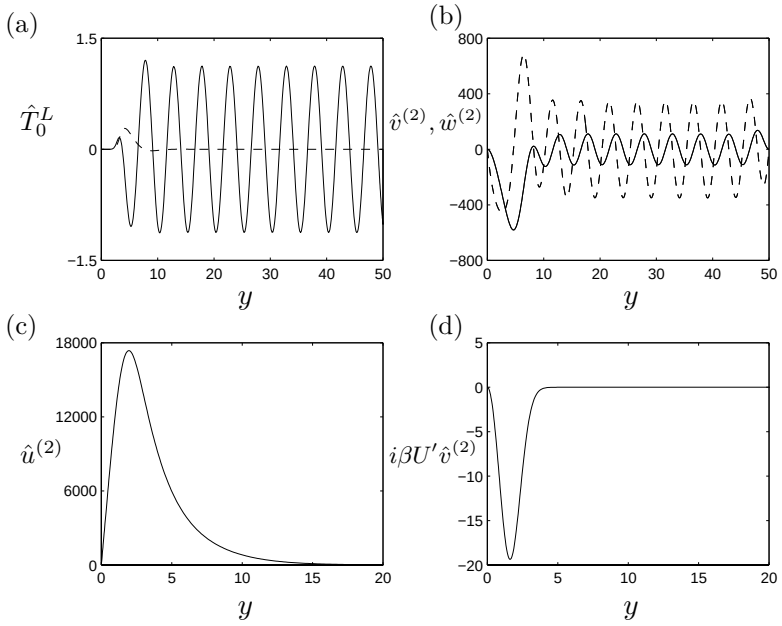

FIGURE 7. Second order solution corresponding to the nonlinear interactions of a couple of oblique Orr-Sommerfeld modes associated to the wave numbers $(0.5, \pm 0.2, 0.628)$, at $Re = 500$: (a) forcing to the Orr-Sommerfeld equation (——) and to the Squire equation (- - -); (b) normal to wall (——) and spanwise component of velocity (- - -); (c) streamwise component of velocity ; (d) forcing to the Squire equation associated to the coupling term $-i\,\beta\,U'\,v^{(2)}$.

The results show that the maximum amplification is attained for $\alpha \approx 2$ and $\beta \approx 0.15$ (thus implying that the streaks are associated to spanwise wave number $\beta \approx 0.3$) independently of the type of forcing modes. The results also indicate that the maximum response is associated to low values of γ ($\gamma \approx 0.25$), i.e. structures of large wall normal extent. We observe that in the case the forcing is given by the Orr–Sommerfeld modes we find a lower maximum for $\alpha \approx 0.1$, $\beta \approx 0.2$ and $\gamma \approx 1.25$.

One should also note that these figures tend to bias high wavenumbers, since they are in practice more damped than low ones. Recall in fact that for simplicity we have put the damping rate of the continuous spectrum modes to zero. This implies, for example, that the increasing amplification for higher values of α in Figs. 8 a), b) and 9 a), b) would be damped for sufficiently high values of the streamwise wavenumber. However this does not present a

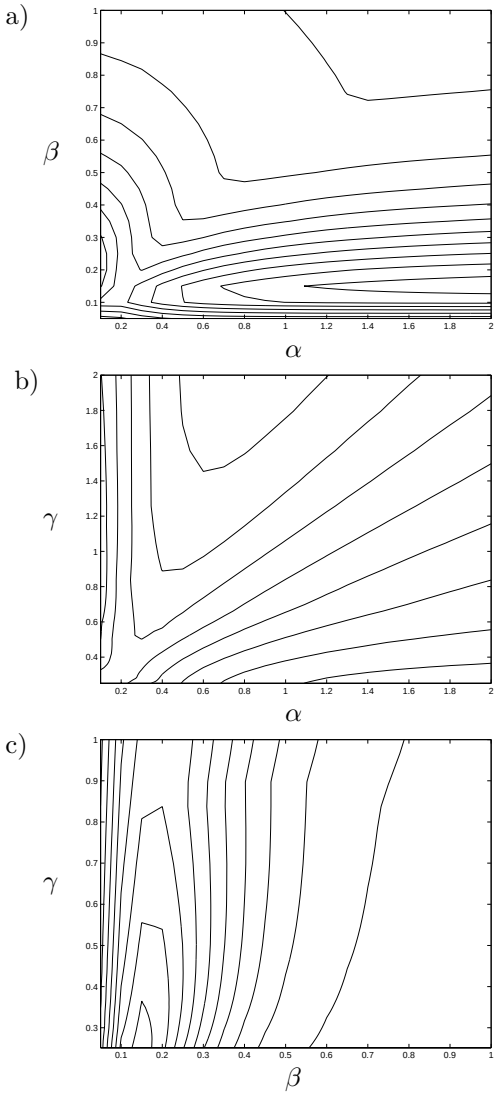

FIGURE 8. Boundary layer response to forcing induced by non-linear interactions of Orr-Sommerfeld modes. Contour levels of the maximum amplification of the streamwise component of velocity at $Re = 300$, $y_\infty = 50$: a) $A(\alpha, \beta)$ for $0.25 < \gamma < 20.9$; b) $B(\alpha, \gamma)$ for $0.05 < \beta < 1$; c) $C(\beta, \gamma)$ for $0.1 < \alpha < 2$. The maximum is 10145 and occurs at $\alpha = 2.$, $\beta = 0.15$, $\gamma = 0.25$. Maximum contour level is 9500 and contour spacing 1000.

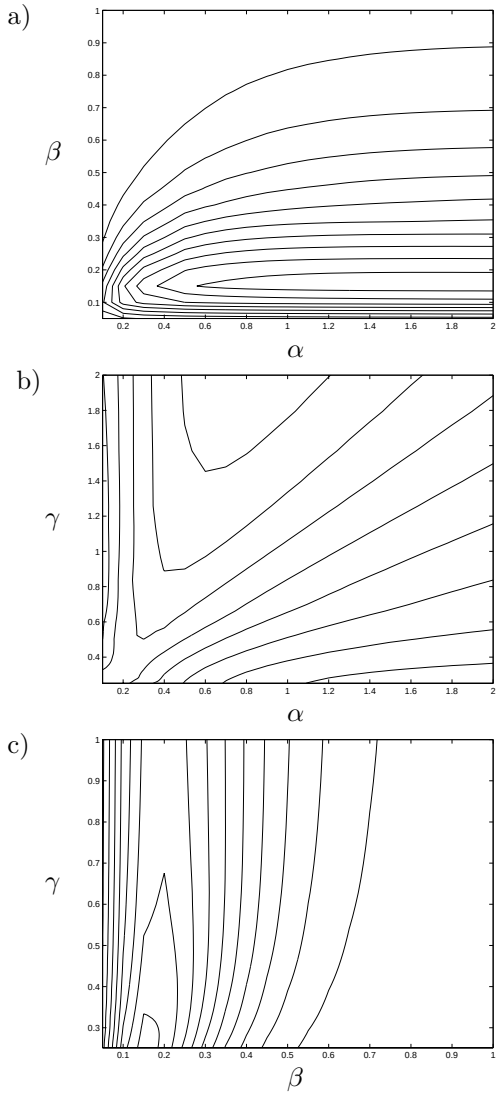

FIGURE 9. Boundary layer response to forcing induced by non-linear interactions of Squire modes. Contour levels of the maximum amplification of the streamwise component of velocity at $Re = 300$, $y_\infty = 50$: a) $A(\alpha, \beta)$ for $0.25 < \gamma < 20.9$; b) $B(\alpha, \gamma)$ for $0.05 < \beta < 1$; c) $C(\beta, \gamma)$ for $0.1 < \alpha < 2$. The maximum is 10586 and occurs at $\alpha = 2.$, $\beta = 0.15$, $\gamma = 0.25$. Maximum contour level is 10000 and contour spacing 1000.

problem in applying the results to a real free-stream turbulence case since realistic free-stream turbulence spectra have little energy content in these higher wavenumbers. This will be discussed in the next session.

4.4. *Filtering with turbulent energy spectrum and streak spacing*

In the results presented so far we assumed unit energy in each Fourier component of the free-stream disturbance. In order to predict which length scales may be important in a real transition initiated by free-stream turbulence, we associate each mode with a coefficient proportional to the energy spectrum of typical homogeneous and isotropic turbulence. We use here the von Kármán spectrum, which is proportional to κ^4 for large scales and matches the Kolmogorov-(5/3)-law for small scales. It has the form

$$E(\kappa) = \frac{2}{3}\,\frac{1.606(\kappa L)^4}{(1.35+(\kappa L)^2)^{17/6}} L\,q \tag{41}$$

where $\kappa = \alpha^2+\beta^2+\gamma^2$, L is an integral length scale and q is the total turbulent kinetic energy, defined as the integral over all κ's of the spectrum. The maximum of the energy is at $\kappa = 1.8/L$. We note that this spectrum, given in Tennekes & Lumley (1972) is a good approximation to homogeneous turbulence. The filtered results are reported in Figs. 10 and 11 for $L = 5$, $q = 1$; the figures show that the filtering moves the more effective α's and γ's to smaller values, while the β's are less affected. The maximum amplification is attained for $\alpha \approx 0.4$ for the case the forcing is given by the Orr-Sommerfeld modes and $\alpha \approx 0.3$ for the Squire case; the corresponding values of β and γ are respectively 0.15 and 0.25 independently of the type of the forcing modes. We note also that in the case the forcing is given by the Orr–Sommerfeld modes, a lower maximum is still present at $\alpha \approx 0.1$, $\beta \approx 0.15$ and $\gamma \approx 0.4$. Similar results were obtained for different choices of the integral length scale L.

The objective of the present work is to find the wavenumbers associated to free-steam disturbances which are most effective in the generations of streamwise vortices. Matsubara & Alfredsson (2001) in their experimental work observed that the spanwise distance to the first minimum of two point velocity correlations, which closely corresponds to half the streak spacing, stays almost constant in the downstream direction. This suggests that the boundary layer growth does not affect the streak development. When scaling these results with the local displacement thickness the characteristic length scale close to the leading edge is approximatively $20\delta^* \pm 10\delta^*$, i.e. centered around a spanwise wavenumber $\beta \approx 0.3$. This is close to the β's for which our simplified temporal model predicts the largest response. In the experiments of Matsubara & Alfredsson (2001) the growth of the boundary layer implies a variation of the spanwise scale with the respect to the local displacement thickness. In our model, we do not account for the growth of the boundary layer, but we are still able to predict the first step of the receptivity process, i.e. the formation of streamwise vortices.

5. Discussion and conclusion

In the present work we have investigated how free-stream disturbances affect a laminar boundary layer. In particular, we have analyzed the receptivity to

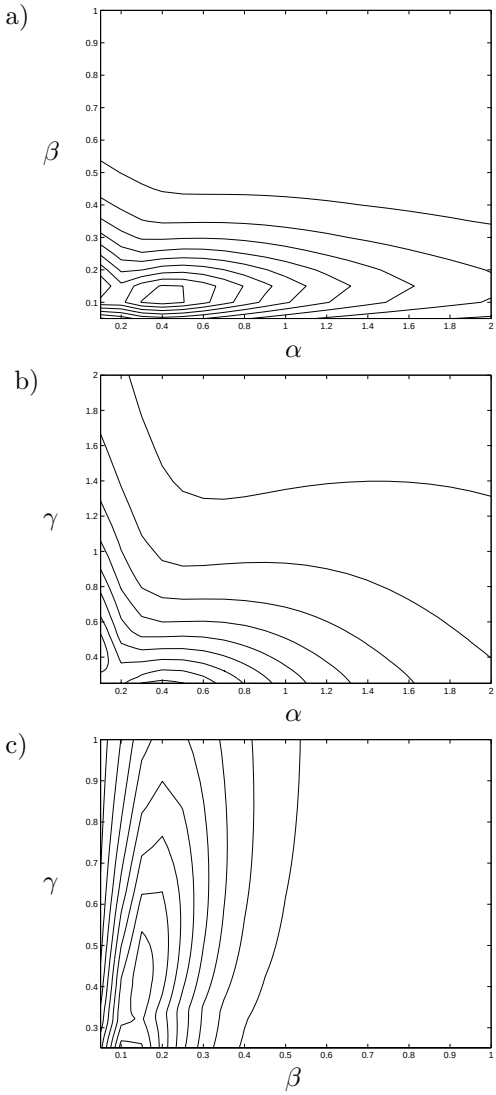

FIGURE 10. Boundary layer response to forcing induced by non-linear interactions of Orr-Sommerfeld modes filtered by turbulent kinetic energy spectrum. Contour levels of the maximum amplification of the streamwise component of velocity at $Re = 300$, $y_\infty = 50$: a) $A(\alpha, \beta)$ for $0.25 < \gamma < 20.9$; b) $B(\alpha, \gamma)$ for $0.05 < \beta < 1$; c) $C(\beta, \gamma)$ for $0.1 < \alpha < 2$. The maximum is 4554 and occurs at $\alpha = 0.4$, $\beta = 0.15$, $\gamma = 0.25$. Maximum contour level is 4500 and contour spacing 500.

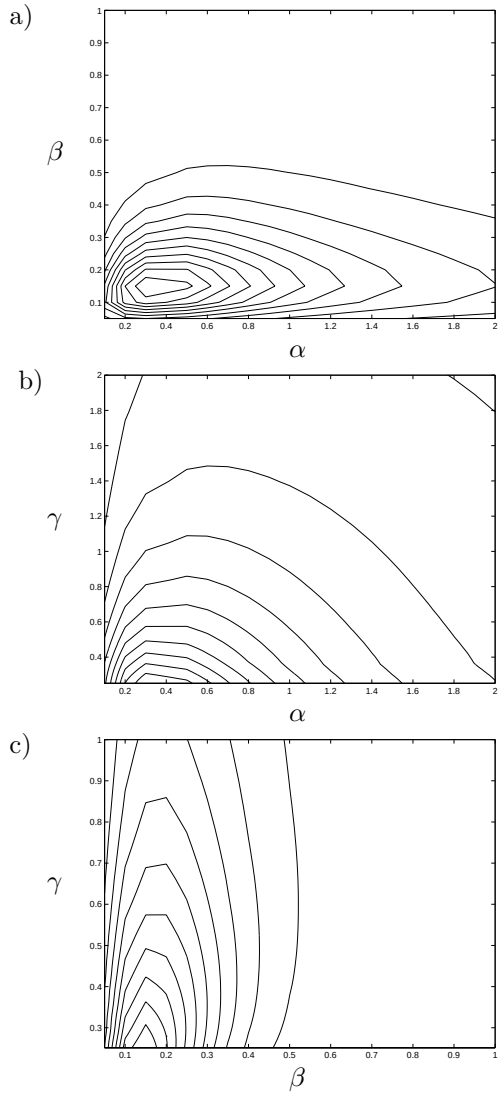

FIGURE 11. Boundary layer response to forcing induced by non-linear interactions of Squire modes filtered by turbulent kinetic energy spectrum. Contour levels of the maximum amplification of the streamwise component of velocity at $Re = 300$, $y_\infty = 50$: a) $A(\alpha, \beta)$ for $0.25 < \gamma < 20.9$; b) $B(\alpha, \gamma)$ for $0.05 < \beta < 1$; c) $C(\beta, \gamma)$ for $0.1 < \alpha < 2$. The maximum is 6273 and occurs at $\alpha = 0.3$, $\beta = 0.15$, $\gamma = 0.25$. Maximum contour level is 6000 and contour spacing 500.

oblique waves in the free-stream and to continuous spectrum modes. In both cases, we observe that the formation of streaks is the dominant feature. The underlying mechanism can be reduced to a two-step process, first the generation of streamwise vorticity and then the formation of streaks.

Previous investigators (Bertolotti 1997; Andersson *et al.* 1999; Luchini 2000) have considered the influence of streamwise vortices present in the free-stream and have shown that the subsequent formation of streaks in the boundary layer can be explained in terms of linear theory by the lift-up mechanism. The most important feature of the process we have investigated is that streamwise vortices are non-linearly generated starting from wave-like disturbances in the free-stream. This non-linear mechanism has already been observed in the numerical experiments of Berlin & Henningson (1999). They isolated the different order interactions to show that the streamwise independent modes are the most excited. Here, we have used a perturbation model which has been shown to provide an efficient theoretical tool to isolate the two-step process, see also Ponziani *et al.* (2000).

The model has been validated by comparisons with DNS data for the case the forcing is given by a couple of oblique waves. In order to apply the model to study the boundary layer receptivity to free-stream turbulence, we have exploited the fact that continuous spectrum modes can be used to represent the free-stream turbulence spectrum (Jacobs & Durbin 2000). This assumption has allowed us to further simplify the study accounting only for the response of the boundary layer to couples of continuous spectrum modes. An extensive parametric study has been carried out to isolate the most effective modes by varying the wave numbers (α, β, γ).

We have concluded that the formation of streaks is due to the second order correction induced by the coupling term in the Orr-Sommerfeld, Squire system and the receptivity is independent of the type of forcing modes. This indicates that disturbances containing normal velocity in the free-stream, are not more likely to force streamwise vorticity in the boundary layer, compared to disturbances not containing v. On the other hand, Berlin & Henningson (1999) draw the conclusion that the normal velocity in the free-stream is more effective than other components. However, their conclusion was based on a type of disturbance which grew in size in the normal direction as the normal velocity increased. Thus their results are also consistent with the present ones which show that this increase in amplification is rather a result of increase in normal scale (or decrease in γ).

The large eddy simulations of Yang & Voke (1993) also indicated the key influence of the wall normal component of the free-stream turbulence intensity in provoking transition. Their results show in fact that the transition process begins with the production of the Reynolds stresses due to the overlapping of regions of non zero fluctuating velocity v and mean shear $\partial U/\partial y$. From our analysis we find that the components with streamwise wave number approximately zero are the ones crucial in generating disturbances inside the

boundary layer, and that can be induced from non-linear interactions of either Orr-Sommerfeld or Squire modes. The capability of modes with frequency and streamwise wavenumber approximately zero to penetrate the shear layer has been demonstrated by different authors (see Westin *et al.* 1994; Jacobs & Durbin 1998; Matsubara & Alfredsson 2001; Hultgren & Gustavsson 1981), and we may thus conclude that v–components active in generating Reynolds stresses are the ones associated with nearly zero frequency and that they are the ones associated with the second order solution in our model.

The results also show that the second order forcing does not depend on the Reynolds number, thus recovering the $O(Re^2)$ scaling of the forced response described by streamwise independent disturbances governed by the Orr-Sommerfeld, Squire system. We may speculate on the implication of this scaling on the Reynolds number dependence of the forced response in the spatial problem. In a number of experiments it has been seen that the growth of the streak amplitude in boundary layers subjected to free-stream turbulence is proportional to Re, or equivalently that the energy growth is proportional to $Re_x \approx Re^2$ or downstream distance. If we assume that the Reynolds number dependence in the spatial case would be the same as in the temporal case investigated here, downstream growth of the streak amplitude predicted would be proportional to Re^2, i.e. over predicted by a factor of Re. However, the result found here assumes a continuous deterministic forcing. Real turbulence would better be described by a stochastic forcing in a number of wavenumbers. Bamieh & Dahleh (1999) have shown that a stochastic forcing reduces the scaling of the maximum response of the temporal problem from Re^2 to $Re^{3/2}$. This is still a factor $Re^{1/2}$ too large. However, the growth in a realistic free-stream turbulence case would probably further be reduced by the fact that free-stream turbulence decays with downstream distance. In our model this would correspond to a forcing which decreases with Re, thus further reducing the growth of the streak amplitude.

Acknowledgments

This research was supported by the Göran Gustavsson Foundation, TFR (Teknikvetenskapliga forskningsrådet), the C.M. Lerici Foundation and the research funding obtained by Prof. R. Piva, University of Rome "La Sapienza".

References

Andersson, P., Berggren, M. & Henningson, D. 1999. Optimal disturbances and bypass transition in boundary layers. *Phys. Fluids.* **11** (1), 134–150.

Bamieh, B. & Dahleh, M. 1999. Disturbance energy amplification in three-dimensional channel flows. In *Proceedings of the 1999 American Control Conference, IEEE, Piscataway, NJ*, pp. 4532–4537.

Berlin, S.& Henningson, D.S. 1999. A nonlinear mechanism for receptivity of free-stream disturbances *Phys. Fluids* **11** , (12), 3749–3760.

Bertolotti, F. P. 1997. Response of the Blasius boundary layer to free-stream vorticity. *Phys. Fluids.* **9** (8), 2286–2299.

Butler, K. M. & Farrell, B. F. 1992. Three-dimensional optimal perturbations in viscous shear flow. *Phys. Fluids A.* **4**, 1637–1650.

DiPrima, R. C. & Habetler, G. J. 1969. A completeness theorem for non-selfadjoint eigenvalue problems in hydrodynamic stability. *Arch. Rat. Mech. Anal.* **32**, 218–227.

Goldstein, M. E. & Hultgren, L. S. 1989. Boundary-layer receptivity to long-wave free-stream disturbances. *Ann. Rev. Fluid Mech.* **21**, 137–166.

Grosch, C. E. & Salwen, H. 1978. The continuous spectrum of the Orr-Sommerfeld equation. Part 1. The spectrum and the eigenfunctions. *J. Fluid Mech.* **87**, 33–54.

Gustavsson, L. H. 1991. Energy growth of three-dimensional disturbances in plane Poiseuille flow. *J. Fluid Mech.* **224**, 241–260.

Henningson, D.S., Lundbladh, A., Johansson, A.V. 1993. A mechanism for bypass transition from localized disturbances in wall-bounded shear flows *J. Fluid Mech.*, **250**, 169-207 .

Hultgren, L. S. & Gustavsson, L. H. 1981. Algebraic growth of disturbances in a laminar boundary layer *Phys. Fluids.* **24** (6), 1000–1004.

Jacobs, R. G. & Durbin, P. A. 1998. Shear sheltering and continuous spectrum of the Orr–Sommerfeld equation. *Phys. Fluids.* **10** (8), 2006–2011.

Jacobs, R. G. & Durbin, P. A. 2000. Bypass transition phenomena studied by computer simulation. Report No. TF-77, Flow Phisycs and Computation Division, Department of Mechanical Engineering, Stanford University, Stanford,California 2000.

Kendall, J. M., 1985. Experimental study of disturbances produced in a pre-transitional laminar boundary layer by weak free-stream turbulence. AIAA Paper 85-1695.

Kerschen, E. J. 1990. Boundary layer receptivity theory. *Appl Mech Rev.* **43** (5, Part 2), S152–157.

Klebanoff, P. S. 1971. Effect of free-stream turbulence on the laminar boundary layer. *Bull. Am. Phys. Soc.* **10**, 1323.

Kreiss, G., Lundbladh, A., Henningson, D. S. 1994. Bounds for threshold amplitudes in subcritical shear flows. *J. Fluid Mech.* **270**, 175–198.

Luchini, P. 2000. Reynolds number independent instability of the boundary layer over a flat surface: optimal perturbations. *J. Fluid Mech.*, **404**, 289–309.

Lundbladh, A., Berlin, S., Skote, M., Hildings, C., Choi, J., Kim, J., Henningson, D. S. 1999. An efficient Spectral Method for Simulation of Incompressible Flow over a Flat Plate TRITA-MEK, Technical Report 1999.11, Royal Institute of Technology, Stockholm,1999.

Matsubara, M., Alfredsson, P.H. 2001. Disturbance growth in boundary layers subjected to free stream turbulence *J. Fluid Mech.*, (In press).

Ponziani, D. 2000. A weakly nonlinear analysis for transition mechanisms in Poiseuille flow *PhD Thesis*, University of Rome, La Sapienza.

Ponziani, D., Casciola, C.M., Zirilli, F., Piva, R. 2000. Weakly nonlinear analysis of a localized disturbance in Poiseuille flow *Stud. Appl. Math.,* **105**, 121-142.

Reddy, S. C. & Henningson, D. S. 1993. Energy growth in viscous channel flows. *J. Fluid Mech.* **252**, 209–238.

Salwen, H. & Grosch, C. E. 1981. The continuous spectrum of the Orr-Sommerfeld equation. Part 2. Eigenfunction expansions. *J. Fluid Mech.* **104**, 445–465.

Schmid, P. J. & Henningson, D.S. 2001. Stability and Transition in Shear Flows. *Springer*.

Tennekes, H. & Lumley, J. L. 1972. A first course in turbulence. *The MIT press*.

Trefethen, L. N., Trefethen, A. E., Reddy, S. C. & Driscoll, T. A. 1993. Hydrodynamic stability without eigenvalues. *Science*. **261**, 578–584.

Westin, K. J. A., Boiko, A. V., Klingmann, B. G. B., Kozlov, V. V. & Alfredsson, P. H. 1994. Experiments in a boundary layer subject to free-stream turbulence. Part I: Boundary layer structure and receptivity. *J. Fluid Mech.* **281**, 193–218.

Yang, Z. Y. & Voke, P. R. 1993. Large eddy simulation of transition under turbulence. *Technical report ME-FD/93.12*, University of Surrey, Dept. Mech. Eng.

Paper 2

2

On the breakdown of boundary layer streaks

By Paul Andersson[†‡], Luca Brandt[†], Alessandro Bottaro[⋆] and Dan S. Henningson[†‡]

[†]Department of Mechanics, Royal Institute of Technology (KTH), S-100 44 Stockholm, Sweden
[‡]FFA, the Aeronautical Research Institte of Sweden, P.O. Box 11021, S–161 11 Bromma, SWEDEN
[⋆]Institut de Mécanique des Fluides de Toulouse (IMFT), Université Paul Sabatier, 118 route de Narbonne, 31062 Toulouse Cedex 4, France

A scenario of transition to turbulence likely to occur during the development of natural disturbances in a flat-plate boundary layer is studied. The perturbations at the leading edge of the flat plate that show the highest potential for transient energy amplification consist of streamwise aligned vortices. Due to the lift-up mechanism these optimal disturbances lead to elongated streamwise streaks downstream, with significant spanwise modulation. Direct numerical simulations are used to follow the nonlinear evolution of these streaks and to verify secondary instability calculations. The theory is based on a linear Floquet expansion and focuses on the temporal, inviscid instability of these flow structures. The procedure requires integration in the complex plane, in the coordinate direction normal to the wall, to properly identify neutral modes belonging to the discrete spectrum. The streak critical amplitude, beyond which streamwise travelling waves are excited, is about 26% of the free-stream velocity. The sinuous instability mode (either the fundamental or the subharmonic, depending on the streak amplitude) represents the most dangerous disturbance. Varicose waves are more stable, and are characterized by a critical amplitude of about 37%. Stability calculations of streamwise streaks employing the shape assumption, carried out in a parallel investigation, are compared to the results obtained here using the nonlinearly modified mean fields; the need to consider a base flow which includes mean flow modification and harmonics of the fundamental streak is clearly demonstrated.

1. Introduction

1.1. *"Lift-up" effect and transient growth*

For quite a long time the fluid mechanics community has recognized transition to turbulence as a fundamental problem and has directed intense research efforts toward its understanding. Even so, our current picture of the physical

processes involved is far from complete. The classical starting point for theoretical investigations of transition is linear stability theory. Here, exponentially growing solutions—in time or space—to the linearised Navier–Stokes equations are sought. If such solutions are not found, the flow is predicted by the theory to be stable. However, experiments show that the route to turbulence is highly dependent on the initial conditions and on the continuous forcing that background noise can provide (see for example Morkovin & Reshotko 1990; Reshotko 1994, for reviews).

Experiments reveal that many flows, including for example Poiseuille and boundary layer flows, may undergo transition to turbulence for Reynolds numbers well below the critical ones from the linear stability theory. For the case of plane Couette flow the theory predicts stability at all Reynolds numbers (Romanov 1973) while numerical and laboratory experiments point to a finite transitional value (Lundbladh & Johansson 1991; Tillmark & Alfredsson 1992; Dauchot & Daviaud 1995).

The reason for this discrepancy between the theory and the experiments has been sought in the nonlinear terms of the Navier–Stokes equations. Examples of nonlinear theories are given by Orszag & Patera (1983), Bayly, Orszag & Herbert (1988) and Herbert (1988). However, examining the Reynolds–Orr equation (Drazin & Reid 1981) a remarkably strong statement can be made on the nonlinear effects: the nonlinear terms redistribute energy among disturbance frequencies but have no net effect on the instantaneous growth rate of the energy. This implies that there must exist a linear growth mechanism for the energy of a disturbance of any amplitude to increase (Henningson & Reddy 1994; Henningson 1996). The apparent need for an alternative growth mechanism based on the linearized equations has recently led to intense re-examination of the classical linear stability theory.

The first convincing alternative was proposed by Ellingsen & Palm (1975). By introducing an infinitesimal disturbance without streamwise variation in a shear layer, they showed that the streamwise velocity component can increase linearly with time, within the inviscid approximation, producing alternating low– and high–velocity streaks in the streamwise velocity component. Landahl (1975,1980) extended this result to the linear evolution of localized disturbances and supplied the physical insight to the linear growth mechanism with what he denoted the *lift-up* effect. He argued that vortices aligned in the streamwise direction advect the mean velocity gradient towards and away from the wall, generating spanwise inhomogeneities.

It is now clear that since the linearized Navier–Stokes operator is non-normal for many flow cases (especially in shear flows) a significant transient growth of a given perturbation might occur, before the subsequent exponential behaviour. Such an algebraic growth involves non-modal perturbations and can exist for subcritical values of the governing parameters.

Indeed, early investigators of the lift-up and transient growth mechanisms found considerable linear energy amplification before the viscous decay (Hultgren & Gustavsson 1981; Boberg & Brosa 1988; Gustavsson 1991; Butler & Farrell 1992; Reddy & Henningson 1993; Henningson, Lundbladh & Johansson 1993). An overview of recent work can be found in the review articles by Trefethen *et al.* (1993) and Henningson (1995). The initial disturbance that yields the maximum spatial transient growth in a non-parallel flat plate boundary layer flow was determined independently by Andersson, Berggren & Henningson (1999a) and Luchini (2000) to consist of vortices aligned in the streamwise direction. These vortices leave an almost permanent scar in the boundary layer in the form of long-lived, elongated streaks of alternating low and high streamwise speed.

1.2. *"Secondary" instability of streamwise streaks*

If the amplitude of the streaks grows to a sufficiently large value, instabilities can develop which may provoke early breakdown and transition, despite the theoretically predicted modal decay. In the remainder of the paper we will refer to the instability of the streak as a "secondary" instability, to differentiate it from the "primary" growth mechanism responsible for the formation of these flow structures. A (secondary) instability can be induced by the presence of inflection points in the base flow velocity profile, a mechanism which does not rely on the presence of viscosity. Controlled experiments on the breakdown of periodically arranged (along the span) streaks produced by an array of roughness elements have been conducted by Bakchinov *et al.* (1995). It was shown that the instability of the streaks causes transition in a similar manner as do the Görtler and cross-flow cases, i.e. via amplification of the secondary wave up to a stage where higher harmonics are generated, and on to a destruction of the spanwise coherence of the boundary layer. Alfredsson & Matsubara (1996) considered the case of transition induced by streaks formed by the passage of the fluid through the screens of the wind-tunnel settling chamber. They report on the presence of a high frequency "wiggle" of the streak with a subsequent breakdown into a turbulent spot.

Today, the description of the *establishment* of steady streaky structures is well captured by the theory. The work presented here aims at understanding the instability of these streaks on the path to boundary layer turbulence. Parenthetically, we note also that streamwise vortices and streaks are an essential ingredient of the near–wall turbulent boundary layer and that the instability of streaky structures is one crucial feature of the near-wall cycle which is thought to lie at the heart of the genesis and dynamics of turbulent coherent structures (Jimenez & Pinelli 1999; Schoppa & Hussain 1997, 1998).

Some work has recently appeared in the literature on the instability of streaks in channel flows (Waleffe 1995, 1997; Reddy *et al.* 1998) and, among the findings reported, it is interesting to note that slip and no-slip boundaries do not display significant differences in the instability scenario (Waleffe 1997).

The present study focuses on the linear, inviscid breakdown of boundary layer streaks. It is believed that the inviscid approximation captures the essential features of the breakdown. This is supported primarily by the controlled experiments of Bakchinov *et al.* (1995), who demonstrate unambiguously the role of the critical layer in the development of the instability. The measurements conducted by Boiko *et al.* (1997) on the instability of a vortex in a boundary layer and the very carefully controlled experiments on the breakdown of streaks in channel flow conducted by Elofsson, Kawakami & Alfredsson (1999) further attest to the inflectional nature of the breakdown. The latter authors generated elongated streamwise streaky structures by applying wall suction, and triggered a secondary instability by the use of earphones. The growth rate of the secondary instability modes was unaffected by a change of the Reynolds number of their flow, over a subcritical range, and the regions of (sinuous-type) oscillations of the streaks in cross-stream planes were reasonably well correlated to the spanwise shear of the main flow. The numerical/theoretical comparative viscous-inviscid investigations on the linear breakdown of longitudinal vortices in a curved channel (Randriarifara 1998) and the numerous studies on the secondary instability of Görtler vortices (Hall & Horseman 1991; Yu & Liu 1991; Bottaro & Klingmann 1996), show that the inviscid approach captures correctly the dominant features of the instability with viscosity playing mainly a damping role. These secondary instability studies bear a close resemblance to the present one.

1.3. *Mean field with optimal streaks and linear stability analysis*

The equations governing the streak evolution are obtained by applying the boundary layer approximations to the three-dimensional steady incompressible Navier-Stokes equations and linearizing around the Blasius base flow. After defining the disturbance energy density as the integral, in the wall-normal direction, of the square of the disturbance velocity components, techniques commonly employed when solving optimal control problems are used to determine the optimal disturbance (streamwise oriented vortices) and its downstream response (streamwise streak). The output streak predicted by the theory of Andersson *et al.* (1999a) and Luchini (2000) is remarkably similar to that measured in the laboratory (see figure 1). The measurements were performed in a pre-transitional flat plate boundary layer, where the largest amplitude of the streamwise velocity was eleven percent of the free-stream velocity. The streak is, in fact, a "pseudo-mode" triggered in a flat-plate boundary layer subject to significant outside disturbances.

The instability of these optimal streaks is studied here with different levels of approximation. Two different representations are used for the mean field: the simpler shape assumption, where the shape of the streak obtained from the linearized equations is considered unmodified even at large amplitudes, and the complete nonlinear development of the streak.

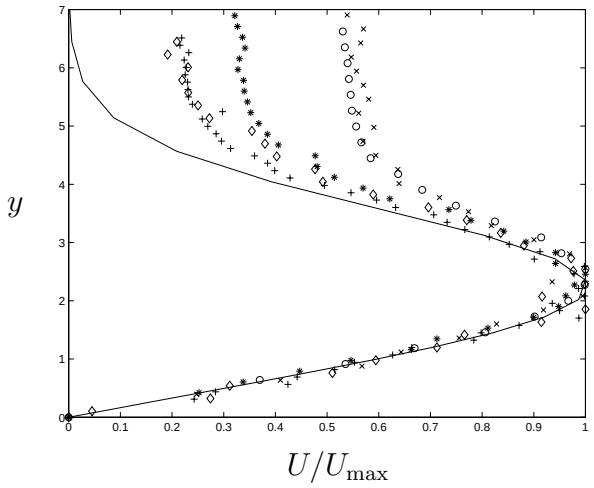

FIGURE 1. Comparison between the streamwise velocity component of the downstream response to an optimal perturbation, and the u-r.m.s. data in a flat-plate boundary layer subject to free-stream turbulence (——, Reynolds-number-independent theory). The symbols represent experiments from Westin *et al.* (1994) (∘, Re_δ=203; +, Re_δ=233; ×, Re_δ=305; ⋆, Re_δ=416; ⋄, Re_δ=517). Here y has been made non-dimensional—and the Reynolds number is defined—using the Blasius length scale $\delta = (L\nu/U_\infty)^{1/2}$.

In both formulations the linear secondary stability calculation are carried out on the basis of the boundary layer approximation, i.e. the mean field to leading order will consist only of the streamwise velocity component (here denoted U), consistent with the scaling hypothesis which led to the definition of the streak. Such a mean field varies on a slow streamwise scale, whereas the secondary instability varies rapidly in the streamwise direction x, as observed in the visualisations by Alfredsson & Matsubara (1996). Hence, our leading order stability problem is the parallel flow problem, with perturbation mode shapes dependent only on the cross-stream coordinates y (wall-normal) and z (spanwise). The same approximation was made previously for the case of the Görtler flow (Hall & Horseman 1991; Yu & Liu 1991; Bottaro & Klingmann 1996).

Due to the spanwise periodicity of the base flow—consisting of streamwise aligned streaks superimposed on a flat-plate Blasius flow—a temporal Floquet analysis is employed with the objective of determining which disturbance pattern shows the highest potential for temporal growth. In particular we are interested in determining if the maximum disturbance growth occurs for a sinuous or a varicose disturbance, and whether it is of fundamental or subharmonic

type. In addition, the critical threshold amplitude of the streak for the onset of the secondary instability is determined.

In § 2 the two-dimensional eigenvalue problem arising from the governing partial differential equation is formulated and the numerical methods adopted are described. In § 3 a scaling property of the mean field calculated by nonlinear simulations is introduced; this property allows a reduced number of simulations to cover a wide range of spanwise scales of the disturbance. Numerical experiments on streak instability are also carried out using DNS and the results are compared with the linear stability calculations. In § 4 a parametric study of the sinuous modes is presented and some comparisons with the shape assumption calculations are discussed. The main conclusions of the work are summarized in § 5.

2. Governing Equations and Numerical Methods

2.1. *Inviscid stability equations*

The dimensionless, incompressible Euler equations linearized around the mean field $(U(y,z),\,0,\,0)$ are

$$u_x + v_y + w_z = 0, \tag{1}$$
$$u_t + Uu_x + U_y v + U_z w = -p_x, \tag{2}$$
$$v_t + Uv_x = -p_y, \tag{3}$$
$$w_t + Uw_x = -p_z, \tag{4}$$

and the system is closed by slip boundary conditions at the solid wall and by decaying disturbances in the free stream;

$$(u,v,w) = (u(x,y,z,t), v(x,y,z,t), w(x,y,z,t))$$

are the perturbation velocities in the streamwise, wall-normal and spanwise directions, respectively, t is time and $p = p(x,y,z,t)$ is the disturbance pressure. All velocities have been scaled with the free-stream speed U_∞ and the pressure with ρU_∞^2, where ρ is the fluid density. The length scale is $\delta = (L\nu/U_\infty)^{1/2}$, with ν kinematic viscosity and L distance from the leading edge. For later use we define two Reynolds numbers using the two different length scales, $Re_\delta = U_\infty\delta/\nu$ and $Re = U_\infty L/\nu$, which relate as $Re = Re_\delta^2$.

The presence of both wall-normal and spanwise gradients in the mean field makes it impossible to obtain an uncoupled equation for either of the velocity components. It is, however, possible to find an uncoupled equation for the pressure by taking the divergence of the momentum equations, introducing continuity and then applying equations (3) and (4) (Henningson 1987; Hall & Horseman 1991). These manipulations yield

$$(\frac{\partial}{\partial t} + U\frac{\partial}{\partial x})\Delta p - 2U_y p_{xy} - 2U_z p_{xz} = 0. \tag{5}$$

We consider perturbation quantities consisting of a single wave component in the streamwise direction, i.e.

$$p(x,y,z,t) = Real\{\tilde{p}(y,z)e^{i\alpha(x-ct)}\},$$

where α is the (real) streamwise wavenumber and $c = c_r + ic_i$ is the phase speed. The equation governing the pressure reduces to

$$(U-c)(\frac{\partial^2}{\partial y^2} + \frac{\partial^2}{\partial z^2} - \alpha^2)\tilde{p} - 2U_y\tilde{p}_y - 2U_z\tilde{p}_z = 0; \tag{6}$$

this constitutes a generalized eigenproblem with c in the role of eigenvalue and needs to be solved for given mean field and streamwise wavenumber. Once the pressure eigenfunctions are computed, the velocity components can be obtained from the explicit expressions

$$i\alpha(U-c)\tilde{v} = -\tilde{p}_y, \tag{7}$$
$$i\alpha(U-c)\tilde{w} = -\tilde{p}_z, \tag{8}$$
$$i\alpha(U-c)\tilde{u} + U_y\tilde{v} + U_z\tilde{w} = -i\alpha\tilde{p}. \tag{9}$$

The pressure component $\tilde{p}$ is expanded in an infinite sum of Fourier modes

$$\tilde{p}(y,z) = \sum_{k=-\infty}^{\infty} \hat{p}_k(y)e^{i(k+\gamma)\beta z}, \tag{10}$$

where β is the spanwise wavenumber of the primary disturbance field and γ is the (real) Floquet exponent. We note two symmetries: first, to within renumbering of the Fourier coefficients γ and $\gamma \pm n$ yield identical modes for any integer n, and second, equation (6) is even under the reflection $z \to -z$. These symmetries make it sufficient to study values of γ between zero and one half, with $\gamma = 0$ corresponding to a *fundamental* instability mode, and $\gamma = 0.5$ corresponding to a *subharmonic* mode (see Herbert 1988 for a thorough discussion on fundamental and detuned instability modes). The mean field is also expanded as a sum of Fourier modes

$$U(y,z) = \sum_{k=-\infty}^{\infty} U_k(y)e^{ik\beta z} \tag{11}$$

and these expansions are introduced into equation (6) to yield an equation that holds for each integer k:

$$\sum_{j=-\infty}^{\infty}\left(U_{k-j}\left[\frac{\partial^2}{\partial y^2} - \beta^2(j+\gamma)^2 - \alpha^2\right] - 2\frac{\partial U_{k-j}}{\partial y}\frac{\partial}{\partial y} + 2\beta^2(k-j)(j+\gamma)U_{k-j}\right)\hat{p}_j$$
$$= c\left[\frac{\partial^2}{\partial y^2} - \beta^2(k+\gamma)^2 - \alpha^2\right]\hat{p}_k. \tag{12}$$

The appropriate boundary conditions are:

$$\frac{\partial\hat{p}_k}{\partial y} = 0 \text{ at } y = 0 \text{ and } \frac{\partial\hat{p}_k}{\partial y} \to 0 \text{ when } y \to \infty. \tag{13}$$

This problem consists of an infinite number of coupled ordinary differential equations which must be truncated in order to find a numerical solution. The complete system must be solved numerically, when the solution is sought for an arbitrary value of the detuning parameter γ. If, however, even and odd solutions in z are sought, the system of equations can be simplified for the fundamental and subharmonic modes. In this case the numerical effort is decreased considerably because the dimension of the matrices arising from the discretisation is halved.

In the fundamental ($\gamma = 0$) case, even (odd) modes are obtained by imposing the condition $\hat{p}_{-k} = \hat{p}_k$ ($\hat{p}_{-k} = -\hat{p}_k$). This is equivalent to introducing either a cosine or a sine expansion

$$\tilde{p}(y,z) = \sum_{k=0}^{\infty} \hat{p}_k(y)\cos(k\beta z), \tag{14}$$

$$\tilde{p}(y,z) = \sum_{k=1}^{\infty} \hat{p}_k(y)\sin(k\beta z), \tag{15}$$

into equation (6), to yield two different systems of ODE's.

In the case of subharmonic disturbances ($\gamma = 0.5$) the spanwise periodicity of the fluctuations is twice that of the base flow. The subharmonic mode also contains a symmetry which renders the decoupling into even and odd modes possible. In this case the cosine and sine expansions are:

$$\tilde{p}(y,z) = \sum_{k=0}^{\infty} \hat{p}_k(y)\cos(\frac{2k+1}{2}\beta z), \tag{16}$$

$$\tilde{p}(y,z) = \sum_{k=0}^{\infty} \hat{p}_k(y)\sin(\frac{2k+1}{2}\beta z). \tag{17}$$

These two expansions produce two new systems of ODE's which clearly yield two different classes of solutions, as in the case of the fundamental modes. Notice, however, that the sinuous fluctuations of the low-speed streaks, represented in the fundamental case by the sine expansion (15) are given, in the subharmonic case, by the cosine expansion (16). This is because the subharmonic sinuous case treats two streaks, which oscillate out of phase (cf Le Cunff & Bottaro 1993). Likewise, varicose oscillations of the low-speed streaks are represented by the cosine series (14) for the fundamental mode, and by the sine expansion (17) in the case of subharmonic perturbations.

For the sake of clarity, in the remainder of the paper only the definitions of *sinuous* or *varicose* modes of instability will be employed, with reference to the visual appearance of the motion of the *low-speed streaks*. A sketch of the different fundamental and subharmonic modes is provided in figure 2: it clearly illustrates how in the subharmonic cases sinuous (varicose) fluctuations of the low-speed streaks are always associated with staggered (in x) varicose (sinuous) oscillations of the high-speed streaks.

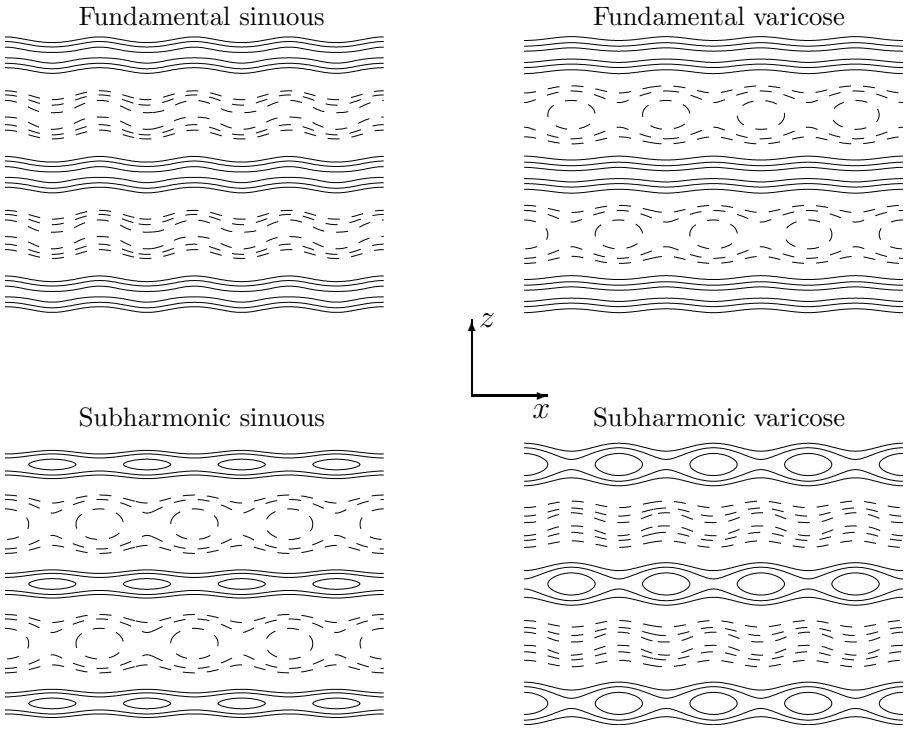

FIGURE 2. Sketch of streak instability modes in the $(x-z)$-plane over four streamwise and two spanwise periods, by contours of the streamwise velocity. The low-speed streaks are drawn with solid lines while dashed lines are used for the high-speed streaks.

2.2. *Chebyshev polynomials in real space*

The temporal eigenvalue system derived in section 2 is solved numerically using a spectral collocation method based on Chebyshev polynomials. Consider the truncated Chebyshev expansion

$$\phi(\eta) = \sum_{n=0}^{N} \bar{\phi}^n T_n(\eta),$$

where

$$T_n(\eta) = \cos(n \cos^{-1}(\eta)) \tag{18}$$

is the Chebyshev polynomial of degree n defined in the interval $-1 \leq \eta \leq 1$. We use

$$\eta_j = \cos\frac{\pi j}{N}, \qquad j = 0, 1, \ldots, N,$$

as collocation points, that is, the extrema of the Nth-order Chebyshev polynomial T_N plus the endpoints of the interval.

The calculations are performed using 121 (N=120) Chebyshev collocation points in y, and with the Fourier series in z truncated after fifteen modes. The wall-normal domain varies in the range $(0, y_{\max})$, with $y_{\max}$ well outside the boundary layer (typically $y_{\max}$ is taken equal to 50). The Chebyshev interval $-1 \leq \eta \leq 1$ is transformed to the computational domain $0 \leq y \leq y_{\max}$ by the use of the conformal mapping

$$y = a\frac{1+\eta}{b-\eta}, \tag{19}$$

where

$$a = \frac{y_i\, y_{\max}}{y_{\max} - 2y_i} \quad \text{and} \quad b = 1 + \frac{2a}{y_{\max}}.$$

This mapping puts half the grid points in the region $0 \leq y \leq y_i$, with y_i chosen to be equal to 8.

The unknown functions $\hat{p}_k = \hat{p}_k(y)$ may now be approximated by

$$\hat{p}_k^N(y) = \sum_{n=0}^{N} \bar{p}_k^n \tilde{T}_n(y),$$

where $\tilde{T}_n(y) = T_n(\eta)$ with $\eta \mapsto y$ being the mapping (19). The Chebyshev coefficients $\bar{p}_k^n$, $n = 0, \ldots, N$ are determined by requiring equation (12) to hold for $\hat{p}_k^N$ at the collocation points y_j, $j = 1, \ldots, N-1$. The boundary conditions (13) are enforced by adding the equations

$$\sum_{n=0}^{N} \bar{p}_k^n \tilde{T}_{n,y}(0) = \sum_{n=0}^{N} \bar{p}_k^n \tilde{T}_{n,y}(y_{\max}) = 0,$$

where subscript n, y denotes the y-derivative of the n-th Chebyshev polynomial.

2.3. *Chebyshev polynomials in complex space*

The discretization leads to a generalized eigenproblem with the two matrices containing only real elements; hence, the solutions will consist of either real eigenvalues or complex conjugate pairs. No strictly damped solutions can be found using these equations together with an integration path running along the real y-axis from 0 to y_{max}, since the neglect of viscosity introduces a continuous spectrum of singular neutral modes. Lin (1944) performed an asymptotic analysis on the Orr–Sommerfeld equation, requiring the inviscid eigenvalue problem (the Rayleigh equation) to be a limit of the viscous one when the Reynolds number approaches infinity. For this to apply, he found that the integration path in the inviscid case could be taken on the real axis if $c_i > 0$

and that it should be taken in the complex plane for $c_i \leq 0$, in such a way that the singularities lie on the same side of the integration path as in the $c_i > 0$ case.

Information on the singularities is contained in the system's determinant. We are satisfied here with the approximate location of the singularities and to simplify the analysis the mean field with the shape assumption is considered, i.e.

$$U(y,z) = U_B(y) + \frac{A_s}{2}u_s(y;\beta)e^{i\beta z} + \frac{A_s}{2}u_s(y;\beta)e^{-i\beta z}, \tag{20}$$

with U_B the Blasius solution, u_s the streak's mode shape provided by the analysis of Andersson *et al.* (1999a) and scaled so that $\max[u_s(y;\beta)] = 1$, A_s the amplitude of the streak and β the spanwise wavenumber. Figure 1 show the streak's mode shape u_s. Introducing expansion (20) into equation (12) yields an equation that holds for each integer k:

$$\begin{aligned}
&\frac{A_s}{2}u_s(\frac{\partial^2}{\partial y^2} - \beta^2(k-1+\gamma)(k-3+\gamma) - \alpha^2)\hat{p}_{k-1} - A_s u_{s,y}\frac{\partial}{\partial y}\hat{p}_{k-1} + \\
&(U_B - c)(\frac{\partial^2}{\partial y^2} - \beta^2(k+\gamma)^2 - \alpha^2)\hat{p}_k - 2U_{B,y}\frac{\partial}{\partial y}\hat{p}_k + \\
&\frac{A_s}{2}u_s(\frac{\partial^2}{\partial y^2} - \beta^2(k+1+\gamma)(k+3+\gamma) - \alpha^2)\hat{p}_{k+1} - A_s u_{s,y}\frac{\partial}{\partial y}\hat{p}_{k+1} = 0,
\end{aligned} \tag{21}$$

plus boundary conditions (13).

By rewriting equations (21) and (13) as a system of first-order equations and studying the system's determinant, the singularities can be identified analytically as the roots of the equation

$$\prod_{k=1}^{K}\{U_B - c + A_s u_s \cos\left(\frac{k\pi}{K+1}\right)\} = 0,$$

where K is the number of Fourier modes. For small values of c_i the approximate location of each singularity in the complex y-plane can be identified with a Taylor expansion around $y = y_r$, i.e.

$$U_B(y_r) + A_s u_s(y_r;\beta)\cos\left(\frac{k\pi}{K+1}\right) = c_r + h.o.t.$$

and to first order these locations are:

$$y_s = y_r + i\frac{c_i}{U_{B,y}(y_r) + A_s u_{s,y}(y_r)\cos\left(k\pi/(K+1)\right)}. \tag{22}$$

These are, as might have been expected, the values of y for which the base flow velocity becomes equal to c at the discrete values of the z coordinate imposed by the truncated Fourier expansion in z. Clearly, y_s crosses the real y axis when c_i changes sign, so that the integration path has to go out into the complex y-plane in order for the singularities to lie on the same side of the

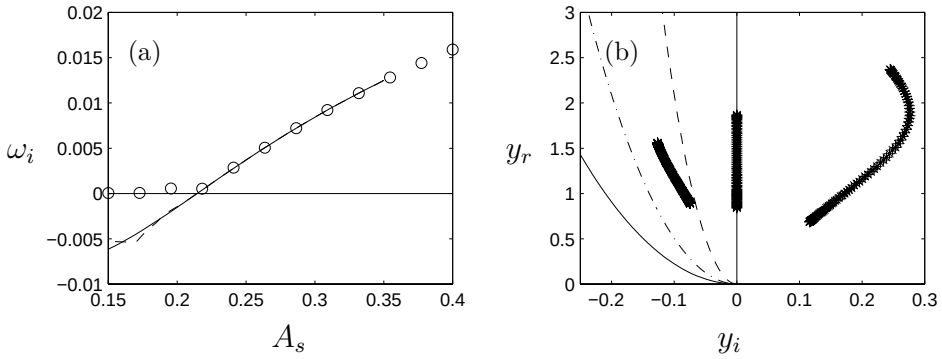

FIGURE 3. (a) Temporal growth rate of the fundamental varicose mode versus the streak's amplitude for α=0.2 and β=0.45 ($\circ$ real integration path, - - - complex integration path with B=0.01, —— complex integration path with B=0.03). (b) The three curved lines denote different integration paths: - - - B=0.01, -·-·- B=0.02, —— B=0.03. The thick segments of stars denote the singular segments for three different streak's amplitudes. From the left: $A_s = 0.15$ (amplified modes do not exist), 0.215 (the least stable discrete mode is neutral) and 0.35 (at least one amplified mode exists). Only for the latter case the real integration path is suitable.

path. Integration in the complex plane is necessary when neutral curves are sought. The mapping

$$y^c = y - iB(y_{\max}\, y - y^2)^{1/2} \tag{23}$$

allows the computation of damped (and neutral) modes. It is introduced into (19), that is $y^c \mapsto \eta^c$, to deliver a curve in the complex plane with endpoints in $\eta^c = -1$ and 1. Complex Chebyshev polynomials $T_n^c(\eta^c)$ are defined by using (18), and the unknown functions are approximated using this new basis. This can be done since the analytic continuation of a polynomial is given by the same polynomial but with a complex argument.

As can be inferred from equation (22) the singularities corresponding to a given set of problem parameters are confined to a finite segment in the complex y-plane. For amplified modes this segment is found in the right half-plane in figure 3(b); for damped modes it is displaced to the left half-plane, whereas for neutral modes the singular segment is a subset of the real axis. In figure 3(a) the results of three calculations of the temporal growth rate are plotted versus the streak amplitude, employing the shape assumption for given streamwise, α=0.2, and spanwise, β=0.45, wavenumbers. The circles are obtained by integrating over the real y-axis; as the amplitude A_s of the streak decreases, so does the largest growth rate of the instability ω_i, until the value $A_S \approx 0.215$ below which only quasi-neutral modes are found. For such modes the real integration path

is located on the wrong side of the singularities. If the complex integration path denoted by a dashed line in both figures (corresponding to B=0.01 in the mapping 23) is employed, the integration correctly follows the damped mode down to an amplitude of about 18%. Clearly one can proceed to even smaller amplitudes simply by increasing B, i.e. by displacing the integration contour further into the negative y_i region. For example, the dotted-dashed contour in figure 3(b) can be used, or the continuous line path (corresponding to $B = 0.03$). The latter integration path has been used and the resulting full spectrum is shown in figure 4 for a streak amplitude of 0.18. The continuous spectrum of singular neutral modes is displaced downward and an isolated, damped mode can be identified at a phase speed close to 0.4. Provided that the singular segment lies on the correct side of the integration path, changes in the path do not affect this eigenvalue; the continuous spectrum is, instead, further moved towards lower values of ω_i for increasing B. Values of B between 0.01 and 0.03 have been used in most of the calculations identifying neutral modes in the present paper.

Clearly also other integration paths are possible; in fact, any complex detour that leaves the singularities to its right side in the complex y-plane will yield the correct physical eigenvalues. Since the physical solutions vanish rapidly at infinity there is no need for the integration path to return to the real axis at $y = y_{\max}$ in order to enforce the boundary conditions at the free stream (Peter Schmid, private communication). In some calculations, the mapping

$$y^c = y - iD(2y_{\max}\, y - y^2)^{1/2} \tag{24}$$

corresponding to a quarter of an ellipse has also been used successfully (D was taken equal to 0.006 in our calculations).

The growing and decaying solutions obtained by our procedure are the asymptotic limits of amplified and damped modes of the viscous stability equations as the Reynolds number approaches infinity (Lin 1955). We re-emphasise here that it is only by the use of this procedure that neutral (and damped) modes can be defined without ambiguities.

2.4. *DNS method*

2.4.1. *Numerical scheme*

The simulation code (see Lundbladh *et al.* 1999) employed for the present computations uses spectral methods to solve the three-dimensional, time-dependent, incompressible Navier–Stokes equations. The algorithm is similar to that of Kim, Moin & Moser (1987), i.e. Fourier representation in the streamwise and spanwise directions and Chebyshev polynomials in the wall-normal direction, together with a pseudo-spectral treatment of the nonlinear terms. The time advancement used is a four-step low storage third-order Runge–Kutta method for the nonlinear terms and a second-order Crank–Nicolson method for the linear terms. Aliasing errors from the evaluation of the nonlinear terms are removed by the $\frac{3}{2}$-rule when the FFTs are calculated in the wall-parallel plane.

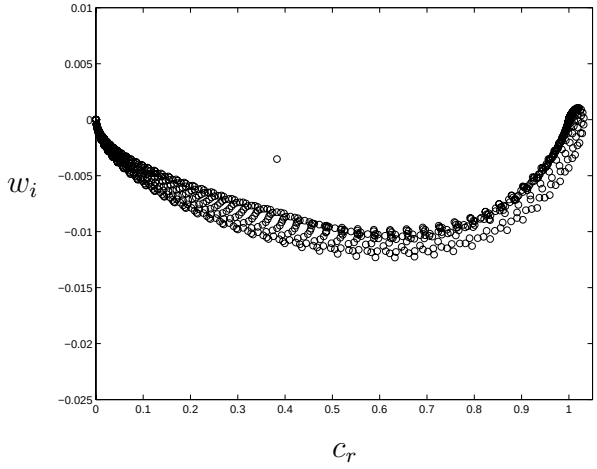

FIGURE 4. Eigenvalue spectrum of the fundamental varicose mode for α=0.2, β=0.45 and A_s=0.18, displayed as temporal growth rate versus phase speed. It is obtained using a complex integration path with B=0.03.

In wall-normal direction it has been found more efficient to increase resolution rather than using dealiasing.

To correctly account for the downstream boundary layer growth a spatial technique is necessary. This requirement is combined with the periodic boundary condition in the streamwise direction by the implementation of a "fringe region", similar to that described by Bertolotti, Herbert & Spalart (1992). In this region, at the downstream end of the computational box, the function $\lambda(x)$ in equation (25) is smoothly raised from zero and the flow is forced to a desired solution $\mathbf{v}$ in the following manner,

$$\frac{\partial \mathbf{u}}{\partial t} = NS(\mathbf{u}) + \lambda(x)(\mathbf{v} - \mathbf{u}) + \mathbf{g}, \tag{25}$$

$$\nabla \cdot \mathbf{u} = 0, \tag{26}$$

where $\mathbf{u}$ is the solution vector and $NS(\mathbf{u})$ the right hand side of the (unforced) momentum equations. Both $\mathbf{g}$, which is a disturbance forcing, and $\mathbf{v}$ may depend on the three spatial coordinates and time. The forcing vector $\mathbf{v}$ is smoothly changed from the laminar boundary layer profile at the beginning of the fringe region to the prescribed inflow velocity vector. This is normally a boundary layer profile, but can also contain a disturbance. A convenient form of the fringe function is as follows:

$$\lambda(x) = \lambda_{max}[S(\frac{x - x_{start}}{\Delta_{rise}}) - S(\frac{x - x_{end}}{\Delta_{fall}} + 1)], \tag{27}$$

where λ_{max} is the maximum strength of the damping, x_{start} to x_{end} the spatial extent of the region where the damping function is nonzero and Δ_{rise} and Δ_{fall}

	xl × yl × zl δ_0	nx × ny × nz (resolution)	Re_{δ_0}
Box1	1940× 34.4× 22.06	576 × 65 × 32	272.2
Box2	1940× 34.4× 22.06	576 × 65 × 32	332.1
Box3	1702× 34.4× 16.68	512 × 81 × 8	264.6
Box4	3096× 34.4× 16.68	1024 × 81 × 8	591.6
Box5	3404× 34.4× 14.71	1024 × 81 × 8	948.7

TABLE 1. Resolution and box dimensions for the simulations presented. The box dimensions includes the fringe region, and are made dimensionless with respect to δ_0, the Blasius length scale at the beginning of the computational box. The parameters zl and nz represent the full span and the total number of Fourier modes, respectively. Note that zl corresponds in all cases to one spanwise wavelength of the primary disturbance.

the "rise" and "fall" distance of the damping function. $S(a)$ is a smooth step function rising from zero for negative a to one for $a \geq 1$. We have used the following form for S, which has the advantage of having continuous derivatives of all orders:

$$S(a) \quad = \quad \begin{cases} 0 & a \leq 0 \\ 1/[1+\exp(\frac{1}{a-1}+\frac{1}{a})] & 0 < a < 1 \\ 1 & a \geq 1 \end{cases} \tag{28}$$

This method damps disturbances flowing out of the physical region and smoothly transforms the flow to the desired inflow state, with a minimal upstream influence.

In order to set the free-stream boundary condition closer to the wall, a generalization of the boundary condition used by Malik, Zang & Hussaini (1985) is implemented. Since it is applied in Fourier space with different coefficients for each wavenumber, it is non-local in physical space and takes the following from,

$$\frac{\partial \hat{\mathbf{u}}}{\partial y} + |k|\hat{\mathbf{u}} = \frac{\partial \hat{\mathbf{v}}_\mathbf{0}}{\partial y} + |k|\hat{\mathbf{v}}_\mathbf{0}, \tag{29}$$

where k is the absolute value of the horizontal wavenumber vector and $\hat{\mathbf{u}}$ is the Fourier transforms of $\mathbf{u}$. Here $\mathbf{v_0}$ denotes the local solution of the Blasius equation and $\hat{\mathbf{v}}_\mathbf{0}$ its Fourier transform.

2.4.2. *Disturbance generation and parameter settings*

The presented numerical implementation provides several possibilities for disturbances generation. The complete velocity vector field from the linear results

by Andersson *et al.* (1999a) is used for the primary disturbance. These optimally growing streaks, here denoted $\mathbf{v_d}$, are introduced in the fringe region by adding them to the Blasius solution to yield the forcing vector $\mathbf{v} = \mathbf{v_0} + \mathbf{v_d}$.

In order to trigger a secondary instability of the streaks a harmonic localized wall-normal volume force is implemented. The harmonic forcing, $\mathbf{g} = (0, F, 0)$, is constructed as an exponentially (in space) decaying function centred at $y = y_0$ and $x = x_{loc}$:

$$F = Cexp\,[-((x - x_{loc})/x_{scale})^2]\,exp\,[-((y - y_0)/y_{scale})^2]g(z)f(t), \qquad (30)$$

where the constant C determines the strength of the forcing and the parameters x_{scale} and y_{scale} its spatial extent. The time dependence is provided by the function

$$f(t) = S(t/t_{scale})\cos(\omega t), \qquad (31)$$

where ω is the angular frequency and the function S has been used again in $f(t)$ to ensure a smooth turn on of the forcing (of duration t_{scale}) in order to avoid problems with transients that may grow and cause transition in the flow. It is also possible to choose the spanwise symmetry of the forcing, to separately excite two classes of secondary disturbances; in

$$g(z) = \cos(\beta z + \phi), \qquad (32)$$

we choose $\phi = 0$ or $\frac{\pi}{2}$ for varicose or sinuous symmetries, respectively.

The box sizes and resolutions used for the simulations presented in this paper are displayed in table 1. The dimensions of the boxes are reported in δ_0, which here denotes the boundary layer thickness at the beginning of the computational box. Box1 is used to produce the non-linear streaks and study their secondary instability, while Box2 is employed to verify the scaling property introduced in section 3.2; Box3, Box4 and Box5 are, instead, used to test the DNS against the linear results (see figure 7(a)). The Reynolds numbers based on δ_0 are also reported in the table. For the calculations presented on the secondary instability induced by harmonic forcing, we use $x_{loc} = 300\delta_0$ from the beginning of the computational box, and $y_0 = 3\delta_0$ with x_{scale} and y_{scale} of $35\delta_0$ and $3\delta_0$, respectively.

3. DNS Results

3.1. *Nonlinear development of the streaks*

Nonlinear mean fields are computed solving the full Navier–Stokes equations in a spatially evolving boundary layer, using the optimal streaks as initial conditions. The complete velocity vector field from the linear results by Andersson *et al.* (1999a) is used as input close to the leading edge and the downstream nonlinear development is monitored for different initial amplitudes of the perturbation. This is shown in figure 5(a), where all energies are normalized by their initial values. The dashed line corresponds to an initial energy small enough for the disturbance to obey the linearixed equations. For this case the maximum of the energy is obtained at x=2.7; note that this location of maximum energy

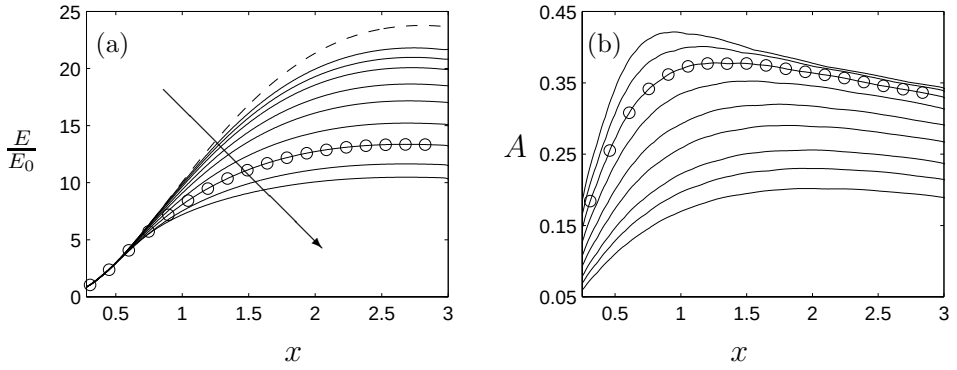

FIGURE 5. (a) The energy of the primary disturbance, E, normalized with its initial value, E_0, versus the streamwise coordinate, x, for β=0.45 and Re_δ=430. Here x has been made non-dimensional using the distance L to the leading edge. The arrow points in the direction of increasing initial energies, E_0= 2.92×10^{-2}, 3.97×10^{-2}, 5.18×10^{-2}, 7.30×10^{-2}, 9.78×10^{-2}, 1.36×10^{-1}, 1.81×10^{-1}, 2.33×10^{-1}, 2.91×10^{-1} (E_0 is computed at x=0.3). The dashed line represents the optimal linear growth. (b) The downstream amplitude development for the same initial conditions as in (a). The amplitude A is defined by equation (34). (The two lines have been circled for future reference).

is weakly dependent on the initial amplitude, even for quite large values of the initial energy.

A contour plot in the (z, y)-plane of the nonlinear mean field corresponding to the circled line in figure 5(a) at $x = 2$ is shown in figure 6(b). This velocity field may be expanded in the sum of cosines

$$U(y, z) = \sum_{k=0}^{\infty} U_k(y) \cos(k\beta z) \tag{33}$$

where U_0 differs from the Blasius solution U_B by the mean flow distortion term. To be able to quantify the size of the primary disturbance field an amplitude A is defined as

$$A = \frac{1}{2}\left[\max_{y,z}(U - U_B) - \min_{y,z}(U - U_B)\right]. \tag{34}$$

When the shape assumption is adopted, A coincides with A_s. Figure 5(b) displays the downstream amplitude development for the same initial conditions as figure 5(a). One can note that the amplitude reaches its maximum value upstream of the position where the energy attains its peak, and starts to decrease at a position where the energy is still increasing. This is due to the thickening of the boundary layer.

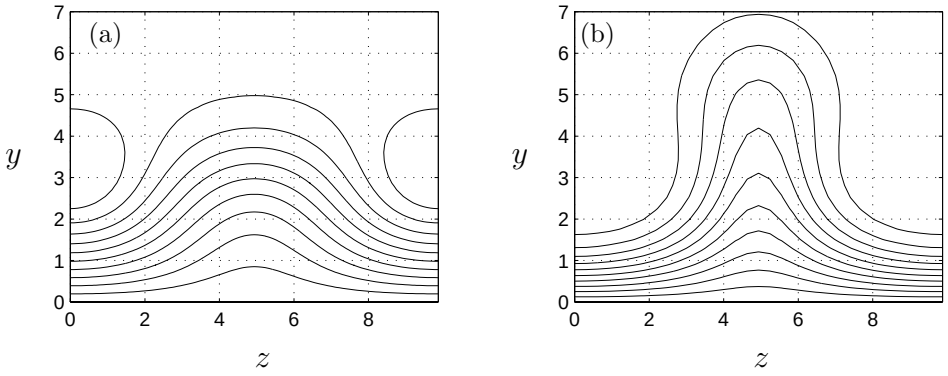

FIGURE 6. (a) Contour plot in a (z, y)-plane of the primary disturbance streamwise velocity using the shape assumption. The spanwise wavenumber is β=0.45, the streamwise position x=2 and the amplitude A_s=0.36. (b) Contour plot in a z-y plane of the nonlinear mean field corresponding to the circled line in figure 5(a) at x=2 (where A=0.36). Here Re_δ=430. In both figures the coordinates y and z have been made non-dimensional using the local Blasius length scale δ, at the streamwise position x=2. In fact, for all y, z plots hereafter the cross-stream coordinates have been scaled using the local Blasius length scale.

The effect of the nonlinear interactions on the base flow are shown by the contour plots in figures 6. Figure 6(a) displays the primary disturbance obtained using the shape assumption with A_s=0.36, while 6(b) shows a fully nonlinear mean field, characterized by the same disturbance amplitude. In the latter case, the low-speed region is narrower, therefore associated with higher spanwise gradients, and displaced further away from the wall.

A base flow like the one presented in figure 6(b) is representative of flat-plate boundary layer flows dominated by streamwise streaks as encountered in experiments (Bakchinov *et al.* 1995; Westin *et al.* 1994; Kendall 1985, 1990) and simulations ( ).

3.2. *Scaling of the mean field*

In Andersson *et al.* (1999a) a scaling property of the optimal streamwise streaks in the flat-plate boundary layer was found to exist. In a linearized setting, they considered an upstream velocity perturbation at the leading edge of the flat plate, $\mathbf{u}_{\rm in}(0)$, and its downstream response, $\mathbf{u}_{\rm out}(x)$, a distance x from the leading edge, and maximized the output energy $E(\mathbf{u}_{\rm out}(x)) = E(x, \beta, E_0, Re)$ over all initial disturbances with fixed energy $E(\mathbf{u}_{\rm in}(0)) = E_0$.

The disturbance energy can be written

$$E(\mathbf{u}(x)) = \int_0^{2\pi/\beta}\int_0^{\infty} (u^2 + \frac{\overline{v}^2}{Re} + \frac{\overline{w}^2}{Re})\, dy\, dz, \tag{35}$$

where $\overline{v} = v\sqrt{Re}$ and $\overline{w} = w\sqrt{Re}$ are the cross-stream velocities in boundary layer scales. The optimal disturbances, which were calculated using the linearized, steady boundary layer approximation, were found to consist of streamwise vortices developing into streamwise streaks. Since streamwise aligned vortices contain no streamwise velocity component, the energy at the leading edge E_0 can be written as

$$E_0 = \frac{\overline{E}_0}{Re}, \quad \text{where} \quad \overline{E}_0 = \int_0^{2\pi/\beta}\int_0^{\infty} (\overline{v}^2 + \overline{w}^2)\, dy\, dz, \tag{36}$$

with $\overline{E}_0$ is independent of the Reynolds number. The boundary layer equations governing $(u, \overline{v}, \overline{w}, \overline{p})$, here $\overline{p}$=pRe, contain no explicit dependence on the Reynolds number; furthermore, all velocities are $O(1)$ a distance sufficiently far downstream of the plate leading edge. Hence, the streamwise velocity component will dominate in the disturbance energy (35) and the output energy obeys the scaling law

$$\overline{E}(x, \beta, \overline{E}_0) = \lim_{\mathrm{Re}\to\infty} E(x, \beta, \overline{E}_0, Re). \tag{37}$$

This scaling property holds also when the solutions are obtained from the Navier–Stokes equations, if $u = 0$ at $x = 0$. In figure 7 both linear and nonlinear solutions obtained from the Navier–Stokes equations are presented which verify (37).

Figure 7(a) displays $\overline{E}/\overline{E}_0$ versus x for the spanwise wavenumber, β=0.45. The solid line corresponds to a solution obtained using the linearized, steady boundary layer approximations. The other three lines represent results obtained from solving the Navier–Stokes equations, for three different Reynolds numbers, with initial disturbance energies small enough to yield a linear evolution. Figure 7(a) shows that the boundary layer approximation is valid and yields solutions in agreement with those obtained from the Navier–Stokes simulations.

Figure 7(b) depicts two curves representing the spatial development of $\overline{E}$ using an initial energy, $\overline{E}_0$, large enough to induce substantial nonlinear effects. The two curves, which represent solutions to the Navier–Stokes equations for the same initial energy and spanwise wavenumber, collapse onto one, although they correspond to two different Reynolds numbers. From figure 7(b) we conclude that the scaling property (37) holds also when the velocity field of the primary disturbance is fully nonlinear.

To clarify the implication of (37), consider the same dimensional problem with the dimensional energy denoted E^* scaled with two different length scales,

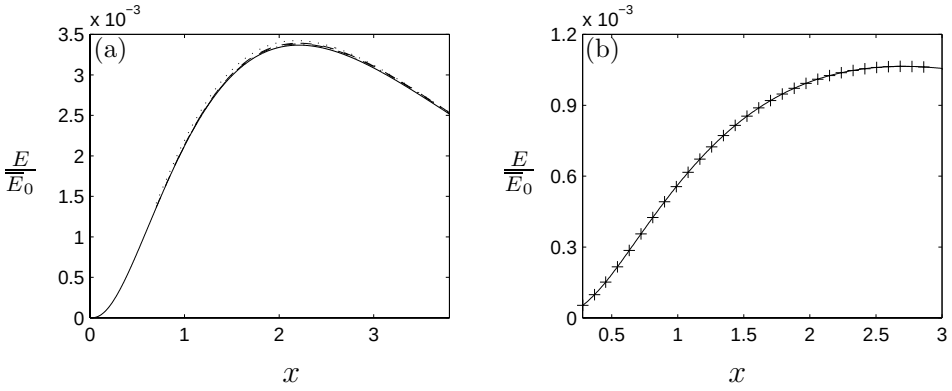

FIGURE 7. The spatial energy growth versus the streamwise coordinate, for the spanwise wavenumber, β=0.45. (a) With three small-amplitude solutions to the Navier–Stokes equations for Reynolds numbers (- - - $Re = 1 \times 10^6$, - ·- · - $Re = 5\times10^5$, $\cdots$ $Re = 1\times10^5$), and (——) one Reynolds number independent solution from the linearized, steady boundary layer approximations. (b) With an initial amplitude large enough to induce considerable nonlinear effects, A=0.30. Here the two curves represent solutions to the Navier–Stokes equations for two different Reynolds numbers (—— $Re = 5 \times 10^5$, and + $Re = 7.5 \times 10^5$).

L and L_1. We write

$$E^*(x, \beta, \overline{E}_0, Re) = E^*(x^1, \beta^1, \overline{E}_0^1, Re^1), \tag{38}$$

where the variables are scaled as

$$x^* = xL = x^1 L_1, \quad \beta^* = \beta\sqrt{\frac{U_\infty}{\nu L}} = \beta^1\sqrt{\frac{U_\infty}{\nu L_1}} \quad \text{and} \quad Re = \frac{U_\infty L}{\nu}, \quad Re_1 = \frac{U_\infty L_1}{\nu}; \tag{39}$$

here x^* and β^* are the dimensional downstream position and spanwise wave number, respectively. The disturbance energies scale as

$$E^* = EU_\infty^2\delta^2 = E^1 U_\infty^2 \delta_1^2 \quad \text{and} \quad \overline{E}_0 = \overline{E}_0^1. \tag{40}$$

Introducing $c^2 = L/L_1 = \delta^2/\delta_1^2$ and rewriting the right-hand expression in (38), in the variables x, β, Re we obtain

$$c^2 E(x, \beta, \overline{E}_0, Re) = E(c^2 x, \beta/c, \overline{E}_0, Re/c^2). \tag{41}$$

Now letting the Reynolds numbers tend to infinity and using (37) we get

$$c^2\overline{E}(x, \beta, \overline{E}_0) = \overline{E}(c^2 x, \beta/c, \overline{E}_0), \tag{42}$$

for each $c > 0$.

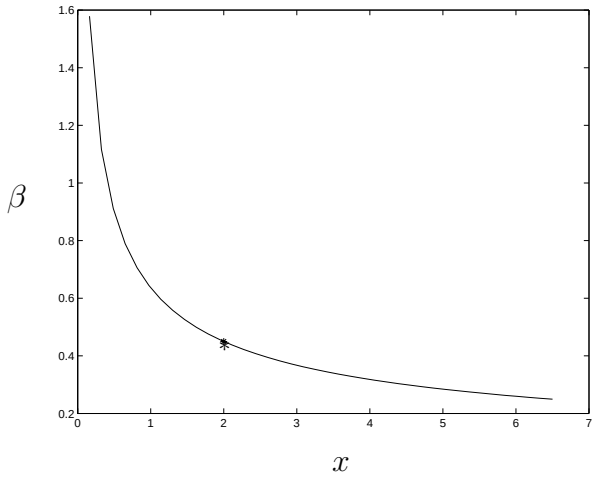

FIGURE 8. Loci of spanwise wavenumbers, β, and streamwise positions, x, representing the known solutions from the linear or nonlinear calculations at x=2 with β=0.45. The streamwise position and the spanwise wavenumber have been made non-dimensional using the distance from the leading edge L and the Blasius length scale $\delta = (L\nu/U_\infty)^{1/2}$, respectively.

An important physical implication of (37) can now be inferred from relation (42). Since (42) is Reynolds number independent, a non-dimensional solution $\overline{E}(x, \beta, \overline{E}_0)$ represent a continuous set of physical solutions in (x^*, β^*)-space, for a fixed $\overline{E}_0$. We have seen that an initial array of streamwise aligned vortices at the leading edge will result in an array of streamwise streaks downstream. Since the streamwise and spanwise length scales are coupled, increasing the spanwise length scale at the leading edge will yield the same downstream behaviour of the solutions but on a larger streamwise length scale.

In figure 8 the curve $(c^2x, \beta/c)$, with x=2 and β=0.45, is shown. From (42) the results along this curve are known and correspond to a rescaling of the solutions calculated at x=2 and β=0.45 (represented by the star in figure 8).

Note that (42) implies that $\overline{E}$ increases linearly as the streamwise coordinate x increases, and the spanwise wavenumber β decreases (cf. figure 8). The increase in the energy of the streak E^* is a result of the widening of the cross-stream spatial extent of the disturbance. Since the shape of the streak velocity profile is the same, this implies that the amplitude remains constant along the curve $x\beta^2$=constant. In contrast, the energy of the corresponding initial vortex E_0^* remains the same for this parameter combination. This implies that the amplitude of the initial vortex, A_v, increases linearly with the spanwise wavenumber, i.e. $A_v \sim \beta$. Thus the amplitude of the initial vortex needed to produce a fixed amplitude of the streak along the curve $x\beta^2$=constant decreases in a manner inversely proportional to the spanwise wavelength.

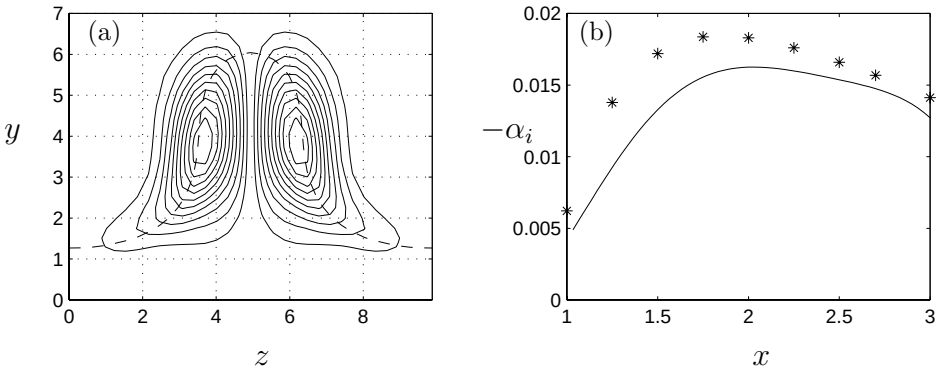

FIGURE 9. (a) Isocontours of r.m.s. values of the streamwise velocity component of the secondary disturbance (ω_r=0.211) for the fundamental sinuous mode at x=2, obtained from the DNS. The dashed line represents the contour of the constant value of the mean field corresponding to the phase speed of the disturbance ($U = c_r = 0.80$). (b) Spatial growth rates, α_i versus x; ——, DNS data with Re_δ=430 and β=0.45; $*$, linear temporal inviscid stability calculations using mean fields at each corresponding x-position and streamwise wavenumber α_r=0.260.

3.3. *Secondary instability results from DNS*

In this section direct numerical simulations of the secondary instability of streaks in a spatially growing flat-plate boundary layer are compared to the results from the inviscid secondary instability theory. This is done to ensure that the inviscid approximation is appropriate and can be used in further investigations and parametric studies of streak instabilities.

The spatial stability problem is defined by the use of a real frequency ω and a complex wavenumber $\alpha = \alpha_r + i\alpha_i$. Here the spatial growth rate $-\alpha_i$ is obtained from the maximum of the streamwise velocity component of the secondary disturbance. The secondary disturbances are triggered using the harmonic forcing introduced in section 2.4.2, allowing for the two symmetries of fundamental type which can be excited separately. The amplitude of the volume force is selected low enough to yield linear secondary disturbances, avoiding the appearance of higher harmonics in the frequency spectra.

To choose the forcing frequency for the DNS, temporal linear secondary stability calculations for the sinuous mode are performed using the nonlinear mean field corresponding to the circled line in figure 5(a), at the local position x=2. The selected mean field has amplitude A=0.36, close to the threshold value for secondary instability in plane channel flow (Elofsson *et al.* 1999). The maximum temporal growth is found for α=0.257, corresponding to a secondary disturbance frequency of 0.211.

The direct numerical simulations for the fundamental sinuous mode of the secondary instability are carried out using this forcing frequency, ω=0.211, and the velocity fields are Fourier transformed in time to obtain the amplitude variation in the streamwise direction and the cross-stream distribution of the disturbance velocity at the frequency of the forcing.

Figure 9(a) shows the u_{rms} distribution of the fundamental sinuous mode at x=2. Note how the disturbance fluctuations follow quite closely the dashed line representing the contour of constant value of the mean field velocity corresponding to the phase speed of the secondary instability, $U = c_r = 0.80$. The solid line in figure 9(b) represents the spatial growth rate of the sinuous mode obtained from the direct numerical simulations. Here the secondary instability is excited at the streamwise position x=0.85. However, since the local forcing does not input pure eigenmodes the values of the growth rates are measured from an x-position downstream of the forcing, where the onset of an "eigenfunction" is identified.

Linear temporal stability calculations, using the real part of the streamwise wavenumber obtained from the direct numerical simulations, α_r=0.260, are also performed, employing mean fields extracted at different streamwise positions from the DNS. In order to compare the spatial results to the growth rates obtained from the temporal inviscid stability problem (12), (13) a transformation first proposed by Gaster (1962) is employed:

$$\omega_i = -\frac{\alpha_i}{\partial\alpha/\partial\omega}. \tag{43}$$

From the temporal eigenvalues, Gaster's transformation (43) provides estimates of spatial growth rates (cf. the stars in figure 9(b)). The agreement between the stability theory and the full simulation results can be regarded as good, since the linear stability calculations are inviscid and performed under the assumptions of parallel mean flow. Note that, as one could expect, the inviscid approximation provides a slight overestimate of the amplification factors, and that closer agreement is found as the Reynolds number increases; here Re=500 000 at the streamwise position x=2.7.

Using the same saturated mean field, direct numerical simulations are also carried out for the fundamental varicose mode of the secondary instability. Attempts to identify instabilities are made with different frequencies and for different streamwise and wall normal positions of the forcing in the direct simulations. Also, linear stability calculations at x=2 and for a range of different streamwise wavenumbers are performed. Both methods produce only stable solutions for this symmetry of the disturbances.

However, linear calculations using as base flow the streaks obtained with the largest initial energy tested (see figure 5), produce small positive temporal growth rates for the fundamental varicose instability. We then proceed as for the sinuous case: the largest growth rate, ω_i, is identified to correspond, at x=2, to a streamwise wavenumber α=0.250 and a frequency ω_r=0.217. This value is used in the DNS forcing and the spatial growth rates obtained are compared

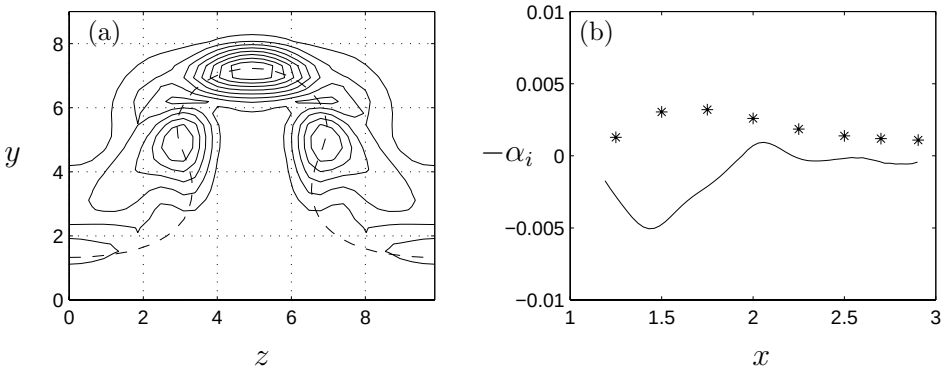

FIGURE 10. (a) Isocontours of r.m.s. values of the streamwise velocity component of the secondary disturbance (ω_r=0.217) for the fundamental varicose mode at x=2, obtained from the DNS. The dashed line represents the contour of the constant value of the mean field corresponding to the phase speed of the disturbance ($U = c_r = 0.863$). (b) Spatial growth rates α_i versus x; ——, DNS data with Re_δ=430 and β=0.45; $*$, linear temporal inviscid stability calculations using mean fields at each corresponding x-position and streamwise wavenumber α_r=0.252.

to linear stability calculations performed at different streamwise positions for α_r=0.252. The results are shown in figure 10(b); the inviscid analysis gives small positive growth rates, while in the DNS the perturbation growth rates remain close to neutral as x exceeds 2.

Figure 10(a) shows the u_{rms} distribution of the fundamental varicose mode together with the contour of constant value of the mean field velocity corresponding to the phase speed of the secondary instability, i.e. $U = c_r = 0.863$. Note also here the close correspondence between the critical layer (displayed in the figure with a dashed line) and regions of intense u-fluctuations.

From the above calculations and comparisons we draw as first conclusion that the secondary instability of streamwise streaks is initially of sinuous type, and that the essential stability features can successfully be captured by an inviscid approach. The above statements are further comfirmed by the results described below.

4. Inviscid Secondary Instability Results

4.1. *The shape assumption versus the nonlinearly developed mean field*

As a preliminary investigation, the secondary instability of streaks approximated by the shape assumption was parametrically studied (Andersson *et al.* 1999b). Comparison of the results with those obtained from calculations where

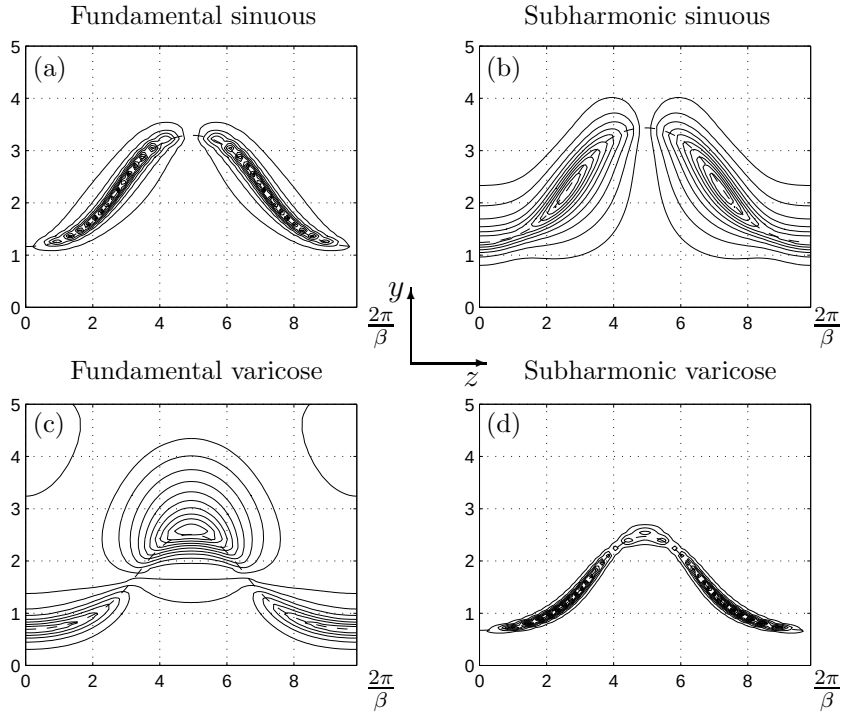

FIGURE 11. Contours of constant absolute values of the streamwise velocity component of four different kinds of modes obtained using the shape assumption. The dashed lines represent the contours of the constant value of the mean field corresponding to the phase velocities of the disturbances. The sinuous modes are calculated with parameters α=0.150, β=0.45 and A_s=0.36 at x=2 (see figure 6a)(c_r = 0.627 and ω_i = 0.00301 for the fundamental mode; c_r = 0.661 and ω_i = 0.0104 for the subharmonic mode). The varicose modes are calculated with parameters α=0.150, β=0.45 and A_s=0.38 at x=2 (c_r = 0.379 and ω_i = 0.00998 for the fundamental mode; c_r = 0.371 and ω_i = 0.00297 for the subharmonic mode). Note that the real and imaginary parts of the subharmonic modes have a period of $4\pi/\beta$. However, their absolute values are $2\pi/\beta$-periodic.

the base flow is the nonlinearly developed streak demonstrate the inapplicability of the shape assumption for this type of studies (except for sinuous symmetries where a qualitative agreement could still be claimed).

In figures 11 and 12 the u-eigenfunctions, obtained with the shape assumption approximation and the nonlinear mean field, respectively, are displayed for the parameters indicated.

Figure 11(a) shows the fundamental sinuous mode which is characterized by out-of-phase oscillations on either side of the low speed-streak, whereas the near-wall region is relatively quiescent. The subharmonic sinuous mode (figure 11b) has real and imaginary parts of u symmetric around the z=0 and z=$2\pi/\beta$ axes. This eigenfunction shows a striking resemblance to that obtained by Ustinov (1998) who solved the linearized Navier–Stokes equations in time; it is also the same high frequency mode triggered in the experiments by Bakchinov *et al.* (1995). In figure 11(c) the fundamental varicose mode is displayed. In-phase fluctuations are spread in a z-range around π/β and halfway through the undisturbed boundary layer height. Some effect is also noticeable around $z = 0$ and $2\pi/\beta$, close to the wall. This mode is also very similar to that computed by Ustinov (1998). The subharmonic varicose mode (figure 11d) is characterized by almost the same phase speed as that of its fundamental counterpart, but here the real and the imaginary parts of this u-eigenfunction are anti-symmetric around the axes $z = 0$ and z=$2\pi/\beta$.

The fundamental u-eigenfunction displayed in figure 12(a) was obtained using the same mean field and streamwise wavenumber as the direct numerical simulations shown in figure 9(a). The agreement between figures 9(a) and 12(a) is very good and in fact, for this symmetry, there is also a fair agreement with the u-eigenfunction displayed in figure 11(a), which was obtained using the shape assumption. Also, the sinuous subharmonic u-eigenfunction 12(b) is in fair agreement with the one obtained using the shape assumption displayed in figure 11(b). In contrast, the fundamental and subharmonic varicose u-eigenfunctions are in poor agreement with both the u_{rms} plot of figure 10(a), obtained from direct numerical simulations, and the u-eigenfunctions of figures 11(c) and 11(d). As shown in figures 12(c) and 12(d) the u-eigenfunctions are considerably less diffuse and strongly concentrated around the isoline $U = c_r$.

The growth rates of the varicose (fundamental and subharmonic) symmetries are highly over-predicted when the shape assumption is used. The positive growth rates of the fundamental varicose case are found to be even larger than those for the fundamental sinuous case, which contradicts experiments and previous, comparable, calculations (Schoppa & Hussain 1997; 1998)

In comparing the mean fields obtained from the shape assumptions to the fully nonlinear ones, we find that the inflection point in the wall-normal direction is smoothed by the nonlinear modification, cf. figure 13(a). This figure shows the streamwise velocity profiles centred on the low-speed streak (i.e. $z = \pi/\beta$) for the two types of mean fields and for a large amplitude. This-z location has been chosen since it is where a wall-normal inflection point first appears when the streak's amplitude is increased, and also where the varicose eigenfunctions achieve their peak values. As reported in a number of experimental and numerical studies (Swearingen & Blackwelder 1987; Yu & Liu 1991; Bottaro & Klingmann 1996; Matsubara & Alfredsson 1998),

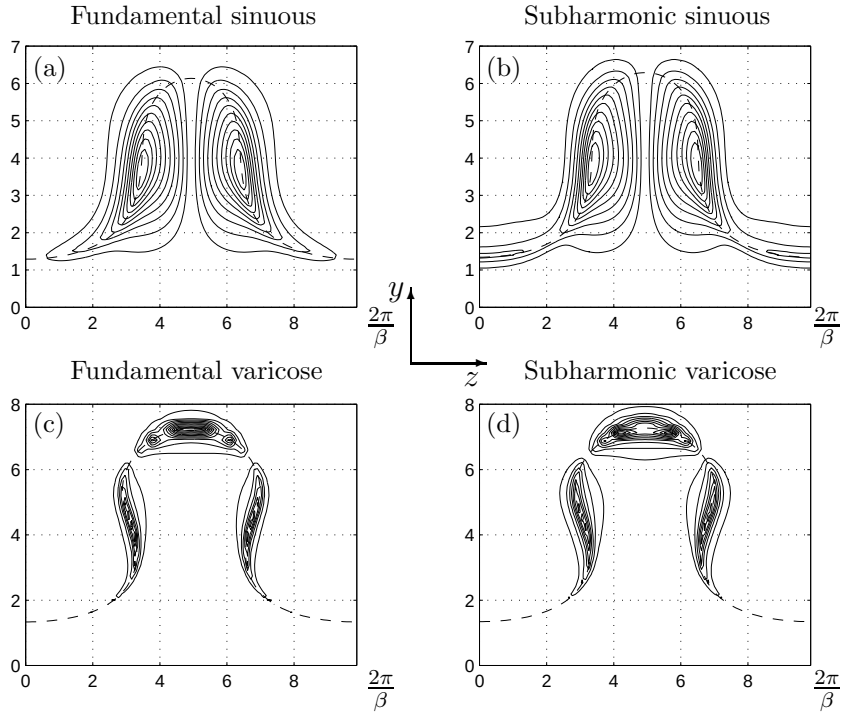

FIGURE 12. Contours of constant absolute values of the streamwise velocity component of four different kinds of modes obtained using the nonlinear mean fields. The dashed lines represent the contours of the constant value of the mean field corresponding to the phase velocities of the disturbances. The sinuous modes are calculated using the nonlinear mean field corresponding to the circled line in figure 5(a), at streamwise position x=2, where $A = 0.36$, for a streamwise wavenumber $\alpha = 0.280$ ($c_r = 0.821$ and $\omega_i = 0.0144$ for the fundamental mode; $c_r = 0.839$ and $\omega_i = 0.0125$ for the subharmonic mode). The varicose modes are calculated using the mean field with largest streak's amplitude (see figure 5(b)) at position $x = 2$, where $A = 0.378$, for a streamwise wavenumber $\alpha = 0.275$ ($c_r = 0.866$ and $\omega_i = 0.00218$ for the fundamental mode; $c_r = 0.876$ and $\omega_i = 0.00243$ for the subharmonic mode). In all calculations Re_δ=430 and β=0.45.

the wall-normal inflection point can be related to the varicose mode, whereas sinuous instabilities correlate well to the spanwise mean shear.

The reason for the overpredicted varicose amplification factor when using the shape assumption can be deduced from inspection of figure 13: an inflection point appears for y close to 3 in this case, but it disappears when the base flow

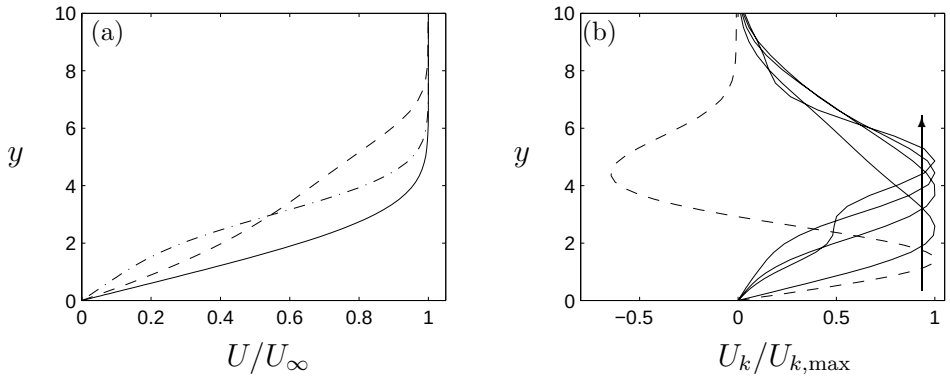

FIGURE 13. (a) The total streamwise velocity versus the wall-normal coordinate at $z = \pi/\beta$ for: - - - -, the nonlinear mean field, and - · - · -, the shape-assumption-approximated mean field. Here both amplitudes are A=A_s=0.33, the streamwise position is x=2 and the spanwise wavenumber is β=0.45; the Blasius profile is drawn, for reference, with a solid line. (b) The different Fourier modes $U_k(y)$ representing the streamwise velocity of the nonlinear mean field in (a) versus the wall-normal coordinate. The dashed line corresponds to the mean flow distortion, $(U_0 - U_B)$, and the arrow points in the direction of higher-order modes. Every mode is normalized with its maximum ($(U_0 - U_B)_{\max}$=0.11, $U_{1,\max}$=0.26, $U_{2,\max}$=6.6×10^{-2}, $U_{3,\max}$=1.1×10^{-2}, $U_{4,\max}$=9.2×10^{-4}.) Here Re_δ=430.

contains all harmonics of the streak. Both the direct numerical simulations and the linear stability calculations using the nonlinearly distorted mean fields produce stable varicose modes for A=0.33. In fact, only for the largest streak studied in this paper, corresponding to an amplitude A=0.373, a slightly unstable varicose mode is found. The discrepancy in the secondary stability results between the two cases can be traced to the mean flow distortion $(U_0 - U_B)$ (see the dashed line in figure 13b). Calculations employing a "nonlinear" mean field constructed without the mean flow distortion (where U_0 is replaced by U_B) result in varicose perturbations with positive growth rates for $A = 0.33$.

Furthermore, the phase speed of the secondary instability is considerably increased when using the nonlinear mean fields. This can be explained by observing that nonlinearities "move" the primary instability outwards from the wall. In figure 13(b) the individual Fourier modes from the cosine expansion of the nonlinear mean field from figure 13(a) are shown, normalized to unit value. Note that higher-order modes are displaced away from the wall. The phase speed of the secondary instability equals the mean field velocity at the critical layer, cf. figure 11. Therefore, as the critical layer is moved outwards, where

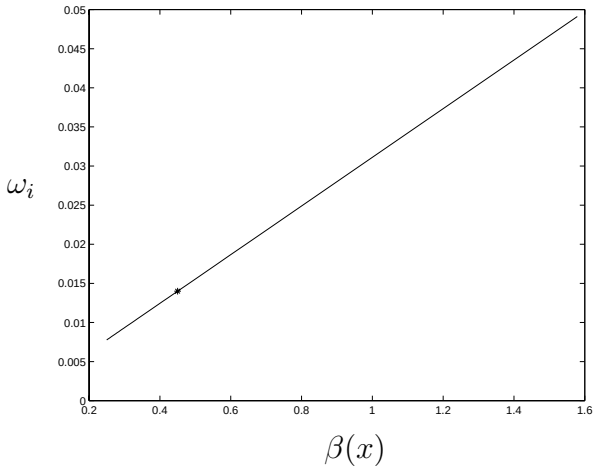

FIGURE 14. Results for the fundamental sinuous growth rates, ω_i, versus the spanwise wavenumbers along the curve in figure 8. The star gives the value of the amplification factor obtained when A=0.36, α=0.30, β=0.45 and x=2, i.e. ω_i=0.014.

the mean flow velocity is higher, the phase speed of the secondary instability is also increased.

4.2. *Parametric study*

In figure 5(b) the downstream amplitude development of streamwise streaks for a spanwise wavenumber β=0.45 and for different initial amplitudes is shown. Most of the linear stability calculations are performed using the velocity fields with the amplitudes found at x=2. This position was chosen since it is close to the point where the primary disturbance energy attains its maximum value.

According to the scaling property of the mean fields derived in section 3.2, the results obtained for the parameters used in this section, x=2 and β=0.45, can be rescaled to apply for all values of β (see figure 8). This implies that a result from a secondary instability calculation obtained using a mean field corresponding to a point on the curve in figure 8 can be rescaled to yield the amplification value for all points on this curve. Since ω_i/β=constant, the value of the constant can be determined from a secondary instability result for a specific parameter combination. The line representing the growth rates of the fundamental sinuous symmetry is displayed in figure 14. In practice, however, the scaling property relating ω_i and β is limited to an intermediate range of β. Since their distance of amplification is so short, large values of β will need a very large initial disturbance amplitude at the leading edge, while disturbances represented by low values of β will saturate far downstream, where Tollmien–Schlichting instabilities may become important and change the

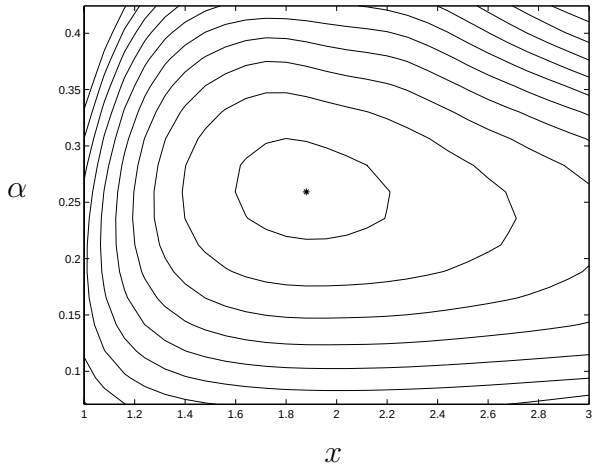

FIGURE 15. Isocontours of the growth rate ω_i, in the (x, α)-plane, for the sinuous fundamental mode, employing the mean field corresponding to the circled line in figure 5. The maximum contour level is 0.014 and the spacing is 0.0014. The $*$ represents the maximum growth rate, ω_i=0.0147, obtained at position x=1.88 and for a streamwise wavenumber α =0.259.

transition scenario. For larger values of β, the corresponding x-position is closer to the leading edge and viscous effects may have a damping influence on the amplification of unstable waves.

Primary disturbances with β in the range $[0.3, 0.6]$ (here considered with respect to a fixed streamwise position, x=1), have the largest transient amplification (Andersson *et al.* 1999a; Luchini 2000). The spanwise distance selected in the controlled experiments by Bakchinov *et al.* (1995) corresponds to a value of β equal to 0.45 (at the location of their roughness elements), and this is also the scale of boundary layer fluctuations in the presence of free-stream turbulence (Westin *et al.* 1994). It could be speculated that this particular range of β is particularly appropriate when dealing with boundary layer streaks, since it corresponds to a spanwise spacing of about 100 wall units once viscous length scales are introduced. The spacing of 100 viscous wall units is not only obeyed by quasi-regular streaks in turbulent but also in laminar and transitional boundary layers (see Blackwelder 1983; Kendall 1985, 1990; Westin *et al.* 1994). It is also the typical transverse 'box' dimension for turbulence to survive in the minimal channel simulations of Jimenez & Moin (1991) and Hamilton, Kim & Waleffe (1995). In the present case, if a simple measure of the friction velocity is adopted by the use of the Blasius wall shear, it is easy to see that streaks spaced 100 wall units apart are present in a subcritical (with respect to TS waves) boundary layer if β is in the range (0.3, 0.63).

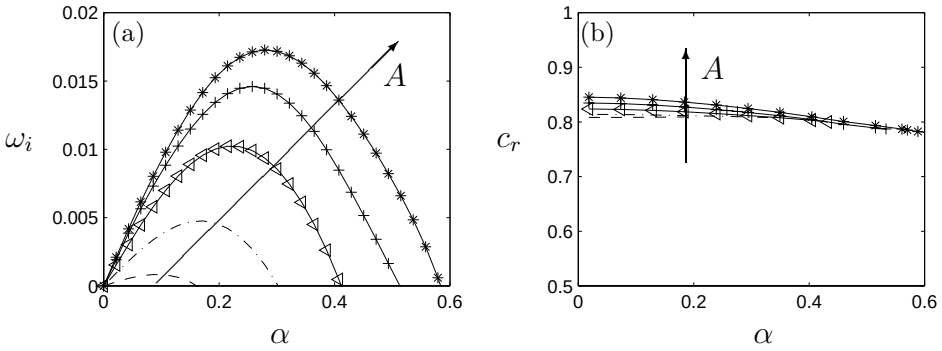

FIGURE 16. Temporal growth rate (a) and phase speed (b) versus streamwise wavenumber for the fundamental sinuous modes for different amplitudes of the primary disturbance (- - - A=28.8,- · - · - A=31.7,—◁— A=34.5, —+— A=36.4, —∗— A=37.3). The arrows point in the direction of increasing A.

Figure 15 shows the isocontours of the growth rate ω_i, for the fundamental sinuous instability in the (x, α)-plane for the mean field corresponding to the circled line in figure 5. The growth rates do not vary significantly for the range of x between $1.6 < x < 2.2$, and in this interval, the maximum growth rate is obtained for nearly the same value of the streamwise wavenumber (α=0.259). Stability calculations are, therefore, performed on the mean field at x=2, where the primary disturbance has saturated and, for the cases with lower initial energy, the streak amplitude achieve its maximum value (cf. figures 5).

An extensive parametric study is carried out for the sinuous fundamental ($\gamma = 0$), arbitrarily detuned ($0 < \gamma < 0.5$) and subharmonic ($\gamma = 0.5$) symmetries, which were the only ones found to be significantly unstable. At first the Floquet parameter is set to zero, i.e. fundamental modes are focused upon. In figure 16(a) the growth rate of the instability $\omega_i = \alpha c_i$ is plotted against the streamwise wavenumber, for the different amplitudes of the streaks, obtained with the DNS. One can note that on increasing the amplitude, not only do the growth rates increase but their maxima are also shifted towards larger values of the streamwise wavenumber α. As shown in figure 16(b) the phase speeds of the fundamental sinuous modes are but weakly dispersive.

Next, we examine the effect of changes in the spanwise wavelength of the secondary disturbance, i.e. we study the effect of the detuning parameter γ. It is often assumed that the preferentially triggered secondary instability modes have the same transverse periodicity as the base flow; this is not at all evident here. The full system of equations (12)-(13) has been solved without resorting to symmetry considerations to yield the results displayed in figures 17, corresponding to a streamwise wavenumber α equal to 0.255 and for mean fields with amplitudes large enough to lead to instabilities for the chosen α. A

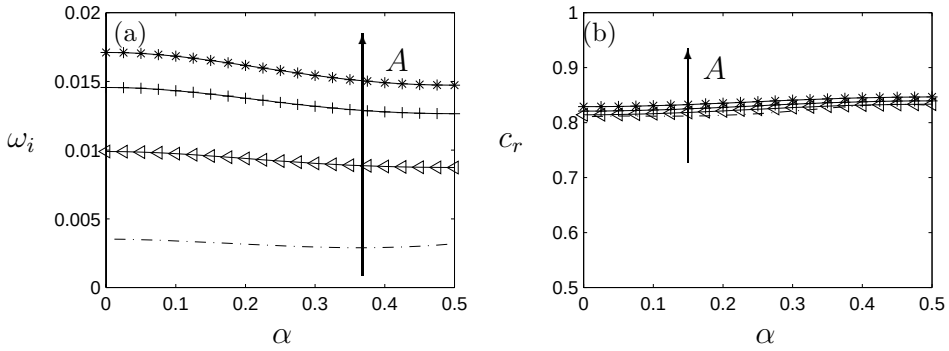

FIGURE 17. Temporal growth rate (a) and phase speed (b) versus the Floquet parameter for sinuous modes, for four different amplitudes of the primary disturbance (symbols as in figure 16).

monotonic behaviour is observed in the γ range of [0, 0.5] except for the case of lower amplitude A.

The behaviour of the amplification factor of the subharmonic modes for different streamwise wavenumbers and different amplitudes of the primary disturbance is shown in figure 18(a). For amplitudes larger than about 0.30, the subharmonic symmetry produces lower maximum growth rates than the fundamental symmetry. Note, however, that for lower amplitudes the sinuous subharmonic symmetry represents the most unstable mode. The phase speed for the subharmonic symmetry, displayed in figure 18(b), is larger than in the fundamental case and the waves are slightly more dispersive.

4.3. *The neutral conditions of streak's breakdown*

A study has been conducted to identify the marginal conditions of breakdown, with each neutral point $\omega_i = 0$ calculated for a range of α by means of the complex integration technique discussed in section 2.3. The steady base velocity profiles obtained with the DNS at x=2 are used here. The results are displayed in figures 19(a-b) for the two sinuous symmetries, together with contour levels of constant growth rates.

It is immediately observed that a streaks amplitude of about 26% of the free-stream speed is needed for breakdown to occur. Although this critical value is achieved for small values of α (where the parallel flow assumption becomes questionable) we are roughly around the values reported by P. H. Alfredsson (private communication, 1998), who stated that "amplitudes of at least 20%" are needed for an instability of the streaks to emerge, and by Bakchinov *et al.* (1995) who in their experiments produced streaks with $A \approx 20\%$ and generated their controlled excitation with a vibrating ribbon. In the case of plane Poiseuille flow, the experiments of Elofsson *et al.* (1999) show that the

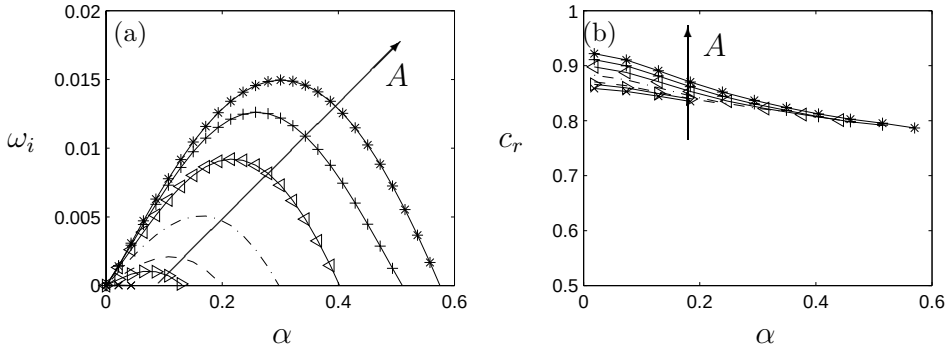

FIGURE 18. Temporal growth rate (a) and phase speed (b) versus streamwise wavenumber for the subharmonic sinuous modes for different amplitudes of the primary disturbance (—×— A=25.6,—▷— A=27.2, - - - A=28.8, -·-·- A=31.7,—◁— A=34.5, —+— A=36.4, —∗— A=37.3).

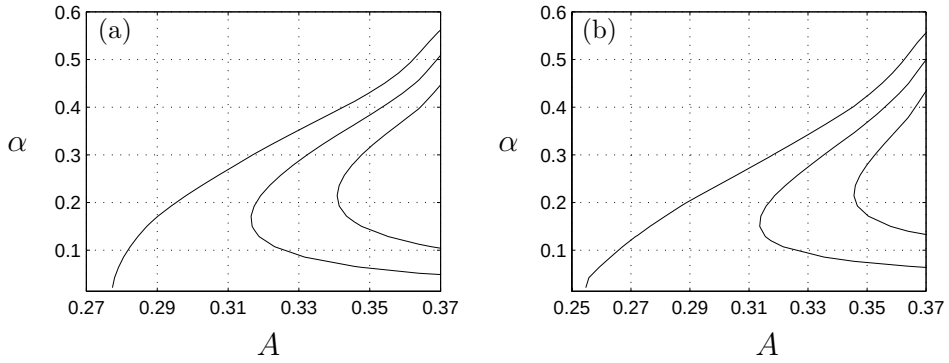

FIGURE 19. Neutral curves for streak instability in the (A, α)-plane for (a) fundamental sinuous mode, (b) subharmonic sinuous mode (contour levels: ω_i=0, 0.0046, 0.0092).

threshold amplitude for streaks' breakdown is 35%, irrespective of the Reynolds number. This Reynolds-number independence was also observed in direct numerical simulations of Couette flow by Kreiss, Lundbladh & Henningson (1994) who reported that "the disturbances in the calculations are found to reach an amplitude of order one for all Reynolds numbers before the rapid secondary instability sets in".

One can notice that the subharmonic mode is unstable for lower amplitudes than the fundamental mode and that the growth rates for larger amplitudes are quite close for the two symmetries. The direct numerical simulations and experiments of oblique transition in a boundary layer conducted by Berlin,

Lundbladh & Henningson (1994) and Berlin, Wiegel & Henningson (1999) show that a subharmonic breakdown of the streaks precedes transition to turbulence.

We do not present any results for the varicose instabilities here. In fact, both the fundamental and the subharmonic symmetries resulted in weak instabilities for amplitudes larger than A=0.37 with growth rates smaller than one fifth of the corresponding sinuous growth rates. Therefore a breakdown scenario triggered by a varicose instability seems unlikely.

It appears then that there is not a dominating mode but rather that fundamental and detuned sinuous instabilities have the same probability of being observed. Hence, the knowledge provided by these results must be combined with that of the inflow disturbance spectrum, i.e. the prevailing receptivity conditions. The present study furnishes possible scenarios which should be confirmed by careful experiments, i.e. with controlled harmonic disturbances to try and trigger specific modes.

5. Conclusions

We have investigated one of the mechanisms which is a possible precursor of transition to turbulence in a boundary layer, namely the linear instability of streaks produced by the non-modal streamwise evolution of free-stream disturbances. Such a breakdown has been observed in experiments carried out by the Swedish (Westin *et al.* 1994; Alfredsson & Matsubara 1996) and the Russian groups (Gulyaev *et al.* 1989; Bakchinov *et al.* 1995): they generated streaky structures and visualized their development, breakdown and the formation of turbulent spots, via smoke injection.

There is starting to be a good correspondence between experiments and theory, and most of the segments of transition induced by the breakdown of streaks are now elucitated (at least qualitatively). Our study aims at the modelling of only one part of this process. More complete pictures are starting to emerge, often based on simple model systems, particurlarly for the description of the self–sustained process that makes near–wall turbulence viable (for a recent account refer to the book by Panton 1997). Although similarities exist between the wall turbulence process and the breakdown of laminar streaks, it is best not to draw definite parallels because of the widely different space and time scales involved in the two cases.

Clearly, other steps can be envisioned to lead to early transition to turbulence (i.e. strong nonlinearities, resonant interactions, etc.) and the present work represents but one brick in the building of a comprehensive picture. One has to further appreciate the fact that in an actual experiment irregular streaky structures are often observed, i.e. with non-uniform spacing and with neighbouring streaks in different stages of development, see Bottin, Dauchot & Daviaud (1998) for an example in plane Couette flow. Thus, these structures do not necessarily become unstable together at a given x-position, but their breakdown will likely occur in an irregular manner. These aspects are linked to the flow

receptivity, the understanding of which is, hence, crucial. For recent progress in this direction the reader is referred to Luchini & Bottaro (1998) and Airiau & Bottaro (1998).

The local, large Reynolds number limit has been considered here, with the implication that this simplified approach captures the essential features of the instability. The inviscid assumption means that one has to be careful in choosing the integration path for the eigenvalue calculation, and a simple procedure for identifying the singularities in the complex y-plane and for integrating around them has been outlined. With our approach, inspired by Lin (1944), neutral and damped inviscid modes can be computed, and a quasi-linear behaviour of the growth rate of the instability with the streak's amplitude is found, in agreement with the careful channel flow measurements by Elofsson *et al.* (1999).

We have shown here that both the linear and nonlinear spatial development of optimal streamwise streaks are well described by the boundary layer approximation and, as a consequence, Reynolds number independent for large enough Reynolds numbers. This results in a boundary layer scaling property that couples the streamwise and spanwise scales, implying that the same solution is valid for every combination of x and β such that the product $x\beta^2$ stays constant. The parameter study of streak instability is therefore representative of a wide range of intermediate values of β for which saturation occurs at a reasonable x: large enough so that the boundary layer approximation may still be valid and small enough so that Tollmien–Schlichting waves may not play a significant role.

The different modes of instability have been catalogued and studied. At a preliminary stage secondary instability calculations of the shape-assumption-approximated mean fields were carried out; however, most results presented here are performed employing the fully nonlinear mean fields. In comparing the two levels of approximations we conclude that the shape assumption must be abandoned in secondary instability studies of streamwise streaks in flat-plate boundary layers. The secondary instability results are very sensitive to a slight change in the shape of the mean field velocity profile and, even if the sinuous modes are reasonably well captured by the shape assumption, the growth rates of varicose modes are widely over-predicted.

When considering the nonlinear mean field we find that the sinuous modes are by far the dominating instabilities. The varicose modes become unstable only for very large amplitudes (around 37% of the free-stream speed) and should, therefore, be rarely observed in natural transition. This is in agreement with DNS and experiments, where the sinuous modes of instability are most often reported for the streak breakdown.

Noticeable is the fact that the sinuous, detuned instability waves can be more amplified than the fundamental modes. The subharmonic modes are in fact found to first become unstable with a critical streak amplitude of about 26% of the free-stream velocity. Plots of the eigenfunctions for fundamental

and subharmonic modes demonstrate clearly that the instability is concentrated around the critical layer, and both types of sinuous modes of breakdown are found to be almost non-dispersive. When the streak amplitude is large enough (around 30% of the free-stream velocity) both the fundamental and detuned modes have positive growth rates; thus, they might both be observed and to decide on their downstream fate is a matter of environmental bias. It is noteworthy that both experiments (Bakchinov *et al.* 1995) and DNS (Berlin *et al.* 1994) did show subharmonic breakdown of the streaks, although neither paper stated so explicitly.

Neutral curves have been obtained here in the amplitude–streamwise wavenumber plane; their identification should prove useful for controlling transition and near-wall turbulence.

Future experiments under controlled conditions may attempt to trigger some of the modes described here. Also, an interesting direction of future research concerns the search for a possible absolute instability of the streaks. Finding a self-sustaining instability mechanism could provide a firmer connection with the birth of turbulent spots.

Acknowledgments

We thank Theo Randriarifara for making his stability code available for some of the validation tests, Paolo Luchini and Peter Schmid for interesting and fruitful discussions, and the referees for valuable comments that helped us produce a more physically relevant account of the breakdown of boundary layer streaks. Part of the work was performed during the first author's stay in Toulouse, supported by "Internationaliseringsmedel för Doktorander" dnr 930-766-95, dossier 71, at the Royal Institute of Technology.

References

Airiau, C. & Bottaro, A. 1998 Receptivity of Tollmien-Schlichting waves via adjoint PSE. Presented at the EUROMECH colloquium 380: *Laminar-Turbulent Transition Mechanisms and Prediction*, Göttingen, Germany, September 14-17, 1998.

Alfredsson, P. H. & Matsubara, M. 1996 Streaky structures in transition In *Proc. Transitional Boundary Layers in Aeronautics.* (ed. R. A. W. M. Henkes & J. L. van Ingen), pp. 373-386, Royal Netherlands Academy of Arts and Sciences. Elsevier Science Publishers.

Andersson, P., Berggren, M. & Henningson, D. S. 1999a Optimal disturbances and bypass transition in boundary layers. *Phys. Fluids* **11**, 134.

Andersson, P., Bottaro, A., Henningson, D. S. & Luchini, P. 1999b Secondary instability of boundary layer streaks based on a shape assmption. *TRITA-MEK Rep.* 199:13. Department of Mechanics, The Royal Institute of Technology, Stockholm, Sweden.

Bakchinov, A. A., Grek, G. R., Klingmann, B. G. B. & Kozlov, V. V. 1995 Transition experiments in a boundary layer with embedded streamwise vortices. *Phys. Fluids* **7**, 820.

Bayly, B. J., Orszag, S. A. & Herbert, T. 1988 Instability mechanisms in shear flow transition. *Ann. Rev. Fluid Mech.* **20**, 359.

Berlin, S. & Henningson, D. S. 1999 A new nonlinear mechanism for receptivity of free-stream disturbances. *Phys. Fluids* **11**, 3749.

Berlin, S., Lundbladh, A. & Henningson, D. S. 1994 Spatial simulations of oblique transition in a boundary layer. *Phys. Fluids* **6**, 1949.

Berlin, S., Wiegel, M. & Henningson, D. S. 1999 Numerical and experimental investigations of oblique boundary layer transition. *J. Fluid Mech.* **393**, 23.

Bertolotti, F. P., Herbert, T. & Spalart, P. R.1992 Linear and nonlinear stability of the Blasius boundary layer *J. Fluid Mech.* **242**, 441.

Blackwelder, R. F. 1983 Analogies between transitional and turbulent boundary layers. *Phys. Fluids* **26**, 2807.

Boberg, L. & Brosa, U. 1988 Onset of turbulence in a pipe. *Z. Naturforschung* **43a**, 697.

Boiko, A. V., Kozlov, V. V., Syzrantsev, V. V. & Shcherbakov, V. A. 1997 A study of the influence of internal structure of a streamwise vortex on the development of travelling disturbances inside it. *Thermoph. and Aeromech.* **4**, 343.

Bottaro, A. & Klingmann, B. G. B. 1996 On the linear breakdown of Görtler vortices. *Eur. J. Mech., B/Fluids.* **15**, 301.

Bottin, S., Dauchot, O. & Daviaud, F. 1998 Experimental evidence of streamwise vortices as finite amplitude solutions in transitional plane Couette flow. *Phys. Fluids* **10**, 2597.

Butler, K. M. & Farrell, B. F. 1992 Three-dimensional optimal perturbations in viscous shear flow. *Phys. Fluids* A **4**, 1637.

Dauchot, O. & Daviaud, F. 1995 Finite amplitude perturbation and spots growth mechanism in plane Couette flow. *Phys. Fluids* **7**, 335.

Drazin, P. G & Reid, W. H. 1981 *Hydrodynamic Stability.* Cambridge University Press.

Ellingsen, T. & Palm, E. 1975 Stability of linear flow. *Phys. Fluids* **18**, 487.

Elofsson, P. A., Kawakami, M. & Alfredsson, P. H. 1999 Experiments on the stability of streamwise streaks in plane Poiseuille flow. *Phys. Fluids* **11**, 915.

Gaster, M. 1962 A note on the relation between temporally-increasing and spatially-increasing disturbances in hydrodynamic stability *J. Fluid Mech.* **14**, 222.

Gulyaev, A. N., Kozlov, V. E., Kuznetsov, V. R., Mineev, B. I., & Sekundov, A. N. 1989 Interaction of a laminar boundary layer with external turbulence *Izv. Akad. Nauk SSSR, Mekh. Zhid. Gaza.* **5**, 55. (in Russian, English transl. 1990 in *Fluid Dyn.* **24**:5, 700)

Gustavsson, L. H. 1991 Energy growth of three-dimensional disturbances in plane Poiseuille flow. *J. Fluid Mech.* **224**, 241.

Hall, P. & Horseman, N. J. 1991 The linear inviscid secondary instability of longitudinal vortex structures in boundary-layers. *J. Fluid Mech.* **232**, 357.

Hamilton, J. M., Kim, J. & Waleffe, F. 1995 Regeneration mechanisms of near-wall turbulence structures. *J. Fluid Mech.* **287**, 317.

Henningson, D. S. 1987 Stability of parallel inviscid shear flow with mean spanwise variation. *Tech. Rep.* FFA-TN 1987-57. Aeronautical Research Institute of Sweden, Bromma.

Henningson, D. S. 1995 Bypass transition and linear growth mechanisms. In *Advances in Turbulence V* (ed. R. Benzi). Kluwer.

Henningson, D. S. 1996 Comment on "Transition in shear flows. Nonlinear normality versus non-normal linearity" [Phys. Fluids 7 3060 (1995)] *Phys. Fluids* **8**, 2257.

Henningson, D. S., Lundbladh, A. & Johansson, A. V. 1993 A mechanism for bypass transition from localized disturbances in wall bounded shear flows. *J. Fluid Mech.* **250**, 169.

Henningson, D. S. & Reddy, S. C. 1994 On the role of linear mechanisms in transition to turbulence. *Phys. Fluids* **6**, 2862.

Herbert, T. 1988 Secondary Instability of boundary layers. *Ann. Rev. Fluid Mech.* **20**, 487.

Hultgren, L. S. & Gustavsson, L. H. 1981 Algebraic growth of disturbances in a laminar boundary layer. *Phys. Fluids* **24**, 1000.

Jimenez,. J. & Moin, P. 1991 The minimal flow unit in near wall turbulence. *J. Fluid Mech.* **225**, 221.

Jimenez,. J. & Pinelli, A. 1999 The autonomous cycle of near wall turbulence. *J. Fluid Mech.* **389**, 335.

Kendall, J. M. 1985 Experimental study of disturbances produced in a pretransitional laminar boundary layer by weak free-stream turbulence. AIAA Paper 85-1695.

Kendall, J. M. 1990 Boundary layer receptivity to free-stream turbulence. AIAA Paper 90-1504.

Kim, J., Moin, P. & Moser, R. 1987 Turbulence statistics in fully developed channel flow *J. Fluid Mech.* **177**, 133.

Kreiss, G., Lundbladh, A. & Henningson, D. S. 1994 Bounds for threshold amplitudes in subcritical shear flows. *J. Fluid Mech.* **270**, 175.

Landahl, M. T. 1975 Wave breakdown and turbulence. *SIAM J. Appl. Math* **28**, 735.

Landahl, M. T. 1980 A note on an algebraic instability of inviscid parallel shear flows. *J. Fluid Mech.* **98**, 243.

Le Cunff, C. & Bottaro, A. 1993 Linear stability of shear profiles and relation to the secondary instability of the Dean flow. *Phys. Fluids* A **5**, 2161.

Li, F. & Malik, M. R. 1995 Fundamental and subharmonic secondary instabilities of Görtler vortices. *J. Fluid Mech.* **297**, 77.

Lin, C. C. 1944 On the stability of two-dimensional parallel flows. *Proc. Nat. Acad. Sci.* **30**, 316.

Lin, C. C. 1955 *The Theory of Hydrodynamic Stability.* Cambridge University Press.

Luchini, P. 2000 Reynolds-number-independent instability of the boundary layer over a flat surface: optimal perturbations. Accepted *J. Fluid Mech.* **404**, 289.

Luchini, P. & Bottaro, A. 1998 Görtler vortices: a backward-in-time approach to the receptivity problem. *J. Fluid Mech.* **363**, 1.

Lundbladh, A., Berlin, S., Skote, M., Hildings, C., Choi, J., Kim, J. & Henningson, D. S. 1999 An efficient spectral method for simulation of incompressible flow over a flat plate. *TRITA-MEK Technical Report* 1999:11, Royal Institute of Technology, Stockholm, Sweden

Lundbladh, A. & Johansson, A. V. 1991 Direct simulation of turbulent spots in plane Couette flow. *J. Fluid Mech.* **229**, 499.

Malik, M. R., Zang, T. A. & Hussaini, M. Y.1985 A spectral collocation method for the Navier-Stokes equations *J. Comp. Phys.* **61**, 64.

Matsubara, M & Alfredsson, P. H. 1998 Secondary instability in rotating channel flow. *J. Fluid Mech.* **368**, 27.

Morkovin, M. V. & Reshotko, E. 1990 Dialogue on progress and issues in stability and transition research. In *Laminar-Turbulent Transition* (ed. D. Arnal & R. Michel). Springer.

Orszag, S. A. & Patera, A. T. 1983 Secondary instability of wall-bounded shear flows. *J. Fluid Mech.* **128**, 347.

Panton, R. l. 1997 (Ed.) *Self–sustaining mechanisms of wall turbulence*. Computational Mechanics Publications, Southampton.

Park, D. S. & Huerre, P. 1995 Primary and secondary instabilities of the asymptotic suction boundary layer on a curved plate. *J. Fluid Mech.* **283**, 249.

Randriarifara, T. 1998 The instability of streamwise vortices in a curved, rotating channel. *submitted to Phys. Fluids.*

Reddy, S. C. & Henningson, D. S. 1993 Energy growth in viscous channel flows. *J. Fluid Mech.* **252**, 209.

Reddy, S. C., Schmid, P. J., Baggett, J. S. & Henningson, D. S. 1998 On the stability of streamwise streaks and transition thresholds in plane channel flows. *J. Fluid Mech.* **365**, 269.

Reshotko, E. 1994 Boundary layer instability, transition and control. AIAA Paper 94-0001.

Romanov, V. A. 1973 Stability of plane-parallel Couette flow. Translated in *Functional Anal. & Its Applics* **7**, 137.

Schoppa, W. & Hussain, F. 1997 Genesis and dynamics of coherent structures in near-wall turbulence: a new look. In *Self-Sustaining Mechanisms of Wall Turbulence.* (ed. R. L. Panton), pp. 385-422. Computational Mechanics Publications, Southampton.

Schoppa, W. & Hussain, F. 1998 Formation of near-wall streamwise vortices by streak instability. AIAA Paper 98-3000.

Swearingen, J. D. & Blackwelder, R. F. 1987 The growth and breakdown of streamwise vortices in the presence of a wall. *J. Fluid Mech.* **182**, 255.

Tillmark, N. & Alfredsson, P. H. 1992 Experiments on transition in plane Couette flow. *J. Fluid Mech.* **235**, 89.

Trefethen, L. N., Trefethen, A. E., Reddy, S. C. & Driscoll, T. A. 1993 Hydrodynamic stability without eigenvalues. *Science* **261**, 578.

Ustinov, M. V. 1998 Stability of streaky structures in boundary layer. Presented at the EUROMECH colloquium 380: *Laminar-Turbulent Transition Mechanisms and Prediction*, Göttingen, Germany, September 14-17 1998.

Waleffe, F. 1995 Hydrodynamic stability and turbulence: Beyond transients to a self-sustaining process. *Stud. Appl. Math.* **95**, 319.

Waleffe, F. 1997 On a self-sustaining process in shear flows. *Phys. Fluids A* **9**, 883.

Westin, K. J. A., Boiko, A. V., Klingmann, B. G. B., Kozlov, V. V. & Alfredsson, P. H. 1994 Experiments in a boundary layer subject to free-stream turbulence. Part I. Boundary layer structure and receptivity. *J. Fluid Mech.* **281**, 193.

Yu, X. & Liu, J. T. C. 1991 The secondary instability in Goertler flow. *Phys. Fluids* A **3**, 1845.

Paper 3

3

Transition of streamwise streaks in zero pressure gradient boundary layers

By Luca Brandt and Dan S. Henningson[1]

Department of Mechanics, Royal Institute of Technology (KTH), S-100 44 Stockholm, Sweden

1. Introduction

A scenario for bypass transition likely to occur in a flat plate boundary layer flow under free–stream turbulence is studied. The disturbances at the leading edge of the flat plate that show the highest potential for transient energy growth consist of streamwise aligned vortices. Due to the lift-up mechanism these optimal disturbances are transformed downstream into elongated streamwise streaks with significant spanwise modulation. The initial disturbance that yields the maximum spatial transient growth in a non-parallel flat plate boundary layer flow was determined by Andersson, Berggren & Henningson (1999) by applying the boundary layer approximations to the three-dimensional steady incompressible Navier-Stokes equations and linearizing around the Blasius base flow. If the disturbance energy of the streaks becomes sufficiently large, secondary instability can take place and provoke early breakdown and transition, overruling the theoretically predicted modal decay. A possible secondary instability is caused by inflectional profiles of the base flow velocity, a mechanism which does not rely on the presence of viscosity. Experiments with flow visualizations by for example Matsubara & Alfredsson (2001) have considered the case of transition induced by streaks formed by the passage of the fluid through the screens of the wind-tunnel settling chamber. They report on the presence of a high frequency "wiggle" of the streak with a subsequent breakdown into a turbulent spot.

In Andersson *et al.* (2001) Direct Numerical Simulations (DNS), using a numerical code described in Lundbladh *et al.* (1999), are used to follow the nonlinear saturation of the optimally growing streaks in a spatially evolving boundary layer. The complete velocity vector field from the linear results by Andersson *et al.* (1999) is used as input close to the leading edge and the downstream nonlinear development is monitored for different initial amplitudes of the perturbation. Inviscid secondary instability calculations using Floquet theory are performed on the obtained mean flows and it is found that the streak critical amplitude, beyond which streamwise traveling waves are excited, is about 26% of the free-stream velocity. The sinuous instability mode (either

[1]Also at FOI, The Swedish Defense Research Agency, Aeronautics Division, S-17290 Stockholm, Sweden

the fundamental or the subharmonic, depending on the streak amplitude) represents the most dangerous disturbance. Varicose waves are more stable, and are characterized by a critical amplitude of about 37%.

Here, also using DNS, we study the transition process resulting from the sinuous secondary instability. A velocity vector field from the simulations presented in Andersson *et al.* (2001) is used as inflow condition. In those simulations a spanwise antisymmetric harmonic volume force was added to the non linear streaks to trigger their sinuous secondary instability in order to check the linear stability calculations. Here the saturated streaks, $\mathbf{v_s}$, and the secondary instability mode, $\mathbf{v_d}$, obtained filtering the velocity field at the frequency ω of the forcing, are introduced as inflow condition by adding them to the Blasius solution to give the forcing vector $\mathbf{v} = \mathbf{v_0} + \mathbf{v_s} + A\mathbf{v_d}e^{i\omega t}$. An amplification factor A is used for the secondary instability to give transition within the computational box. The late stages of the process are investigated and flow structures identified. They are different from the case of transition initiated by Tollmien-Schlichting waves and their secondary instability (see Rist & Fasel 1995 as example) or by-pass transition initiated by oblique waves (Berlin *et al.* 1999). In these latter two scenarios Λ-vortices with strong shear layer on top, streamwise vortices deforming the mean flow and inflectional velocity profiles are observed. Berlin *et al.* (1999) speculated that the pattern of Λ-vortices appearing is then independent on the presence of Tollmien-Schlichting waves, but depends only on the streawise streaks and the oblique waves. These two are key elements also in the present case, but a different spatial symmetry property of the amplifying disturbance gives different flow structures. The present case shows analogies with streak instability and breakdown found in the near wall region of a turbulent boundary layer (see Schoppa & Hussain 1997 or Kawahara *et al.* 1998).

2. Results

In this section we give an overview of the full transition of a streamwise streak subjected to sinuous secondary instability. Time averaged statistics and Fourier analysis of the results are presented while instantaneous flow structures are discussed in the next section. Our simulation starts at $Re_{\delta_0^*} = 875$ ($x = 0$) and if not stated differently, in the results presented the coordinates are made non dimensional using the inflow boundary layer thickness δ_0^*. The computational box is 6.86 δ_0^* wide, corresponding to one spanwise wavelength of the streak, and 10.7 δ_0^* high. A simulation with the inlet moved further downstream ($Re_{\delta^*} = 1044$) is also performed to have some fully developed turbulence within the computational box using the same number of modes. The length of the boxes is 380 δ_0^*. $1440 \times 97 \times 72$ spectral modes are used respectively in the streamwise, wall-normal and spanwise directions.

To extract information on the frequency content of the flow, sixteen velocity field are saved during one period of the secondary instability mode. We then transform these velocity fields in time and in the spanwise direction to Fourier

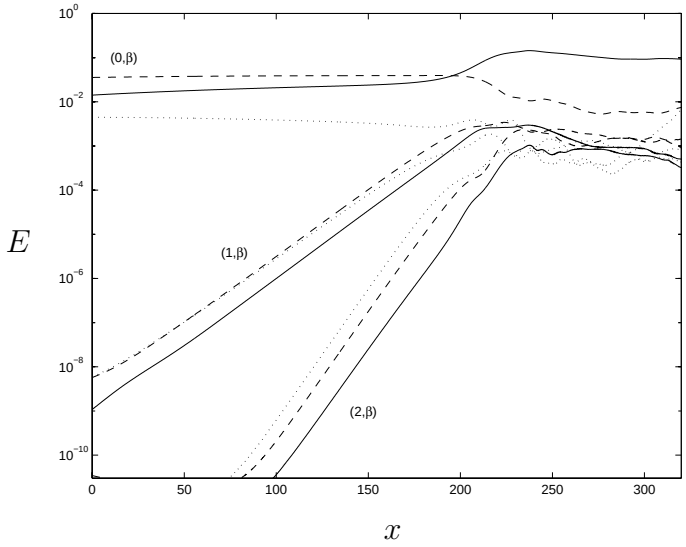

FIGURE 1. Energy in different Fourier modes (ω, β) versus the downstream position. Frequencies: zero (streak), one (secondary instability), two (higher harmonic). — $\beta = 0$, - - - $\beta = 1$, $\cdots$ $\beta = 2$.

space and use the notation (ω, β), where ω and β are the frequency and spanwise wavenumber, each normalized with the corresponding fundamental frequency and wavenumber. The energy in some of the modes is displayed in figure 1, where the zero frequency mode represents the streak. The secondary instability mode ($\omega = 1$) is present at the beginning of the computation, while the higher harmonics are excited as the flow evolves downstream. The energy growth is exponential for a long streamwise extension and the growth rate of the first harmonic ($\omega = 2$) is twice the one of the fundamental secondary instability, and similarly for higher frequencies (not reported here), the growth rate is proportional to the harmonic order.

It is interesting to note that the energy content is of the same order for modes with different spanwise wavenumbers but with the same frequency. This result is different from the one obtained when the same analysis is applied to a case of transition initiated by two oblique waves (Berlin *et al.* 1999) or by Tollmien–Schilichting waves (Laurien & Kleiser 1989; Rist & Fasel 1995). In these cases nonlinear interactions are important to select the modes dominating the transition process, namely the streamwise independent ones, while here streaks are induced from the start and they develop to a highly nonlinear stage before they become unstable to time dependent disturbances; thus the harmonics in the spanwise direction are generated during the streak growth and are responsible for the large spanwise shear of the flow. The instability of such a flow is then characterized by modes strongly localized in the spanwise

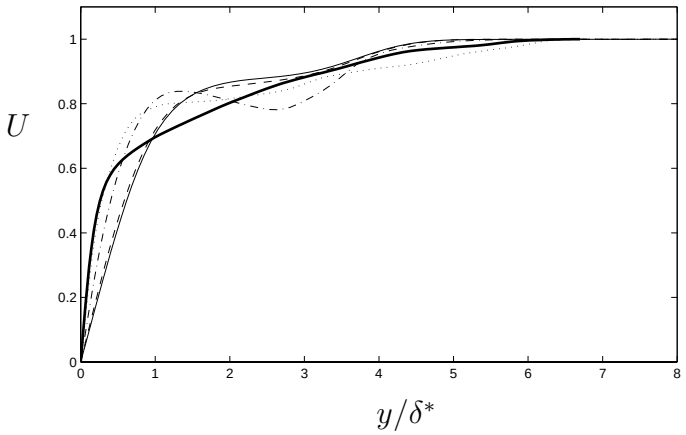

FIGURE 2. Average streamwise velocity in outer coordinates at different streamwise positions;$x = 126$: —— (thin line), $x = 185$: - - - , $x = 215$: - · - , $x = 268$: ··· , $x = 399$:—— (thick line).

direction so that a number of wavenumbers β is needed to correctly capture them (see Andersson *et al.* 2001). The growth in the different harmonics starts to saturate around position $x = 200$ and soon the energy becomes of the same order for the different ω's. From this point ($x \approx 220$) the Fourier transform in time of the whole velocity fields is no longer accurate since not enough frequencies are resolved. In fact higher and higher harmonics are excited until the energy spectra fill out.

Mean velocity profiles at various locations in the transitional zone are displayed in figure 2, where the wall normal coordinate is made non dimensional with the local boundary layer thickness δ^*. The evolution from the laminar flow to a turbulent one can be seen. At position $x = 215$ a strong inflectional mean profile is present exactly during the large growth of the skin friction coefficient, not reported here. In the outer part of the boundary layer one can see an over–shoot of the velocity before approaching the final value. The same behavior of the mean flow was observed by Wu *et al.* (1999) in their simulations of transition induced by free–stream turbulence.

At the early stages of transition, the averaging of the streamwise velocity provides information on the evolution of the streak during the process, since the spanwise modulation dominates in the *rms* values. These are displayed in figure 3 also for the other two velocity components. In the experiments of Matsubara & Alfredsson (2001) of transition induced by upstream–generated grid turbulence the u_{rms} value attained by the streaky structure before the breakdown is about $11 - 12\%$. In our case, instead, the streak amplitude at the beginning of transition is about 19%, but we do not have a continuous forcing by the free–stream turbulence which is able to locally nonlinearly trigger the

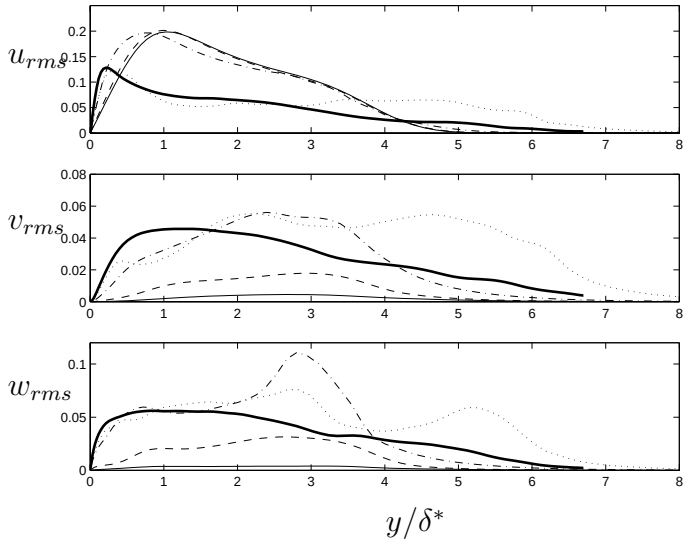

FIGURE 3. Time averaged Reynolds stresses in outer coordinates at different streamwise positions;$x = 126$: —— (thin line), $x = 185$: - - - , $x = 215$: - · - , $x = 268$: ··· , $x = 399$:—— (thick line).

inflectional instability of the flow. However, the same qualitative behavior of the u_{rms} is observed compared to the experiments, i.e. the peak is sharpening, moving closer to the wall and reaching values of approximatively $12 - 13\%$.

As the flow develops downstream, the rms values of the wall normal and spanwise velocity components increase especially in the outer part of the boundary layer, around $y \approx 3$. This corresponds to the wall normal region where the secondary instability is localized. One can also note that the spanwise velocity fluctuations are larger than the wall normal ones, and a considerable value of $w_{rms} \approx 11\%$ is attained at $x = 215$. It is also interesting to notice that at $x = 268$ the mean velocity profile, figure 2, and the u_{rms} are very close to the turbulent ones, especially close to the wall, but the v_{rms} and w_{rms} are characterized by large values in the upper part of the boundary layer. These oscillations represent periodic structures, formed in the transition region which survive downstream.

Profiles of the time-averaged turbulence kinetic energy production normalized with wall parameters are shown in figure 4 at the three different streamwise locations within the turbulent region and compared with the DNS data of Skote (2001). Spalart (1988) noticed that his DNS profiles of turbulent production at three different momentum thickness Reynolds numbers are self-similar. He explained it with the fact that the decrease of Reynolds stresses is compensated

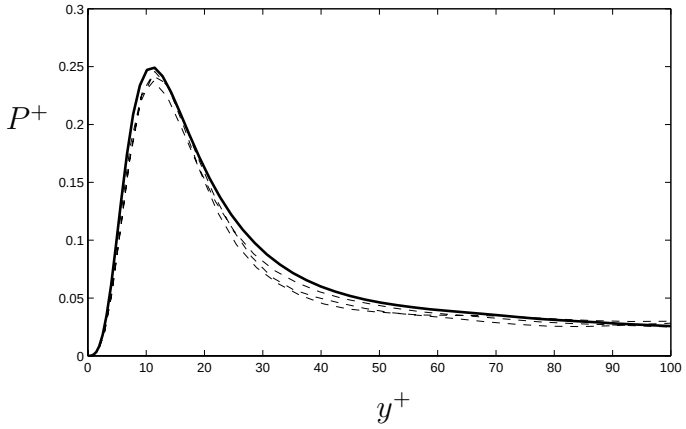

FIGURE 4. Time averaged non-dimensional turbulence kinetic energy production, $P^+ = -\overline{uv}^+ \frac{\partial U^+}{\partial y^+}$, near the wall. - - - : present simulations at $Re_\theta = 845$ ($x = 360$), $Re_\theta = 875$ ($x = 375$) and $Re_\theta = 910$ ($x = 400$); ——: Skote's simulations at $Re_\theta = 685$.

by the increase of mean velocity gradient for these relatively low Reynolds numbers. This seems to be true also in the present case, since all the profiles show a maximum of $P^+ = 0.25$ at $y^+ = 12$. The agreement in the profile of the kinetic energy production let us believe that the dynamics of turbulence is active at the downstream end of our computational box. Thus the flow observed is still influenced by the deterministic inflow conditions and by the transitional process only in the upper part of the boundary layer.

3. Instantaneous flow structures

A three-dimensional picture of the secondary instability mode is displayed in figures 5 and 6. These are obtained from the Fourier transformed velocity fields discussed in the previous section, filtering at the fundamental frequency. The mode is characterized by a streamwise wavelength $\lambda_x = 11.9$ and a frequency $\omega = 0.43$; only one wavelength λ_x is shown in the figures. Isosurface of positive and negative streamwise velocity are plotted in figure 5 to show the antisymmetry of this kind of instability. The low speed region is located around $z = 0$, where the fluctuations are stronger. The result is a spanwise oscillation of the low speed streak. The spanwise velocity, seen in figure 6, is in fact characterized by alternating positive and negative values, with a symmetric distribution of the disturbance with respect to the streak.

As observed in a number of experiments and numerical studies, see Le Cunff & Bottaro (1993) as example, the sinuous instability can be related to the spanwise inflectional points of the mean flow. Andersson *et al.* (2001) have shown that the secondary instability modes are concentrated around the critical

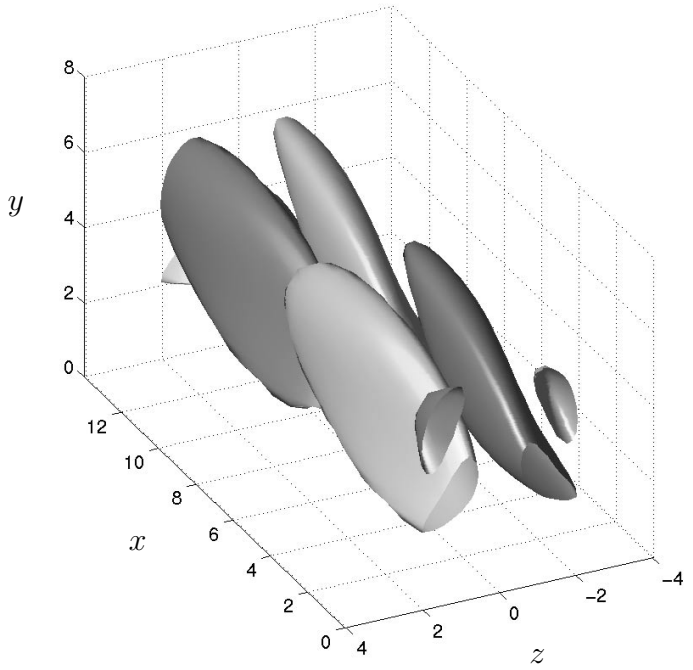

FIGURE 5. Isosurface of positive (dark grey) and negative (light grey) streamwise velocity component of the secondary instability eigenmode. The coordinates are made non dimensional using the local boundary layer thickness.

layer, i.e. the layer of costant value of the mean field velocity corresponding to the phase speed of the disturbance which is $u = 0.81U_\infty$ in the present case, thus confirming the inviscid nature of the considered instability.

In figure 7 the instantaneous streamwise velocity component of the perturbation is shown in a longitudinal plane perpendicular to the wall for $z = 0$, corresponding to the center of the undisturbed low speed streak and in a plane parallel to the wall, at $y = 0.47$. The perturbation velocity field is defined as the difference between the solution velocity field and the mean value in the spanwise direction for each value of x and y. It can be clearly seen that the sinuous instability consists of harmonic antisymmetric streamwise oscillations of the low speed region.

In figure 7a) one can note that the perturbation is first seen in the outer part of the boundary layer. The disturbance moves then towards the wall until the wall-shear is considerably increased. At the end of the computational box some periodicity can still be seen in the disturbance in the outer part of the boundary layer, while close to the wall the flow is now turbulent. In figure 7b) two streaks can be seen within the computational box at the end of the transition process,

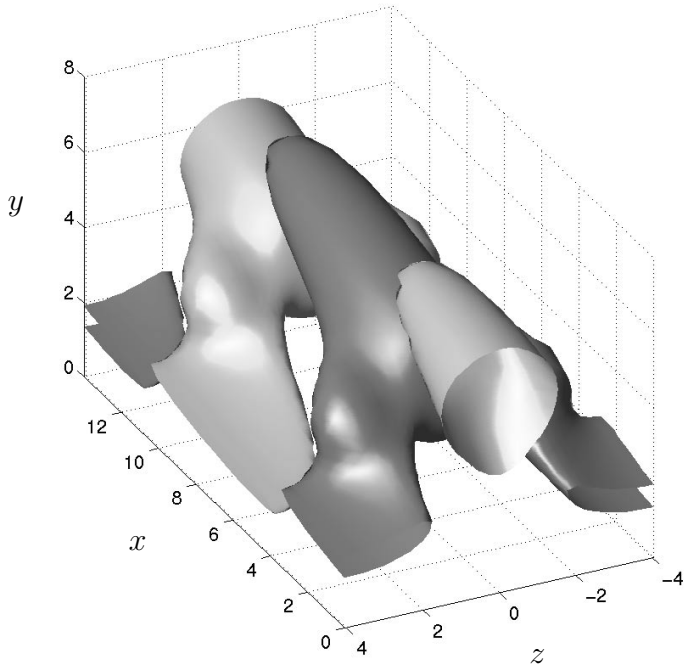

FIGURE 6. Isosurface of positive (dark grey) and negative (light grey) spanwise velocity component of the secondary instability eigenmode. The coordinates are made non dimensional using the local boundary layer thickness.

with a spacing of about $130z^+$. The spanwise dimension of the box is in fact for $x > 350$ less than 275 plus units, larger than the minimal channel studied by Jiménez & Moin (1991), in which a turbulent flow could be sustained. On the other hand, the computational box is apparently too small to allow the formation of some of the large structures present in the outer region.

The flow field from the laminar to the turbulent region is shown in figure 8. The light grey isosurface represents the low speed streaks, while the dark grey represents regions of low pressure. These corresponds to strong rotational fluid motions and are used to identify vortices. Also visualizations using negative values of the second largest eigenvalue of the Hessian of the pressure (see Jeong & Hussain 1997) are performed and no relevant differences are observed. The main structures observed during the transition process consist of elongated quasi-streamwise vortices located on the flanks of the low speed streak. Vortices of alternating sign are overlapping in the streamwise direction in a staggered pattern and they are symmetric counterparts, both inclined away from the wall and tilted in the downstream direction towards the middle of the undisturbed low speed region. The strength and extension of these vortices and the spanwise motion of the low speed streak increase downstream before the

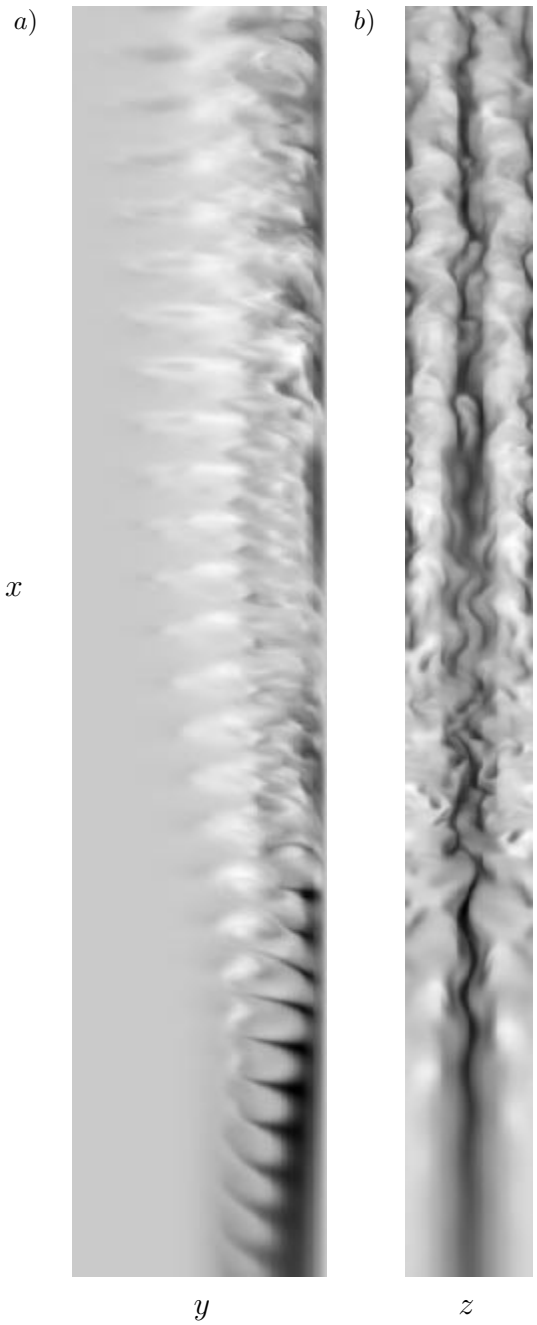

FIGURE 7. Visualization of streaks breakdown using streamwise velocity component of the perturbation in a wall normal x–y plane and wall parallel x–z plane. Grey scale from dark to light corresponding to negative to positive values. The flow is from bottom to top. $x-y$-plane at $z = 0$, $x-z$ plane at $y = 0.47$. $185 \leq x \leq 360$ in the streamwise direction.

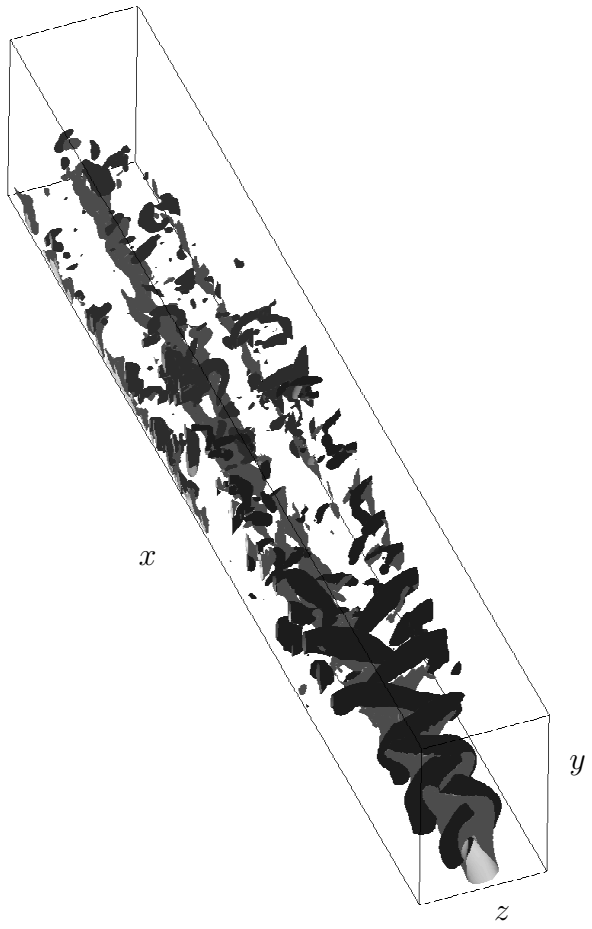

FIGURE 8. The flow field from the laminar to the turbulent region. The x-values correspond to the range $185 \leq x \leq 360$. The light grey structures are the low speed streaks and the darker ones are regions with low pressure. Contours level are -0.14 for the steamwise velocity fluctuations and -0.014 for the pressure for $x < 268$ and -0.0065 further downstream. The streamwise scale is one third of the cross stream ones.

breakdown. Towards the end of the box the flow has a more turbulent nature and more complicated low-pressure structures occur. It also seems that there is no connection between the laminar and turbulent-region low speed streak,

since the streak is disrupted at transition and those which appear downstream are not a continuation from upstream.

In other studied transition scenarios (Rist & Fasel 1995, Berlin *et al.* 1999), positive and negative streamwise vortices are also present on the side of the low speed region but they are not staggered in the streamwise direction so that the typical Λ-structures are seen. This is due to the different symmetry of the streamwise vorticity of the fundamental secondary instability; in the present case the vorticity disturbance is symmetric, while in the varicose case, observed in the simulations of oblique transition by Berlin *et al.* (1999), the streamwise vorticity is antisymmetric.

The vortex structures present in a turbulent boundary layer seem to be related to streak instabilities. Waleffe (1997) found that the dominating instability is sinuous and it is correlated with the spanwise inflection of the basic mean flow. Kawahara *et al.* (1998) and Schoppa & Hussain (1997) also used a similar approach and showed that the varicose mode is stable. The identified structures show a close resemblance to the one detected in our transitional boundary layer (Schoppa & Hussain 1997). On the other hand, Skote et al. (2001) show that the appearance of an unstable wall-normal velocity profile is a precursor to the appearance of horseshoe vortices, thus associated to varicose instability of the turbulent streaks.

References

Andersson, P., Berggren, M. and Henningson, D. S., 1999. Optimal disturbances and bypass transition in boundary layers. *Phys. Fluids*,**11**, pp. 134-150.

Andersson, P., Brandt, L., Bottaro, A. and Henningson, D. S., 2001. On the breakdown of boundary layer streaks. *J. Fluid Mech.*,**428**, pp. 29-60.

Berlin, S., Wiegel, M. and Henningson, D. S., 1999. Numerical and experimental investigations of oblique boundary layer transition. *J. Fluid Mech.*, **393**, pp. 23-57.

Jeong, J. and Hussain, F., 1997. Coherent structures near the wall in a turbulent channel flow. *J. Fluid Mech.*, **332**, pp. 185-214.

Jiménez, J. and Moin, P., 1991. The minimal flow unit in near-wall turbulence. *J. Fluid Mech.*, **225**, pp. 213-240.

Kawahara, G., Jiménez, J., Uhlmann, M. and Pinelli, A., 1998. The instability of streaks in near-wall turbulence. Center for Turbulence Research, Annual Research Briefs 1998, pp 155-170.

Le Cunff, C. and Bottaro, A., 1993. Linear stability of shear profiles and relation to the secondary instability of the Dean flow. *Phys. Fluids A*, **5**, pp. 2161.

Laurien, E. and Kleiser, L., 1989. Numerical simulation of boundary-layer transition and transition control. *J. Fluid Mech.*, **199**, pp. 403-440.

Lundbladh, A., Berlin, S., Skote, M., Hildings, C., Choi, J., Kim, J. and Henningson, D. S., 1999. An efficient spectral method for simulation of incompressible flow over a flat plate. TRITA-MEK Technical Report 1999:11, Royal Institute of Technology, Stockholm, Sweden.

Matsubara, M. and Alfredsson, P.H., 2001. Disturbance growth in boundary layers subjected to free-stream turbulence. *J. Fluid Mech.*, **430**, pp. 149-168.

Rist, U. and Fasel, H., 1995. Direct numerical simulation of controlled transition in a flat-plate boundary layer. *J. Fluid Mech.*, **298**, pp. 211-248.

Schoppa, W. and Hussain, F., 1997. Genesis and dynamics of coherent structures in near-wall turbulence: a new look. In *Self-Sustaining Mechanisms of Wall Turbulence.* (ed. R. L. Panton), pp. 385-422. Computational Mechanics Publications, Southampton.

Skote, M., Haritonidis, J. H. and Heningson, D. S., 2001. Instabilities in turbulent boundary layers. *Phys. Fluids*, submitted.

Skote, M., 2001. Studies of turbulent boundary layer flow through direct numerical simulation, PhD thesis, Royal Institute of Technology, Stockholm, Sweden.

Spalart, P. R., 1988. Direct siulation of a turbulent boundary layer up to $Re_\theta = 1410$. *J. Fluid Mech.*, **197**, pp. 61-98.

Waleffe, F., 1997. On a self-sustaining process in shear flows. *Phys. Fluids*, **9**, pp. 883-900.

Wu, X., Jacobs, R. G., Hunt, J. C. R. and Durbin, P. A., 1999. Simulation of boundary layer transition induced by periodically passing wakes. *J. Fluid Mech.*, **398**, pp. 109-153.